# Seismological and geotechnical aspects of the $M_w$=6.3 l'Aquila earthquake in central Italy on 6 April 2009

**Giuseppe Lanzo**, *Professor, University of Rome, Italy; email: giuseppe.lanzo@uniromal.it*
**Giuseppe Di Capua**, *INGV Rome, Italy; email: giuseppe.dicapua@ingv.it*
**Robert E. Kayen**, *USGS Menlo Park, USA; email: rkayen@usgs.gov*
**D. Scott Kieffer**, *Professor, Graz University of Technology, Austria; email: kieffer@TUGraz.at*
**Edward Button**, *ETH Zurich, Switzerland; email: button@erdw.ethz.ch*
**Giovanna Biscontin**, *Professor, Texas A&M University, USA; email: gbiscontin@civil.tamu.edu*
**Giuseppe Scasserra**, *University of Rome, Italy; email: giuseppe.scassera@gmail.com*
**Paolo Tommasi**, *CNR-IGAG, Rome, Italy; email: paolo.tommasi@uniromal.it*
**Alessandro Pagliaroli**, *CNR-IGAG, Rome, Italy; email: alessandro.pagliaroli@uniromal.it*
**Francesco Silvestri**, *Professor, University of Naples, Italy; email: francesco.silvestri@unima.it*
**Anna d'Onofrio**, *Professor, University of Naples, Italy; email: donofrio@unima.it*
**Crescenzo Violante**, *CNR-IAMC, Naples, Italy; email: crescenzo.violante@iamc.cnr.it*
**Armando Lucio Simonelli**, *Professor, University of Sannio, Benevento, Italy; email: alsimone@unisannio.it*
**Rodolfo Puglia**, *INGV, Milan, Italy; email: puglia@mi.ingv.it*
**George Mylonakis**, *Professor, University of Patras, Greece; email: mylo@upatras.gr*
**George Athanasopoulos**, *Professor, University of Patras, Greece; email: gaa@upatras.gr*
**Vasil Vlahakis**, *University of Patras, Greece*
**Jonathan P. Stewart**, *Professor and Vice Chair Civil and Environmental Engineering Department, University of California, Los Angeles, USA; email: jstewart@seas.ucla.edu*

**ABSTRACT**: *The L'Aquila earthquake occurred on April 6 2009 at 03:32:39 local time. The earthquake ($M_w$=6.3) was located in the central Italy region of Abruzzo. Much of the damage occurred in the capital city of L'Aquila, a city of approximate population 73000, although many small villages in the surrounding region of the middle Aterno river valley were also significantly damaged. In the weeks following the earthquake, the Geo-Engineering Extreme Events Reconnaissance (GEER) international team, comprised of members from different European countries and the U.S., was assembled to provide post-earthquake field reconnaissance. The GEER team focused on the geological, seismological, and geotechnical engineering aspects of the event. We describe the principal seismological findings related to this earthquake including moment tensors of the main shock and two triggered events, the aftershock pattern and its variation with time, tectonic deformations associated with the main shock, surface fault rupture, and the inferred fault rupture plane. We describe damage patterns on a village-to-village scale and on a more local scale within the city of L'Aquila. In many cases the damage patterns imply site effects, as neighbouring villages on rock and soil had significantly different damage intensities (damage more pronounced on softer sediments). The April 6 mainshock was the best-recorded event to date in Italy. We present metadata related to the recording sites and then present preliminary comparisons of the data to GMPEs. Those comparisons support the notion of faster distance attenuation in Italy relative to the average for active regions as reflected in NGA GMPEs. Several incidents of ground failure are then discussed, including a number of rockfalls and minor landslides. Perhaps the most significant incidents of ground failure occurred at Lake Sinizzo, for which we describe a number of slumps and spreads around the lake perimeter. This is documented using field observations as well as LIDAR and bathymetric data.*

**KEYWORDS:** L'Aquila Earthquake, seismic source, ground motion parameters, site effects, ground failure, structural damage, dams, retaining structures

Submitted: 8 October 2009; Published: 22 April 2010
Reference: Lanzo G., Di Capua G., Kayen R.E., Kieffer D.S., Button E., Biscontin G., Scasserra G., Tommasi P., Pagliaroli A., Silvestri F., d'Onofrio A., Violante C., Simonelli A.L., Puglia R., Mylonakis G., Athanasopoulos G., Vlahakis V., Stewart J.P., (2010). *Seismological and geotechnical aspects of the $M_w$=6.3 l'Aquila earthquake in central Italy on 6 April 2009.* International Journal of Geoengineering Case histories, http://casehistories.geoengineer.org, Vol.1, Issue 4, p.206-339.

**SITE LOCATION:** IJGCH-database.kmz (requires Google Earth)

## INTRODUCTION

The L'Aquila earthquake occurred on April 6 2009 at 03:32:39 local time. The earthquake was located in the central Italy region of Abruzzo. Much of the damage occurred in the capital city of L'Aquila, a city of approximate population 73000, although many small villages in the surrounding regions were significantly damaged including Paganica, Castelnuovo, and Onna. Collapsed and damaged structures in L'Aquila included both older masonry buildings and relatively modern reinforced concrete structures. At the time of this writing, 307 people are known to have died from the earthquake, most in collapsed structures, making this the deadliest earthquake to strike Italy since the 1980 Irpinia earthquake.

A number of reconnaissance teams were mobilized to the affected region in the weeks following the earthquake. The national institute of geophysics and volcanology (Istituto Nazionale di Geofisica e Vulcanologia, INGV) mobilized a team of geologists (EMERGEO Working Group) to look for evidence of surface rupture and other effects; some of their findings are discussed in this report. The Geo-Engineering Extreme Events Reconnaissance (GEER) team was assembled to investigate geological, seismological and geotechnical engineering aspects of the event (GEER Working Group, 2009). The international GEER team is comprised of members from Italy, Austria, Switzerland, Greece, and the United states. Team members were selected to provide needed expertise in geology, engineering geology, GIS applications, earthquake ground motions, and geotechnical earthquake engineering. The team includes individuals highly experienced in post-earthquake reconnaissance and relatively young professionals investigating their first earthquake.

The GEER team did not focus on structural engineering or lifeline aspects of the event, which were investigated by an EERI team. The GEER and EERI activities were closely coordinated to optimize resources in the documentation of the valuable, perishable data associated with the earthquake effects.

The GEER team employed a number of innovative technologies to facilitate effective reconnaissance. All teams mobilized for field work had a common GPS unit and laptop with a Google Earth (GE) GIS database actively maintained over the course of the work. The GE database was used to keep track of visited locations, but also contained maps of surface geology, locations of aftershocks, strong motion stations, and other information relevant to investigators in the field. Another valuable use of technology involved LIDAR mapping of a site having significant incidents of ground failure (Lake Sinizzo).

This paper presents the GEER findings, which have been previously documented in a GEER report (GEER Working Group, 2009). Following this introduction, we describe seismological aspects of the earthquake sequence, including the geologic and tectonic setting, moment tensor solutions for the mainshock and several triggered events, analysis of aftershock patterns, and analysis of GPS and InSAR data. Included in that discussion is a preliminary model of the ruptured fault. We then describe the ground motions recorded during the mainshock by a digital instrument array. Metadata associated with the recordings is presented, trends in the recorded ground motions are presented, and preliminary comparisons to ground motion prediction equations are made. In the next section, we describe damage patterns both within L'Aquila and through comparisons of damage intensities in adjacent villages with similar construction. The results provide valuable insights into possible site effects on ground motion in regions where recordings are not available. We then describe our findings on ground failure, defined as permanent ground deformations induced by the earthquake. Observed ground failures included several rockfalls, seismic compression of fill materials, and apparent strength loss of soil materials leading to inward movement of the banks of a lake. The performance of dams and earth retaining structures is then reviewed, with such structures having generally been found to perform well.

## EARTHQUAKE SETTING AND SOURCE CHARACTERISTICS

### Geological and Tectonic Setting

Geodynamic Evolution

The area affected by the earthquake of April 6, 2009 is located within the central section of the Apennines. This mountain chain, which traverses most of the length of the Italian peninsula, is the result of the convergence between the African and European tectonic plates and the subsequent collision of the two continental margins, a geodynamic process illustrated in

Figure 1 that began in the Neogene age (about 23 MY before present) and was responsible for the closing of the Mesozoic Tethys Ocean.

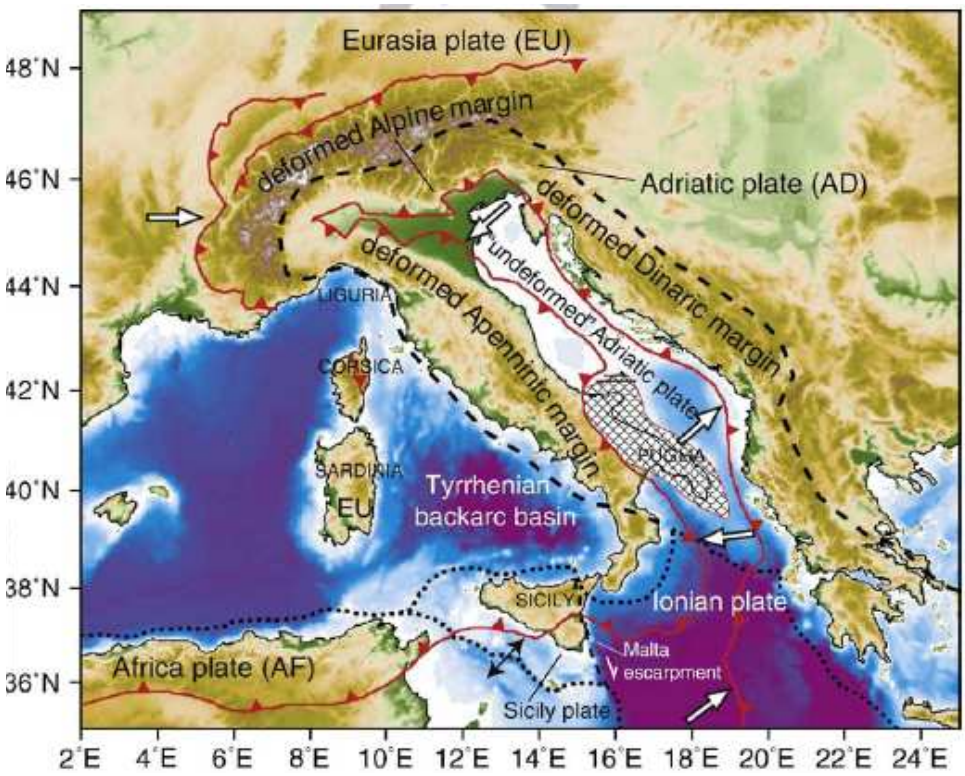


*Figure 1. Geodynamic model for the central Mediterrannean (Devoti et al., 2008).*

The compressive phase significantly deformed the extensive layers of marine deposits accumulated along the margins of the African Plate, uplifting them into a mountain chain. Over time, orogenic thrusts acted in an asynchronous manner along the Apennine chain, deforming this sector of the continental crust from the Miocene epoch to the Upper Pliocene sub-epoch (24 My to 3.6 My BP).

The geodynamic model most often cited and used to describe recently observable phenomena is based on a thrust belt-foredeep-foreland system progressively migrating away from the Tyrrhenian and towards the Adriatic flank. As schematically depicted in Figure 2, this system describes a transition from continental compression in the front of the chain (Adriatic side) to extension behind the chain (Tyrennian sector).

Most of the central zone of the Apennine chain is formed of stiff calcareous successions of carbonate platforms and turbiditic deposits that were deposited in the foredeep basins and progressively incorporated in the chain migrating from West to East. The deposits were folded and faulted. The older deposits overlie more recent ones, indicating the formation of an orogenic structure known as a tectonic duplex. The resulting effect is characterized by significant crustal shortening, some of which is evident in this segment of the Apennine chain. Furthermore, later structural complications contributed to the rotation of rigid blocks and isostatic movements in response to strong crustal thickening. At a certain point the chain emerges from the seabed, rising in some places to peaks higher than 3000 m above sea level. The emergence of the chain would have begun at the end of the Messinian age (7 My BP; in the more internal, Tyrrhenian sectors) and continued until the Upper Pliocene epoch (3.6 My BP; for the more external, Adriatic sectors) (Cavinato and De Celles, 1999). A map of the portion of the Apennine chain near L'Aquila is shown in Figure 3.

The thrust belt-foredeep-foreland system's progressive migration towards the Adriatic flank would have occurred in response to a mechanism of sinking with the flexural retreat of the Apulian foreland plate. The flexural retreat could be attributed to the existence of movements in the upper mantle that have a direction contrary to that of the subduction of the Apulian plate towards the Tyrrhenian flank (Doglioni, 1990 and 1991).

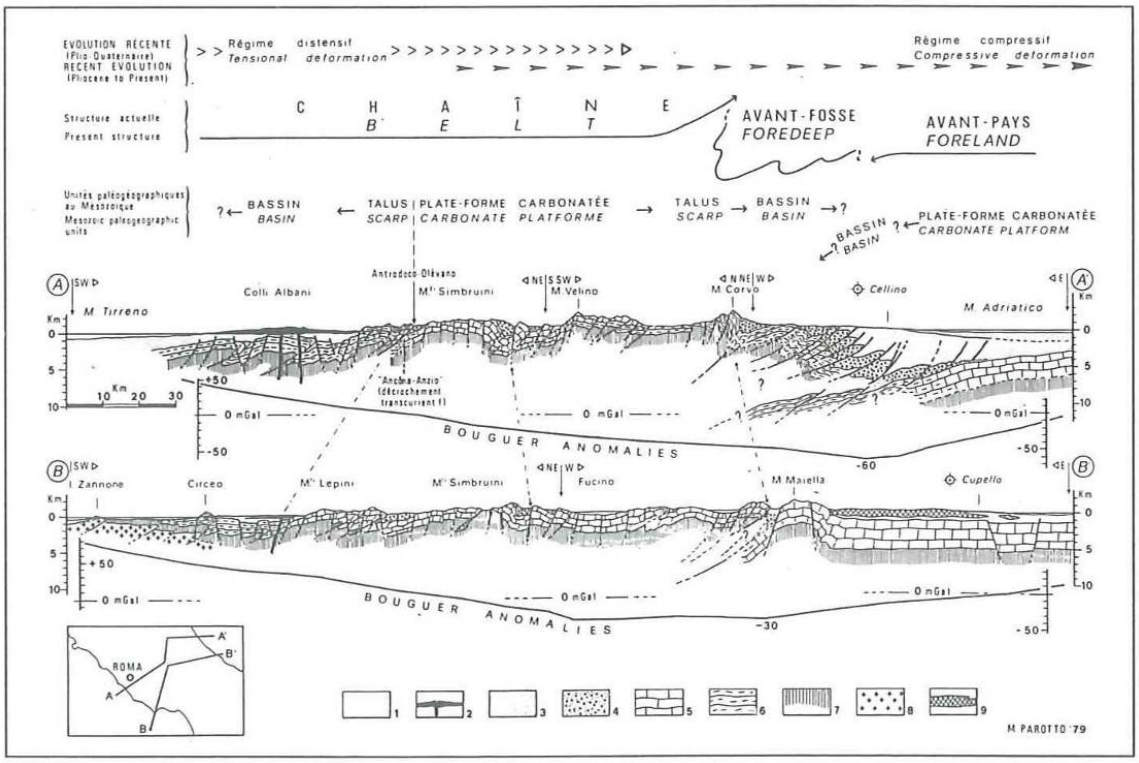



*Figure 2. Geologic cross-sections across the central Apennines. The area affected by the earthquake is located between M. Velino and M. Grande (Tozzi, 1993 from Parotto, 1980).*

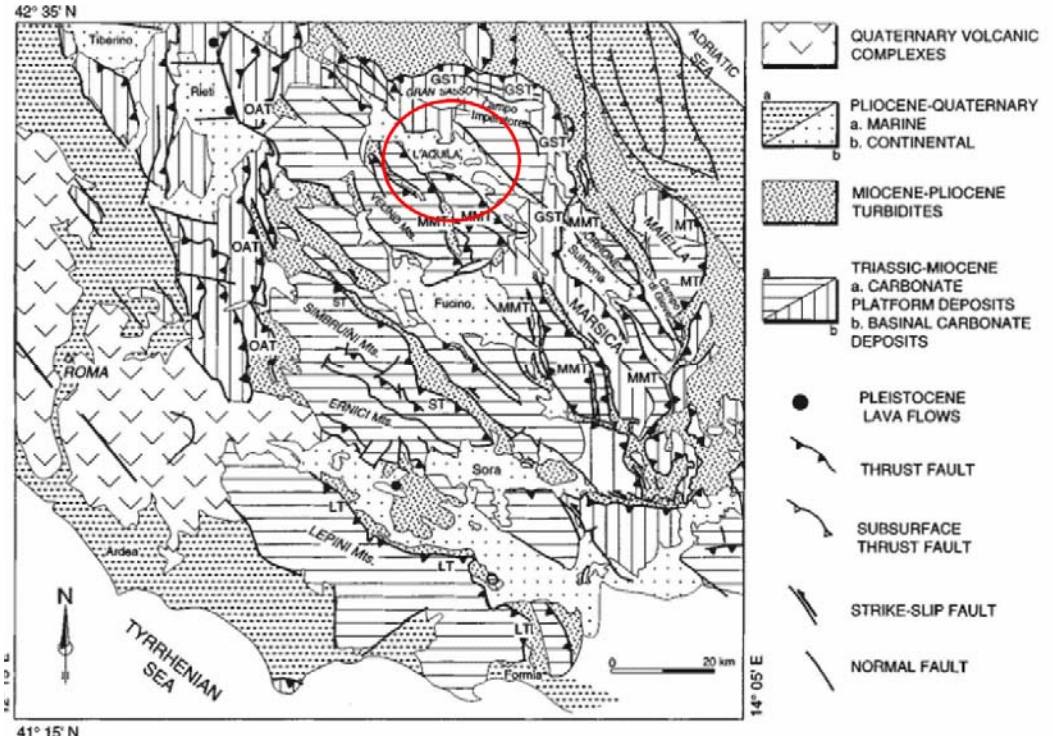



*Figure 3. Geologic-structural map of the central Apennines (Cavinato and De Celles, 1999). In the L'Aquila basin (inside the red circle) there are continental Quaternary deposits (in white with black dots) encased between carbonate platform deposits (horizontal and vertical hatching lines).*

Finally, beginning in the Messinian-Tortonian age (11.6 My BP) the area experienced a process of crustal thinning accompanied by the oceanization of the Tyrrhenian Sea (retroarc basin). Since the Lower Pleistocene (1.8 My BP), these extensional movements, which in the peri-Tyrrhenian area cause the development of Tuscany-Lazio-Campania volcanism, have been progressively migrating towards the Adriatic sectors, to the point that they have affected the Apennine chain's watershed. However the portion of the chain between the watershed and the Adriatic area would have undergone a process of gravitational settling and collapses due to isostatic instability, with the consequent formation of several intra-Apennine basins, including the L'Aquila basin (Ghisetti and Vezzani, 2000 and 2002).

The deformations associated with crustal thinning and the gravitational collapse are primarily accommodated by normal faults formed in part by reactivating pre-existing thrusts associated with the emplacement of the Apennine tectonic slices, making these structures important pre-, syn- and late-orogenic normal features that define the plano-altimetric configuration (basin and range). This pattern displays alternating ridges (Simbruini-Ernici, Velino-Sirente, Gran Sasso, Maiella e Morrone, etc.) and depressions under tectonic control (Valle del Sacco, Val Roveto, Piana del Fucino, Valle dell'Aterno, Conca dell'Aquila, Piana di Sulmona, etc.) as illustrated in Figure 3 (Cavinato and De Celles, 1999).

The foredeep of the tectonic system described above extends with a sort of geographic continuity from the great Padan Plain down to the Bradanic area (Puglia) and encompasses thousands of meters of silico-clastic sediments. The compression is active in the Adriatic coastal area.

Geological Setting

The central sector of the Apennine chain consists of deposits that were formed on the continental crust of the African plate in different paleogeographic domains. In general terms two great Meso-Cenozoic depositional systems are distinguishable. The first is characterized by Mesozoic carbonate platforms (limestones and dolomites) evolving towards carbonate slope and basin environments (calcarenites and marls) and was subject to active deposition until the mid-Miocene (16.5 My BP). The second consists of impressive foredeep silico-clastic deposits (clays and sandstones) datable to the Upper Miocene-Pliocene interval (11 to 5 My BP).

The emergent chain then underwent an intense erosive Plio-Pleistocene phase (5 to 1.7 My BP). The sedimentary erosive-depositional cycles produced slope deposits and vast alluvial and lacustrine deposits that filled the intra-Apennine basins. The Pleistocene glacial cycles interacted with the tectonic deformations, through fluctuations in fluvial base level and variations of the predominant morphodynamic regime. Figure 4 shows a distribution of the Quaternary deposits present within the L'Aquila basin and the Aterno River Valley, which comprises the principal hydrographic feature of this sector.

Elongation in the NW-SE direction (parallel to many of the active normal faults) is notable in these intra-Apennine basins, which include the localities – among them the city of L'Aquila – that were affected by the earthquake of April 6.

Figure 5 is a detail of Figure 4 in the L'Aquila area, showing the outcropping Meso-Cenozoic carbonate rocks (with a small part of Meso-Cenozoic marly-arenaceous rocks just east of L'Aquila) along with Quaternary sediments distinguished as Pleistocene (beige) or Holocene (light blue).

The area that was most intensely affected by the April 6 mainshock roughly corresponds to the valleys of the Aterno River, its right tributary Raio Creek and the plateau extending to the west of the Aterno Valley. The bedrock of the area is comprised of limestone formations, deposited from the Jurassic to the Miocene age, that largely outcrop along the valley flanks and on the ridges located within the Aterno Valley. These limestones (shown in green on the cross sections in Figures 6 and 7) vary in texture from micritic to bioclastic and calcareous sandstones are also common. Several formations are associated with thick chert bands and/or layers. Glauconite rich layers are found in several of the Cretaceous formations. Bedding thickness ranges from thinly bedded to very thickly bedded massive limestones. The pelagic content of the limestone varies and several formations vary between marly limestone and calcareous marls, which tend to be thinly bedded. Calcareous conglomerates form the thickest and most competent layers within these formations. Locally the substratum consists of Miocene sandstones with marly intercalations. These outcropping formations (shown in light brown to dark brown in Figure 6) tend to be thick to very thickly bedded and in sections contain turbidite deposits composed primarily of marls and clays. Marl-dominated formations also tend to be thickly bedded, within these formations the clay content can vary resulting in more clayey marls. Marly limestones are also present in these formations together with chert and glauconite.

In the central inhabited zone of L'Aquila there are vast deposits associated with Quaternary paleolandslides. These deposits are comprised of Pleistocene heterometric breccias with varying degrees of cementation, known as "Megabreccias", at times of noteworthy dimensions (up to several cubic meters), comprised of primarily calcareous elements immersed in sandy silty matrices (Blumetti et al., 2002).

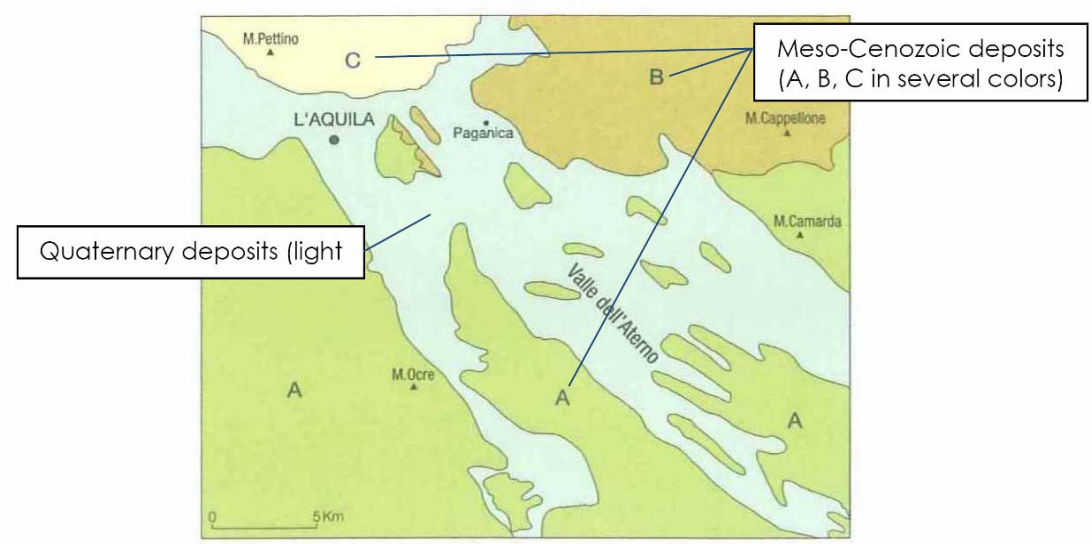



*Figure 4. Distribution of Quaternary deposits (in light blue) and Meso-Cenozoic deposits (in other colors) in the L'Aquila basin and the Aterno River Valley (from Sheet no. 359 of the Geologic Map of Italy at scale of 1:50000 – APAT, 2006).*

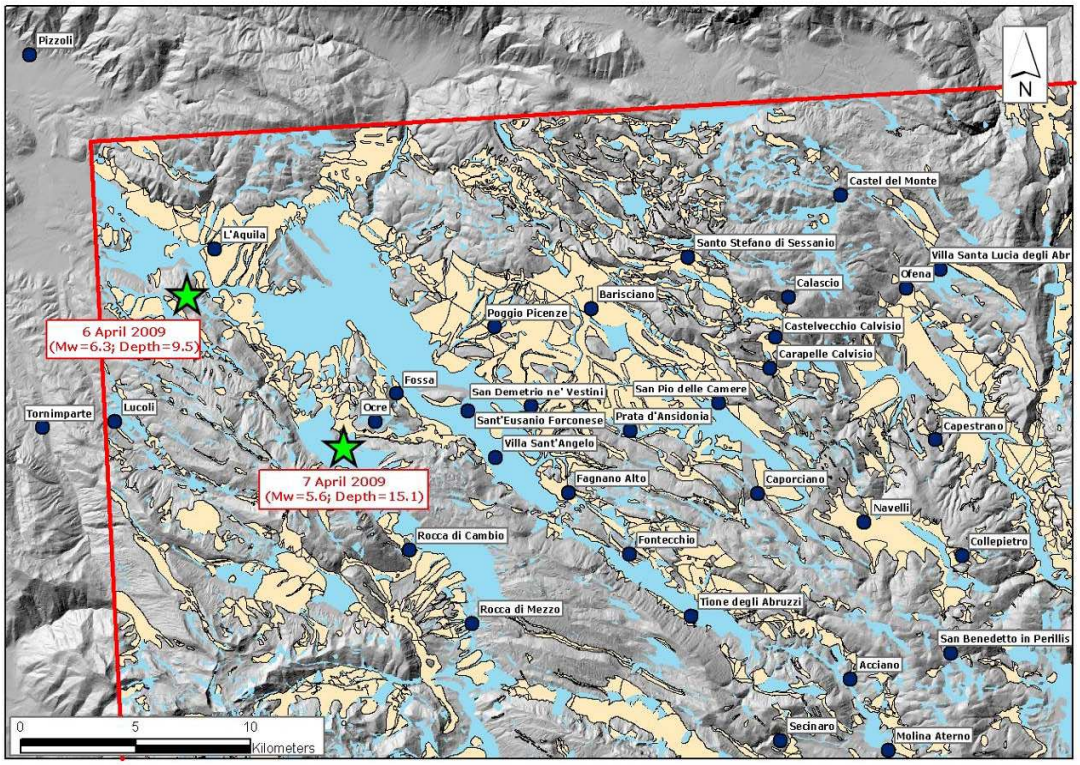



*Figure 5. Detail of the L'Aquila area. Within the red line, the areas in gray are where the Meso-Cenozoic deposits outcrop. The Pleistocene deposits are in beige, and the Holocene deposits are in light blue.*

According to Bertini and Bosi (1970) and Bertini et al. (1989) the Aterno Valley is partly filled by Pleistocene lacustrine deposits formed by a complex sequence of pelitic and coarse grained units, with frequent lateral variations, overlying the bedrock. On the left side of the Aterno river drainage basin (drainage from NW to SE), old breccias with large blocks are interposed between the bedrock and the lacustrine sequence (Valle Valiano formation).

The older (bottom) unit of the lacustrine sequence is the S. Nicandro formation. It consists of silts locally characterized by a significant clay fraction. On the left side of the drainage basin, alternations of silts with breccia layers are locally found at the base of the lacustrine sequence.

More recent (shallower) components of the lacustrine sequence are formed by coarse-grained units, often cemented, ranging from sands with gravels to breccias with large blocks, which can present finer intercalations (silts, fresh or weathered pyroclastites, paleosols). The units differ by clast shape, abundance of finer intercalations and overall degree of cementation.

The valley bottom is topped by Holocene alluvial deposits whereas the foot of the valley flanks and of the ridges located within the valley are covered by talus debris and locally by large debris alluvial fans.

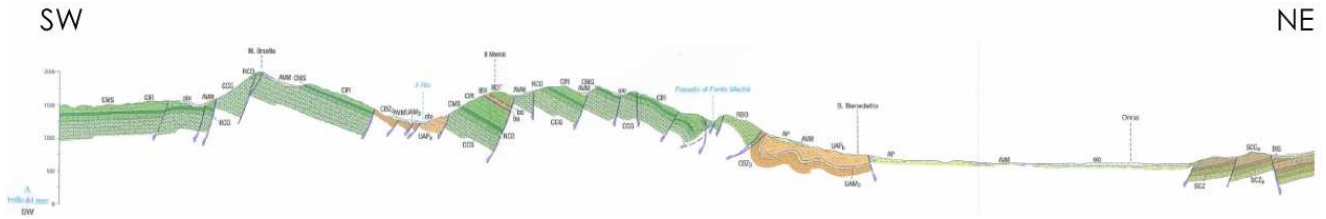



*Figure 6. SW-NE Geologic cross-section, crossing the L'Aquila basin and passing through the inhabited center of Onna, where the highest macroseismic level was surveyed (IX-X MCS) (from the Geologic Map of Italy at scale 1:50000)*




*Figure 7. SW-NE Geologic cross-section of the Aterno River Valley (Bosi and Bertini, 1970).*

Tectonic Setting

The Quaternary deposits of the L'Aquila area were deposited in morphological depressions inside the uplifted and emergent chain. These sedimentary basins are primarily delimited by high-angle (70°) normal faults with an Apennine trend that vertically break up, at different elevations, the orogenic structure, thereby forming a Horst and Graben structure. The normal fault system has its origins in a Quaternary phase (1.8 My BP). In general, the intra-chain basins are delimited by master faults and synthetic faults (i.e., a type of minor faults whose strike and sense of displacement is similar to their associated major fault) on the eastern sides of the depressions and by antithetic faults on the western sides.

In the area southeast of L'Aquila it is possible to see morphological limestone ridges outcropping with monoclinalic attitude. Some ridges are located in the center of the old Quaternary lacustrine basin. These ridges are the surface evidence of uplifted structures (Horst wedges) surrounded by depressed areas (Grabens) filled with Quaternary deposits.

Figure 6 shows a geologic cross-section that cuts from SW to NE through the Aterno Valley, taken from the Geologic Map of Italy at scale 1:50000; this section gives an idea of the tectonic structure of this sector. The right side of Figure 6 shows an intra-Apennine basin alongside an area of the chain that was overlain during the compressive phases by Apennine

orogeny. If the cross-section were to extend towards the right it would include the high reliefs of the Gran Sasso, bordered in turn by normal faults that lower the carbonate platforms towards the Southwest. The cross-section coincidentally crosses the L'Aquila basin at the elevation of Onna, a severely damaged village.

Figure 7 shows another geologic cross-section (SW-NE) at scale 1:25000, across the Quaternary basin. The carbonate ridges (Horsts) in green form the rigid substrate overlain by Quaternary deposits (in other colors) that fill the morphologic depressions (Grabens). The limestone ridges, with a generally NW-SE trend, are bounded by normal faults that lower them at various elevations.

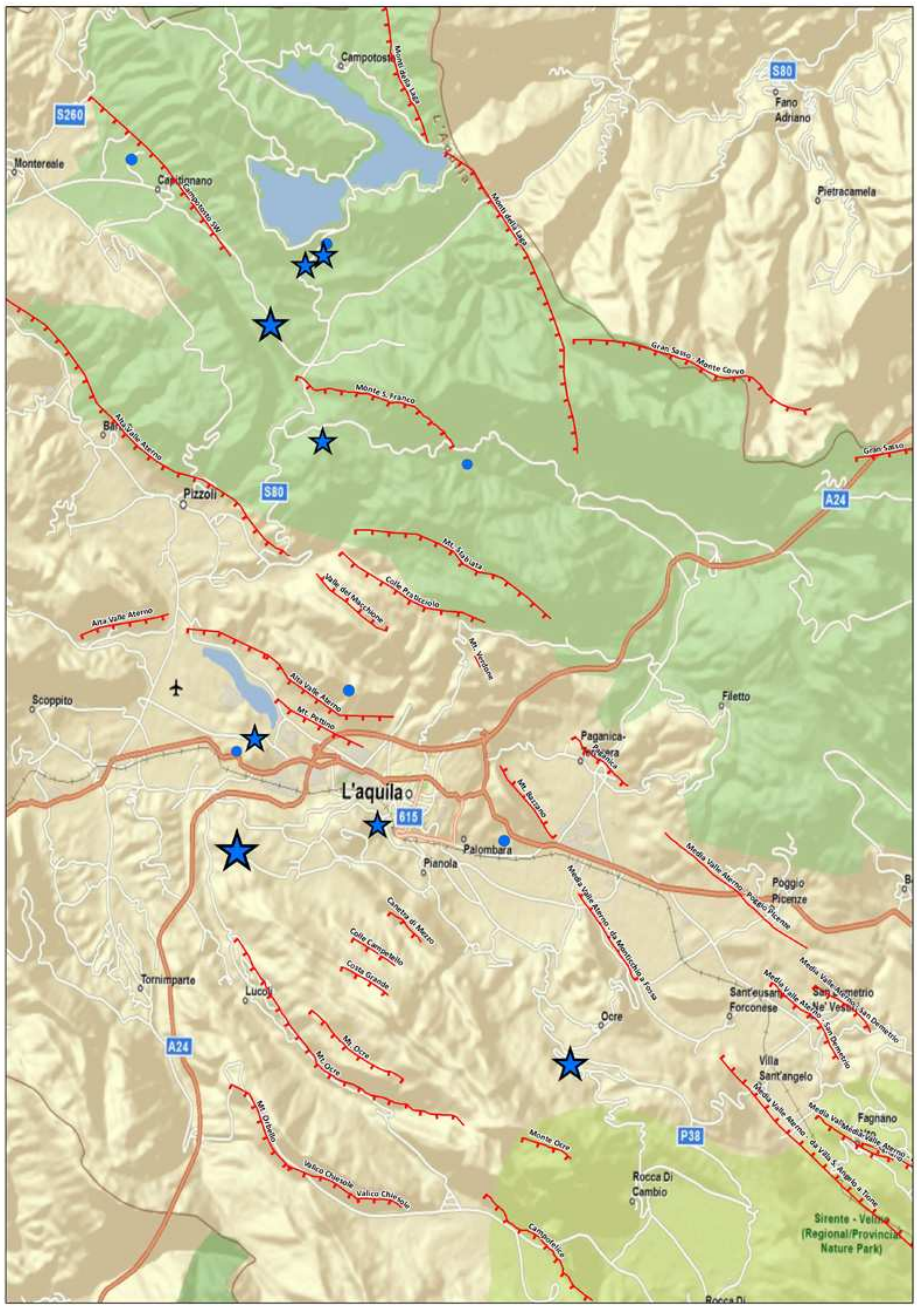



*Figure 8. Active faults (in red) of the L'Aquila area (from INGV website: http://www.ingv.it). The features are oriented towards the hanging wall. The stars indicate the locations of some epicenters with $M_w$>4.0 associated with the recent seismic sequence.*

The extensional system comprised of normal faults (master faults, synthetic and antithetic faults) present in the area is active, as demonstrated by this earthquake and the regional geomorphology. As described below, extension is also demonstrated by the normal fault focal mechanism of the present earthquake. The activity of the tectonic structures, with larger movements on the eastern edges of the basins, is also evidenced by the presence of important Quaternary alluvial fans on the Northeast side of depressions. With their movement the normal faults have in fact produced a rejuvenation of the relief in the NE areas, resulting in the increased effectiveness of the erosive processes and the deposition of coarse material in the valley zones in the SW areas. Figure 8 indicates the active faults of the L'Aquila area. These are normal faults of variable length that predominantly strike NW-SE (Bagnaia et al., 1992; Boncio et al., 2004; Galadini and Galli, 2000; Galadini and Messina, 2001). Southeast of L'Aquila, the active faults have a strongly rectilinear trend dipping either towards the Southwest or the Northeast.

**Seismological Aspects (Seismo-Kinematic Characteristics and Macroseismic Studies)**

Mainshock

The principal seismic event began on April 6, 2009 at 01:32:39 (UTC) and was recorded by the centralized national seismological network Rete Sismometrica Nazionale Centralizzata, operated by the national earthquake center (Centro Nazionale Terremoti, CNT) of the National Institute of Geophysics and Volcanology (Istituto Nazionale di Geofisica e Vulcanologia, INGV, www.ingv.it). The parameters calculated for this earthquake are given in Table 1.

*Table 1. Parameters for mainshock (in bold) and principal triggered events.*

| Date | Hour (UTC) | Lat. (N) | Long. (E) | Depth (kM) | $M_w$ |
|---|---|---|---|---|---|
| 2009/03/30 | 13:38:38 | 42.326 | 13.362 | 10.6 | 4.4 |
| **2009/04/06** | **01:32:39** | **42.348** | **13.380** | **9.5** | **6.3** |
| 2009/04/07 | 17:47:37 | 42.275 | 13.464 | 15.1 | 5.6 |
| 2009/04/09 | 00:52:59 | 42.484 | 13.343 | 15.4 | 5.4 |

The focal mechanism shows that the event took place along a normal fault trending NW-SE (strike 147°) with dip SW < 50°, demonstrating the same direction as many of the major tectonic structures visible on the surface (Figure 9).

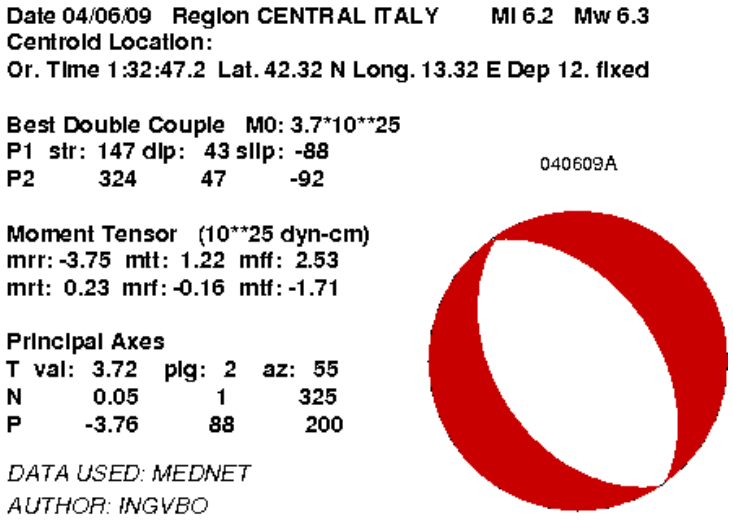



*Figure 9. Quick Regional Centroid Moment Tensors for the earthquake of April 6, 2009 (http://earthquake.rm.ingv.it/qrcmt.php).*

Seismic Sequence

The earthquake of April 6, 2009 was the largest event in a seismic sequence that started a few months earlier and had its most significant previous event on March 30, 2009. The focal mechanism of this event is shown in Figure 10. Since April

6, an active seismic sequence, not concluded as of this writing, has occurred with events as large as $M_w$ 5.6. Figures 11-12 show the focal mechanisms, and key attributes are given in Table 1.

The instrument locations and the sequence of aftershocks (Figure 13, updated on July 16, 2009) clearly identify two principal areas of crustal rupture: the main area in which the main shock of April 6 occurred and a second area associated with another tectonic structure, probably of lesser dimensions, on which the earthquake of April 9 occurred. Even the latter structure demonstrates that it had extensional movement along a plane oriented in the Apennine direction and dipping towards the SW by about 50° (Figure 12). The earthquake of April 7, whose focal mechanism also shows a component of oblique movement (Figure 11), occurred at a greater depth than the other two events. Both the April 7 and April 9 earthquakes are considered triggered events and not aftershocks of the April 6 mainshock.

Figure 14 shows several transverse sections (sections 1, 2 and 3) and one longitudinal section (section 4) of the L'Aquila basin that illustrate hypocenter distributions. The sections also show the surface positions of the active faults expressed at the surface (Chiarabba and De Gori, in Cocco, 2009). It should be noted that the hypocenter locations used in Figure 14 refer to a time interval in the seismic sequence previous to the one referenced in Figure 13, and therefore in Figure 14 several recent events are not shown.

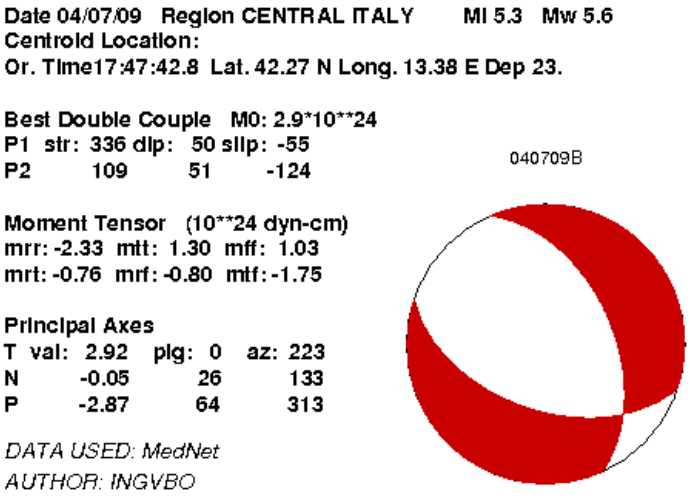



*Figure 10. Quick Regional Centroid Moment Tensors for the earthquake of March 30, 2009 (http://earthquake.rm.ingv.it/qrcmt.php).*

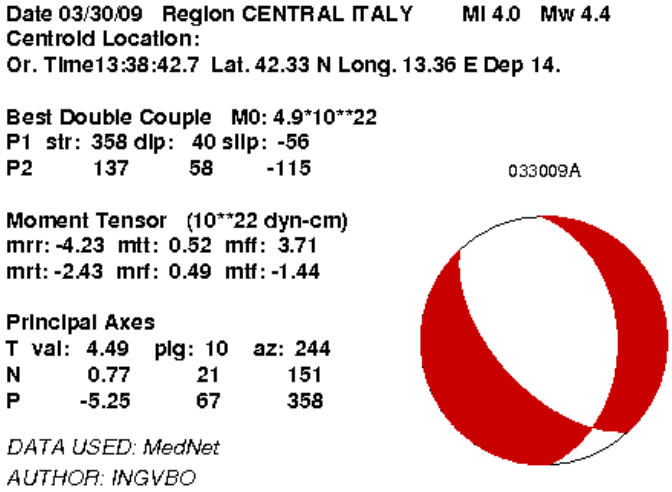



*Figure 11. Quick Regional Centroid Moment Tensors for the earthquake of April 7, 2009 (http://earthquake.rm.ingv.it/qrcmt.php).*

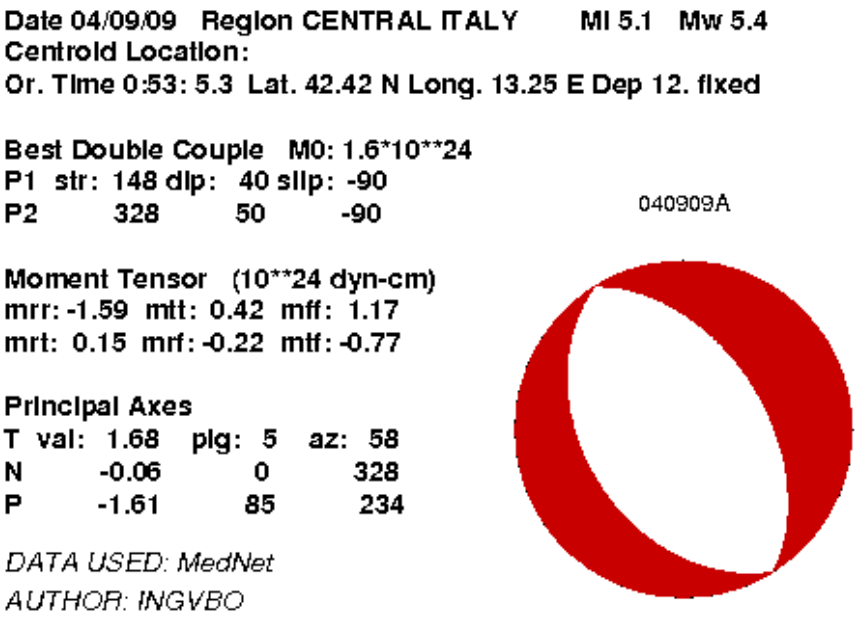



*Figure 12. Quick Regional Centroid Moment Tensors for the earthquake of April 9, 2009 (http://earthquake.rm.ingv.it/qrcmt.php).*

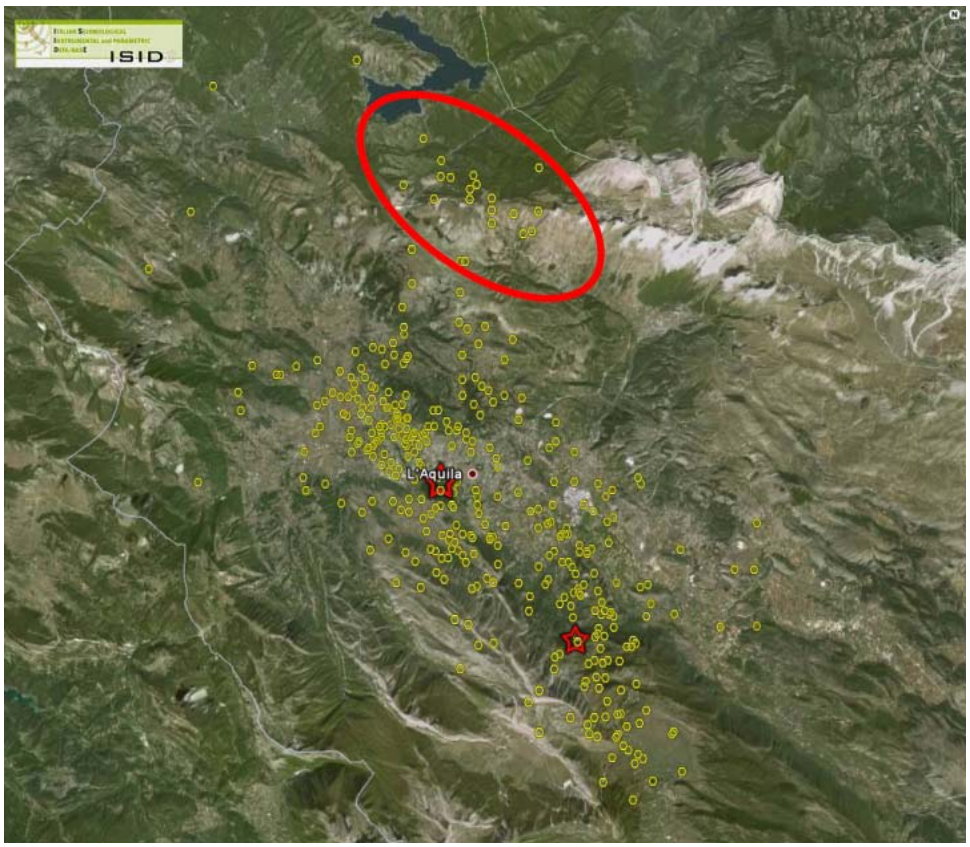
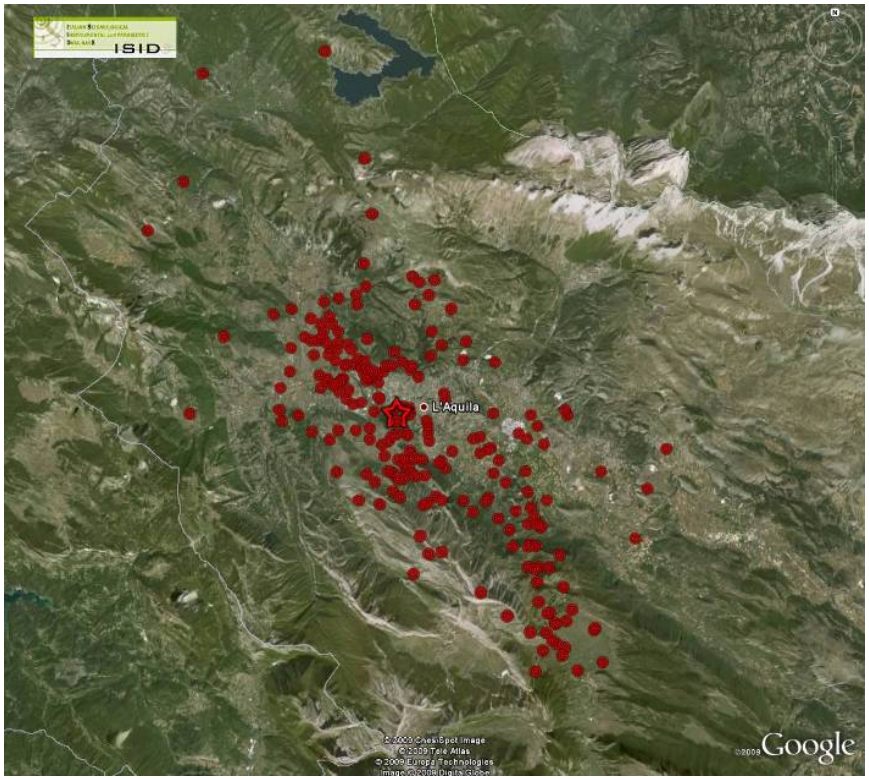
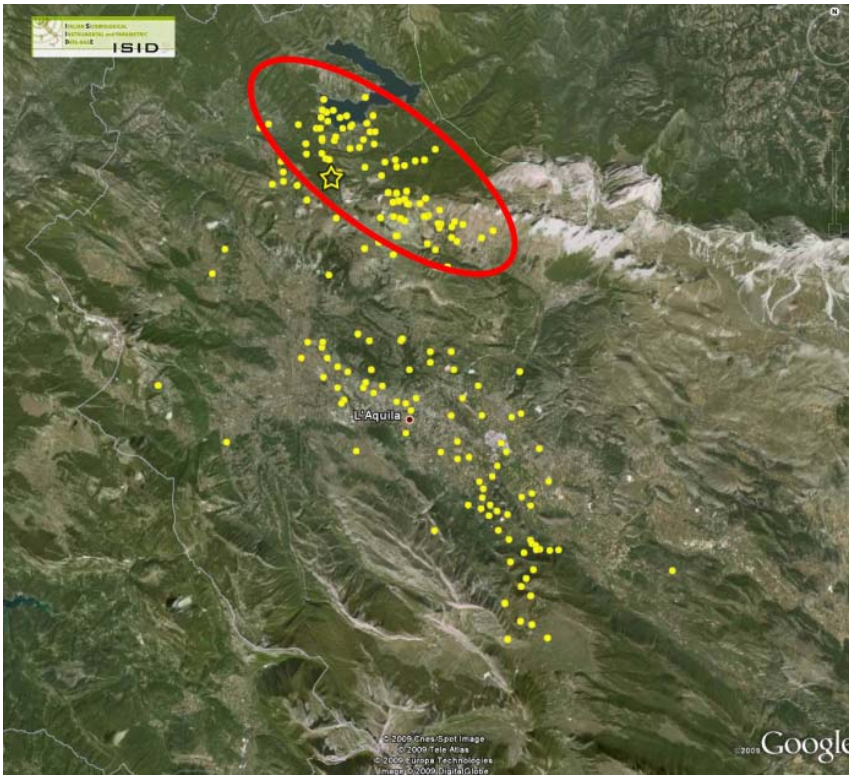


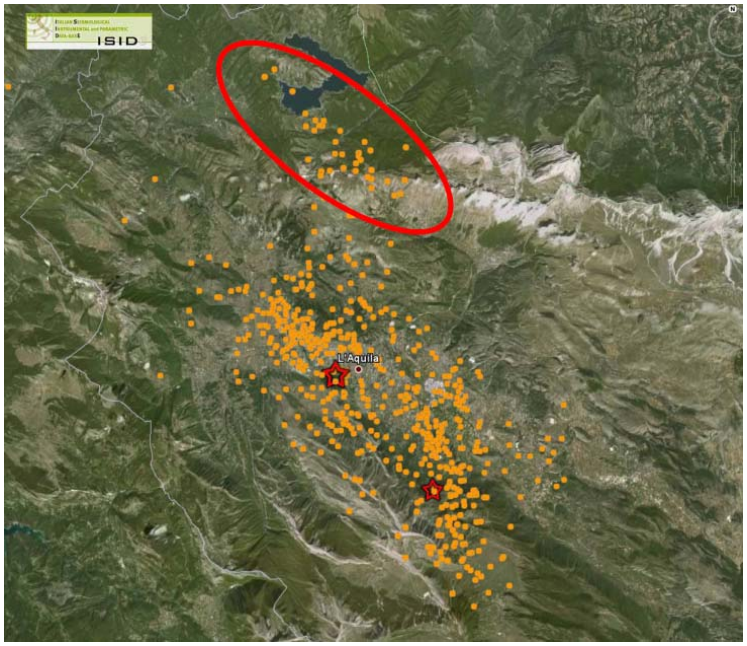

*Figure 13. Seismic sequence in the L'Aquila area using data from ISIDE (Italian Seismological Instrumental and Parametric Data-Base: http://iside.rm.ingv.it/iside/standard/index.jsp). The locations of the epicenters was updated on July 16, 2009 (www.ingv.it). An animation of the time sequence of aftershocks is available at http://dl.getdropbox.com/u/164400/ABRUZZO/index.html.(A) April 6, 2009: epicenters for main-shock and aftershocks on 6 April.*



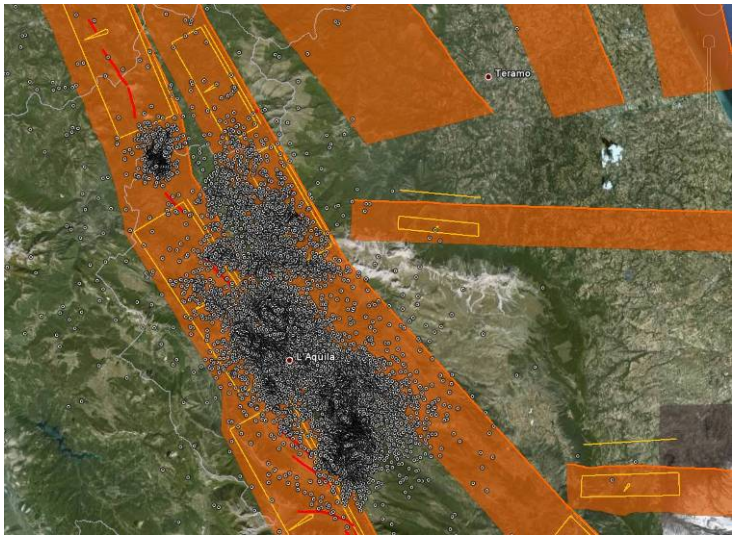

*(B) April 6-7, 2009: on April 7 new seismic events began to appear in the north of the area struck by the April 6 earthquake (towards Campo-tosto lake). A triggered event $M_w$=5.6 occurs SE of L'Aquila (red star).*




*(C) April 6-8, 2009: on April 8 seismicity near Campo-tosto Lake increases, with events oriented NW/SE. The seismic sequence near L-Aquila continues.*




*(D) April 9, 2009: A second event is triggered near Campotosto Lake on April 9 at location marked with yellow star.*




*(E) January 1 – July 16, 2009: Yellow boxes and lines denote individual sources and orange zones are composite sources from DISS Working Group (2009).*

Section 4 in Figure 14 shows a concentration of hypocenters between 5 and 10 km depth. Note that the epicenters indicate lack of seismic activity at shallow depths (upper 2-3 km). The stars indicate the three principal events of the sequence. The one in the center is the main shock. Left of the main shock is the hypocenter of the April 9 triggered event that occurred north of L'Aquila; on the right is the April 7 triggered event along the Aterno Valley (Southeast of L'Aquila), located at about 15 km depth in a crustal area with a cluster of minor events. The other sections show hypocenters of events occurring after the main shock, located at various depths progressing towards the surface and distributed primarily along inclined planes that have surface expressions in the traces of the active faults shown in Figure 15 (Bagnaia et al., 1992; Boncio et al. 2004; Galadini and Galli, 2000; Galadini and Messina, 2001). Section 2 shows an apparent dip of the ruptured fault, as evidenced from the hypocenter pattern, that is somewhat shallower than that of the surface-expressed faults. The other sections do not illustrate a clear dip angle. In Figure 15, the purple triangles indicate waypoints where EMERGEO geologists observed coseismic phenomena, particularly ground fractures and/or remobilization of the recent talus laid on the fault planes.

The earthquake of April 6 was anticipated by a seismic sequence (Figure 16) with hypocenters at depths of 8-12 km, apparently without causing movement on specific fault planes but rather concentrating inside a low angle crustal ramp. The April 6 main shock (at a depth of 9.46 km) was located in the middle of this area of crustal rupture.

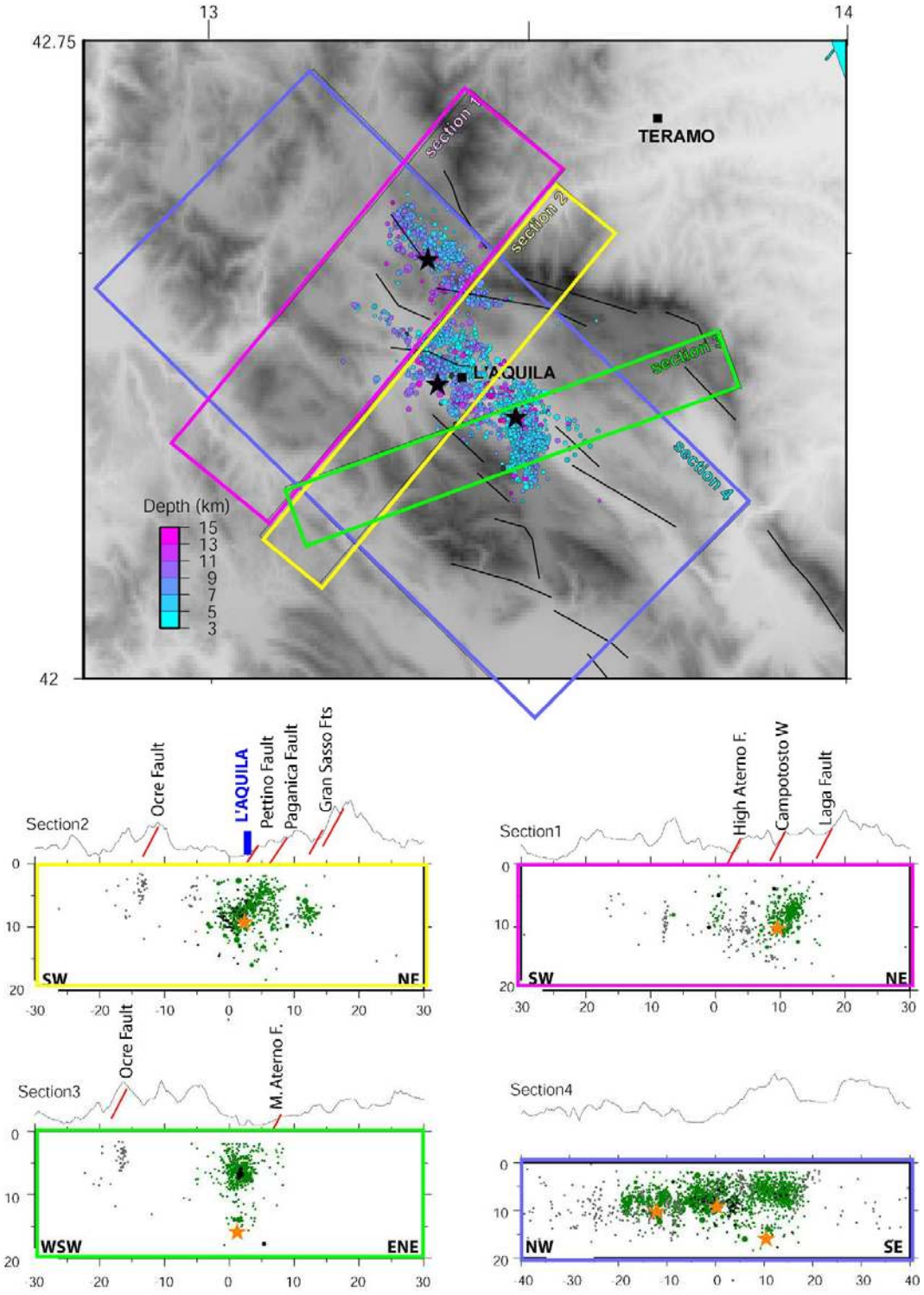



*Figure 14. Seismic sequence in the L'Aquila area. Epicenter locations (at top) and sections showing hypocenter locations (Chiarabba and De Gori, in Cocco, 2009).*

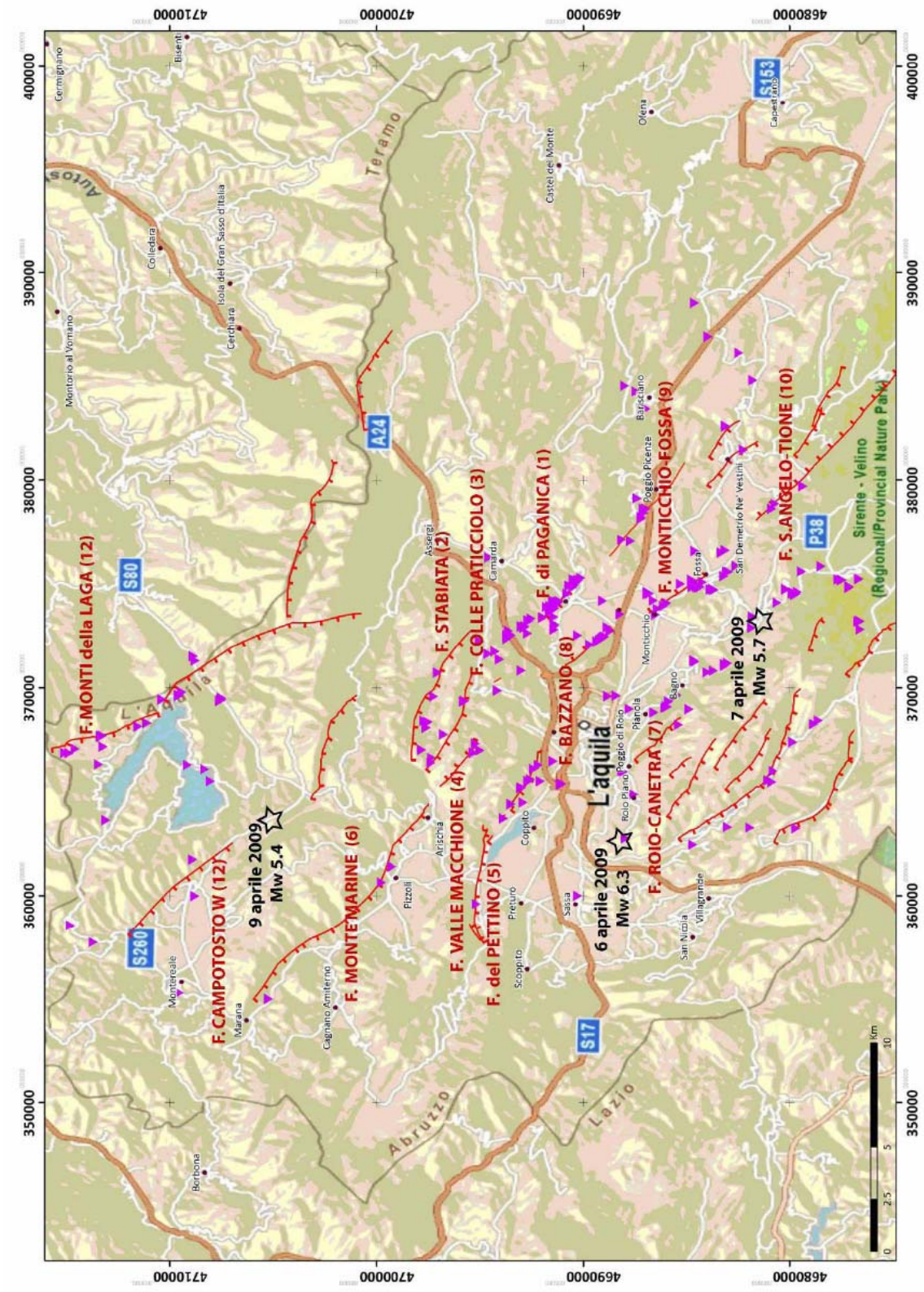



*Figure 15. Active faults of the L'Aquila area and locations of the three principal events of the active seismic sequence (EMERGEO Working Group, 2009). Mainshock epicenter coordinates not updated per Table 1.*

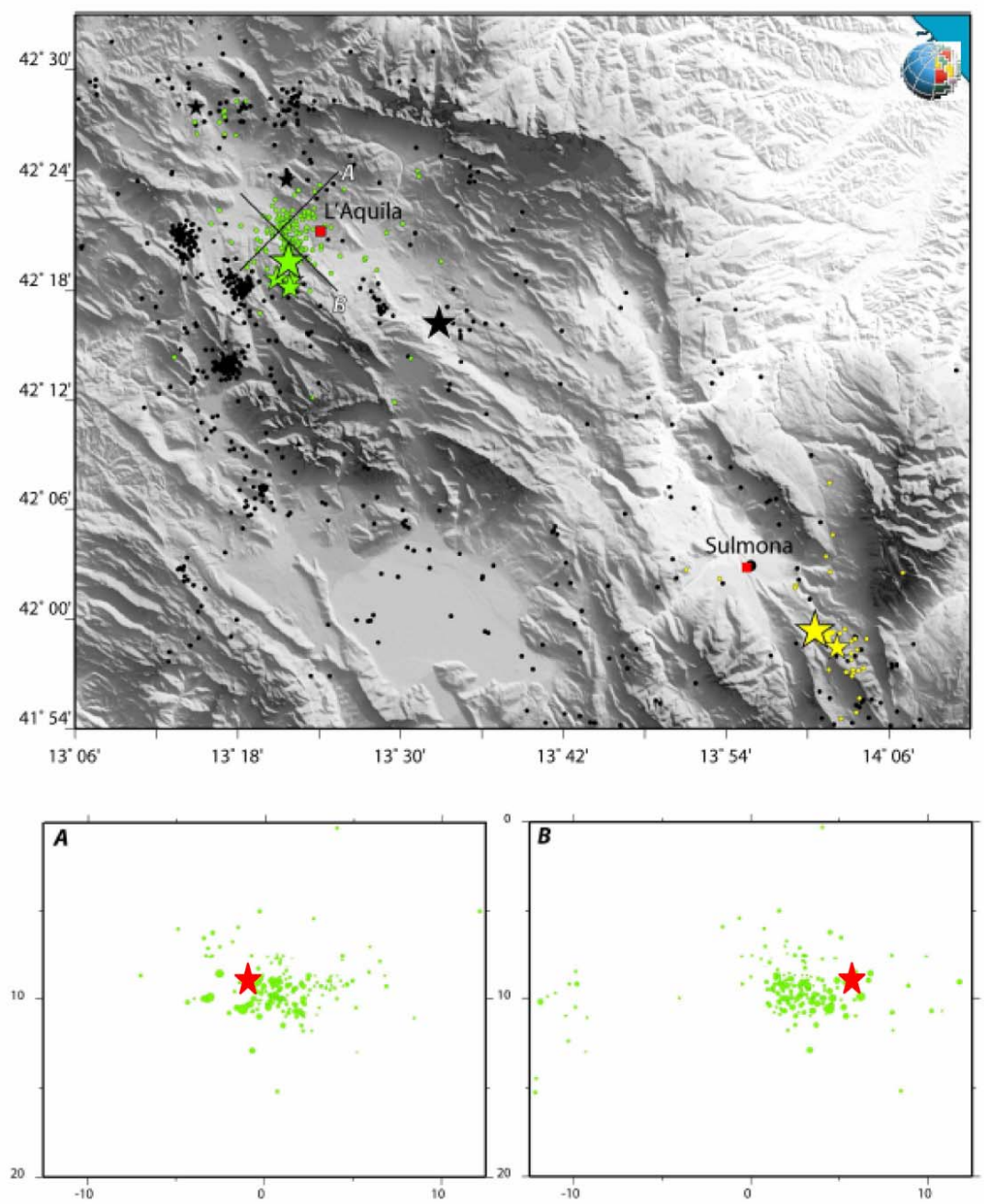



*Figure 16. Sequence of foreshock hypocenters illustrating their position relative to the mainshock (red star) Modified image from INGV web site [http://portale.ingv.it/primo-piano/archivio-primo-piano/notizie-2009/terremoto-6-aprile/cgr_31_3_2009.pdf](http://portale.ingv.it/primo-piano/archivio-primo-piano/notizie-2009/terremoto-6-aprile/cgr_31_3_2009.pdf).*

Recent and Historical Seismicity and Macroseismic Observations

The earthquake occurred in a central Apennine area that had low seismic activity from 1980-2008 and lies between two areas with higher levels of activity. Those areas are the Umbria-Marche area to the Northwest (struck by the 1997 seismic sequence) and the Lazio-Molise area to the Southeast. Figure 17 shows a plan view and transverse cross-section of a portion of the chain passing through L'Aquila, with the locations of the hypocenters of earthquakes during the time period in question. The red points indicate the hypocenters of the events of the active seismic sequence, and the stars mark the three principal events of April 6, 7 and 9, 2009 (Chiarabba and De Gori, in Cocco, 2009). The active sequence is therefore occurring in an area whose seismic characteristics affirm that seismic events are probable, even if they are not predictable.

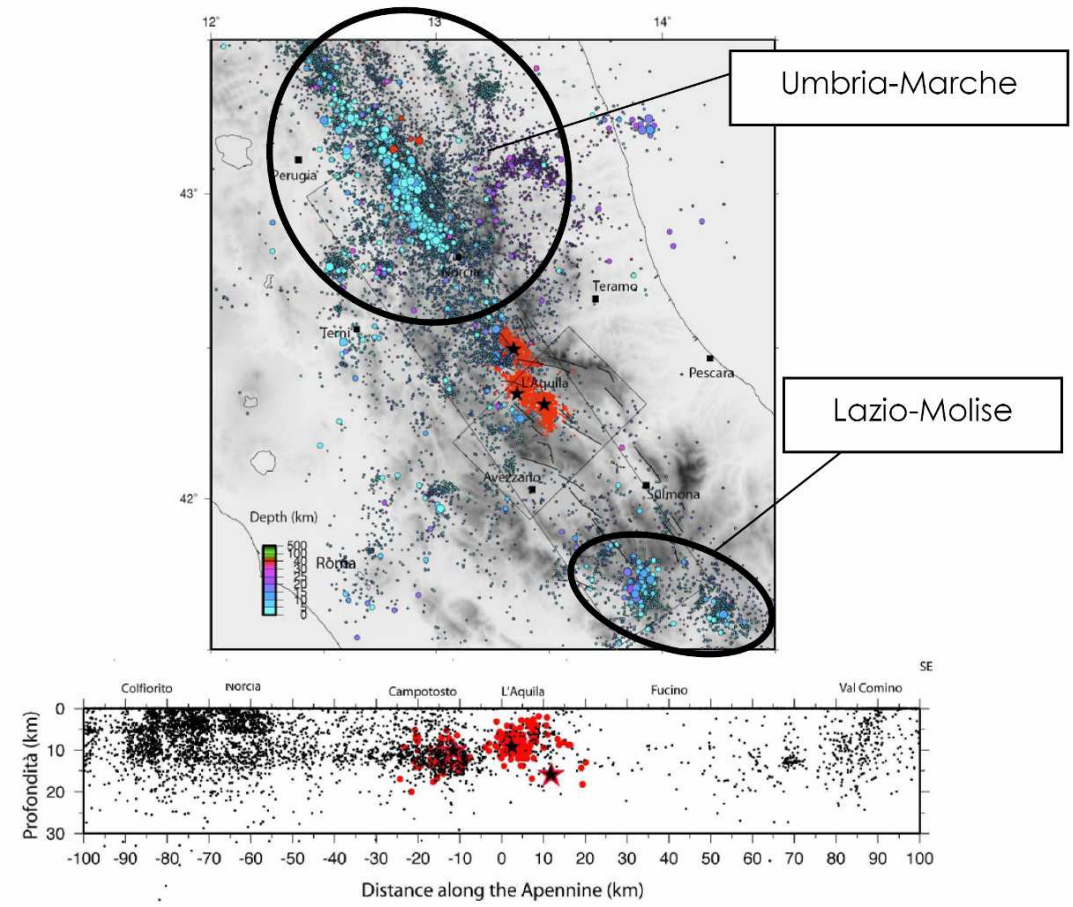



*Figure 17. Seismicity in the central Apennines in the period 1980-2008 and location of the events of the active seismic sequence. The cross-section was drawn through the NW-SE running rectangle shown in the plan (Modified from Chiarabba and De Gori, in Cocco, 2009).*

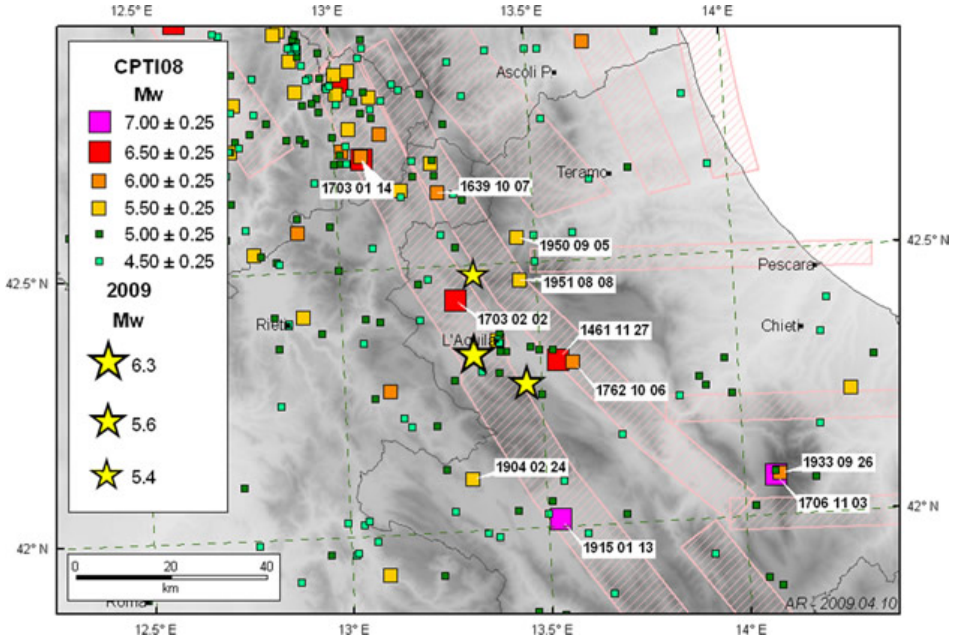



*Figure 18. Historic seismicity of the central Apennines near L'Aquila (Rovida et al., 2009).*

The high seismic risk of the L'Aquila area has been known for some time, thanks to historical seismic studies that have put in evidence numerous important earthquakes (Figure 18) that affected the central Apennines. These events are included in the parametric catalog of Italian earthquakes Catalogo Parametrico dei Terremoti Italiani, version 4 (Gruppo di Lavoro CPTI, 2004), and for each one of them there is a record of the assumed location based on macroseismic observations and an estimate of $M_w$ based on the dimensions of the area of maximum intensity. The most significant earthquakes in this area are those of 1315 ($M_w$>6.7), 1349 ($M_w$>6.5), 1461 ($M_w$>6.5), 1703 ($M_w$>6.7), and 1915 ($M_w$>7.0).

One of the principal events to hit the city of L'Aquila was the earthquake of 1461, which produced macroseismic effects in the same area of maximum intensity as this earthquake. The area of maximum intensity was located between the city of L'Aquila and the inhabited center of Paganica, passing through Onna (Figure 19, macroseismic intensity distribution from http://emidius.mi.ingv.it/DBMI04/; Stucchi et al., 2007). This event has geographic and parametric characteristics similar to those of the earthquake of April 6, 2009, since it has a maximum intensity equal to IX-X MCS and an estimated $M_w$ of 6.5, close to the $M_w$=6.3 of the April 6 event.

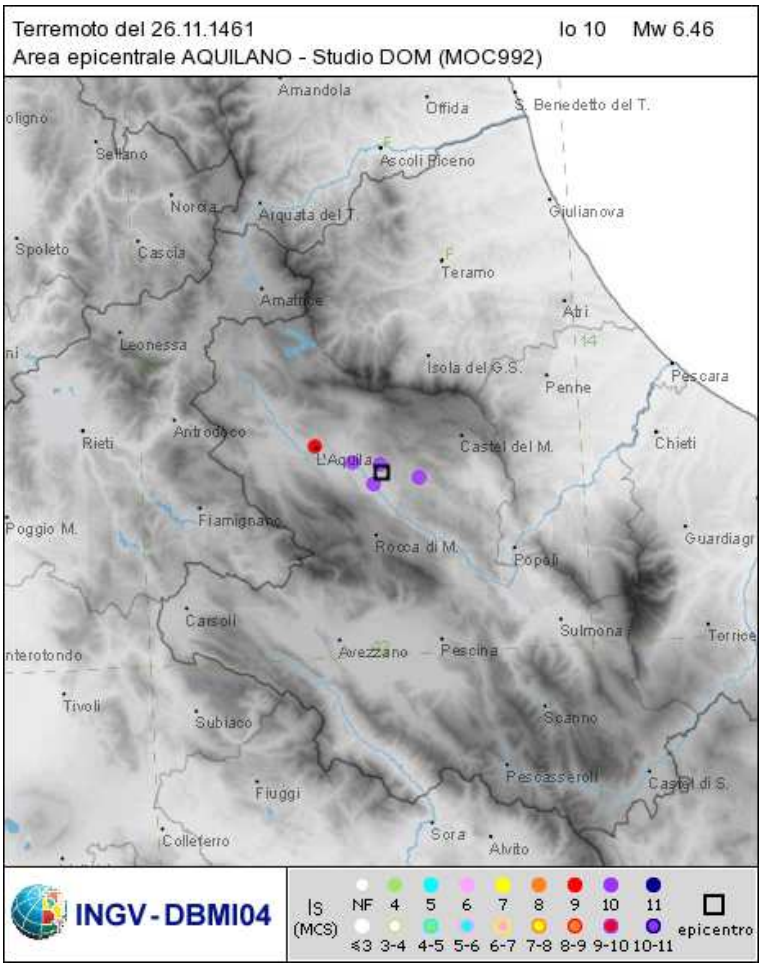
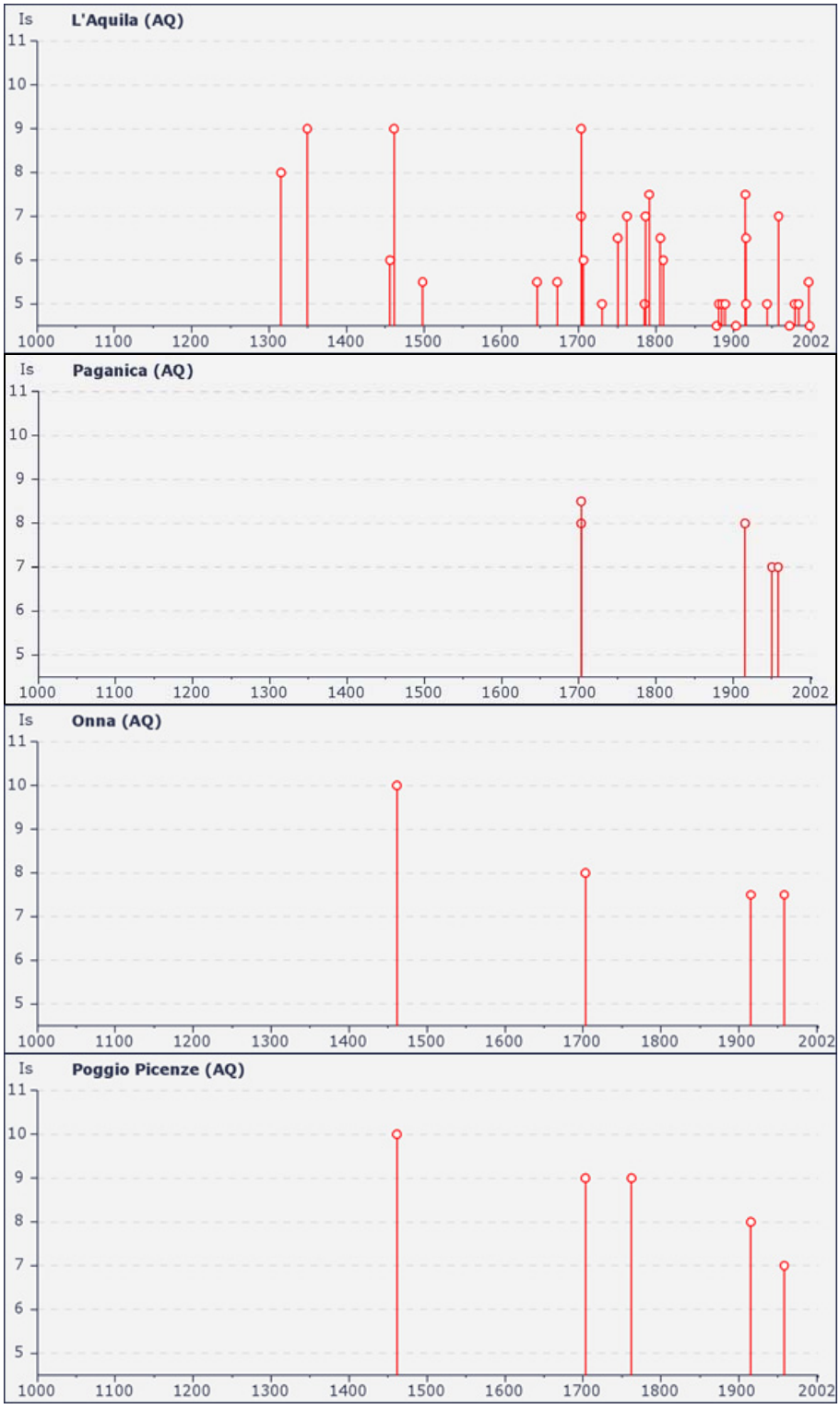



*Figure 19. Macroseismic intensity distribution determined for 1461 earthquake (Stucchi et al., 2007).*

The information contained in the historical documents make it possible to compile a seismic history for each Italian region, in the form of a graph with years on the abscissa and macroseismic intensity (MCS) on the ordinate. Figure 20 shows macroseismic histories of several locations affected by the April 6 earthquake. The various macroseismic histories indicate particularly strong intensities during the earthquake of 1461 especially in Onna and Castelnuovo, which were also significantly damaged by the 2009 sequence. Using these graphs one can compare intensities experienced at various inhabited village centers for the same earthquake. It is notable, for example, that there is a paucity of historical information for the inhabited center of San Pio delle Camere, located near the relatively well-documented inhabited center of Castelnuovo, because the two sites experienced very different damage patterns during the recent earthquake. In fact,

although the two towns are characterized by very similar construction types with “poor” stonework and masonry buildings, San Pio delle Camere (Intensity MCS=V-VI) consistently has much less damage than Castelnuovo (Intensity MCS=IX-X). These different damage levels likely result from variations in local seismic response, primarily due to the lithostratigraphic characteristics of the subsoil in the two areas (details presented in the subsequent section on Damage Patterns).



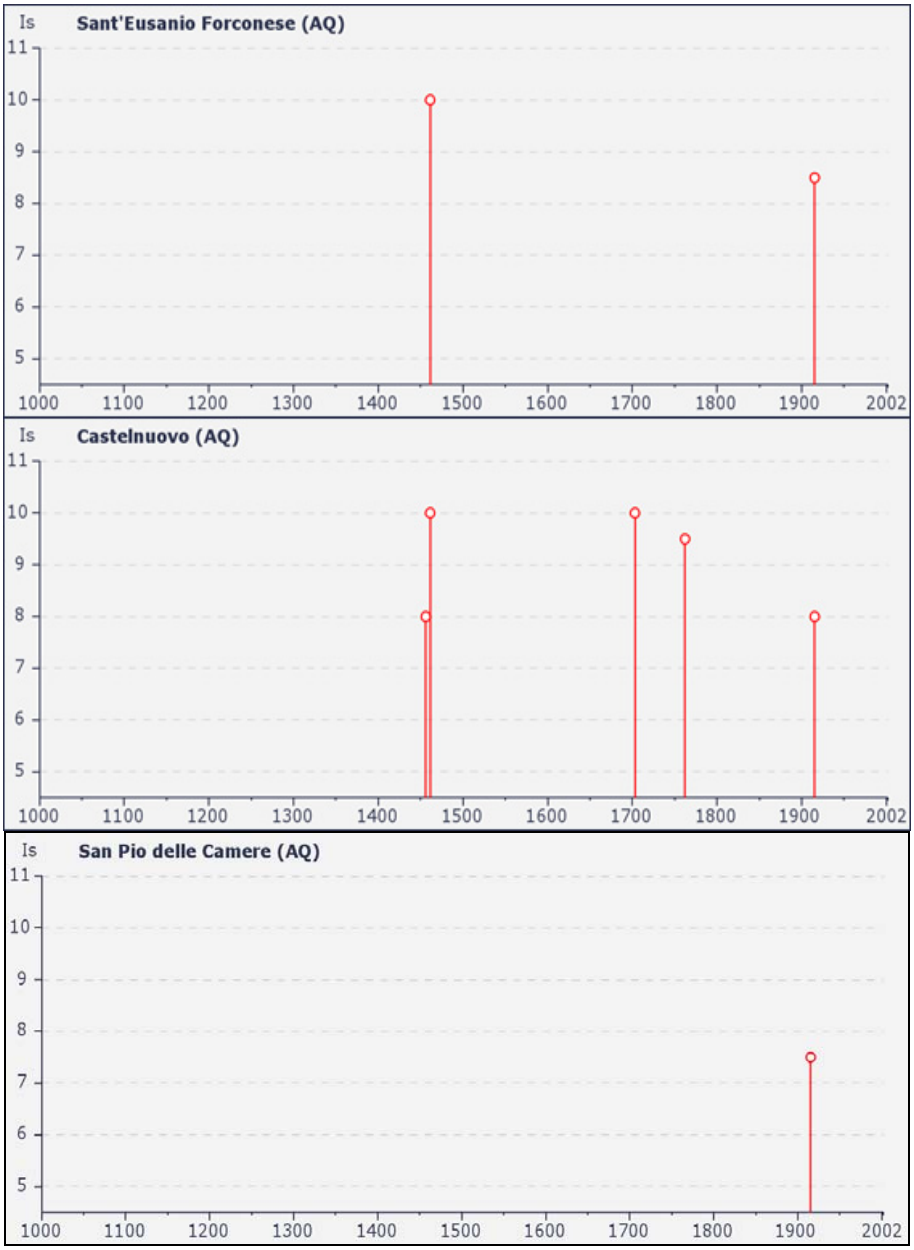



*Figure 20. Seismic history of several inhabited centers that were affected by the earthquake of April 6, 2009 (http://emidius.mi.ingv.it/DBMI04/; Stucchi et. al., 2007).*

In the days following the main shock of the current seismic sequence, the Quick Earthquake Survey Team, comprised of researchers from various agencies and institutions supported by the activities of the Department of Civil Protection, compiled a macroseismic survey of the effects of this earthquake on the built-up/inhabited areas in more than 180 localities of the L'Aquila, Pescara, Teramo and Rieti provinces. The results of the survey are presented in Figure 21 (Galli and Camassi, 2009: http://portale.ingv.it/real-time-monitoring/quest/macrodef_sito.pdf).

The map shows an asymmetric distribution of damage with respect to the earthquake's epicenter. Damage is limited north and west of the epicenter (black star), with macroseismic intensities no higher than VI MCS. Conversely in the area southeast of L'Aquila, the intensities reach IX-X MCS within an elongated area of high intensity and damage. Macroseismic intensities ≥ VI (MCS) attributed to some villages are reported in Table 2. Also the value V-VI (MCS) for San Pio delle Camere is indicated. Additional macroseismic data, not reported in Table 2, is still being withheld because it is in the process of being made official.

*Table 2. Selected sites affected by the earthquake and surveyed macroseismic intensities (Galli and Camassi, 2009).*

| Locality | Municipality | Province | Lat. (N) | Lon. (E) | I (MCS) |
|---|---|---|---|---|---|
| Castelnuovo | San Pio delle Camere | AQ | 42.295 | 13.628 | IX-X |
| Onna | L'Aquila | AQ | 42.327 | 13.480 | IX-X |
| San Gregorio | L'Aquila | AQ | 42.327 | 13.496 | IX |
| Sant'Eusanio Forconese | Sant'Eusanio Forconese | AQ | 42.288 | 13.525 | IX |
| Tempera | L'Aquila | AQ | 42.366 | 13.458 | IX |
| Villa Sant'Angelo | Villa Sant'Angelo | AQ | 42.269 | 13.538 | IX |
| L'Aquila (city centre) | L'Aquila | AQ | 42.356 | 13.396 | VIII-IX |
| Poggio Picenze | Poggio Picenze | AQ | 42.320 | 13.541 | VIII-IX |
| Bazzano | L'Aquila | AQ | 42.337 | 13.455 | VIII |
| Casentino | Sant'Eusanio Forconese | AQ | 42.278 | 13.510 | VIII |
| Paganica | L'Aquila | AQ | 42.358 | 13.473 | VIII |
| Roio Piano | L'Aquila | AQ | 42.327 | 13.357 | VIII |
| Tussillo | Villa Sant'Angelo | AQ | 42.267 | 13.531 | VIII |
| Fossa | Fossa | AQ | 42.296 | 13.487 | VII-VIII |
| Castelvecchio Subequo | Castelvecchio Subequo | AQ | 42.130 | 13.731 | VII |
| Goriano Sicoli | Goriano Sicoli | AQ | 42.080 | 13.775 | VII |
| Pettino | L'Aquila | AQ | 42.375 | 13.355 | VII |
| Pianola | L'Aquila | AQ | 42.322 | 13.404 | VII |
| Carapelle Calvisio | Carapelle Calvisio | AQ | 42.298 | 13.684 | VI-VII |
| Coppito | L'Aquila | AQ | 42.366 | 13.344 | VI-VII |
| Prata d'Ansidonia | Prata d'Ansidonia | AQ | 42.277 | 13.609 | VI-VII |
| San Demetrio ne' Vestini | San Demetrio ne' Vestini | AQ | 42.288 | 13.558 | VI-VII |
| Santo Stefano di Sessanio | Santo Stefano di Sessanio | AQ | 42.343 | 13.645 | VI-VII |
| Stiffe | San Demetrio ne' Vestini | AQ | 42.256 | 13.545 | VI-VII |
| Assergi | L'Aquila | AQ | 42.414 | 13.505 | VI |
| Barete | Barete | AQ | 42.450 | 13.283 | VI |
| Barisciano | Barisciano | AQ | 42.325 | 13.592 | VI |
| Bominaco | Caporciano | AQ | 42.244 | 13.658 | VI |
| Bussi sul Tirino | Bussi sul Tirino | PE | 42.210 | 13.826 | VI |
| Campotosto | Campotosto | AQ | 42.558 | 13.369 | VI |
| Capestrano | Capestrano | AQ | 42.266 | 13.769 | VI |
| Caporciano | Caporciano | AQ | 42.250 | 13.674 | VI |
| Castel del Monte | Castel del Monte | AQ | 42.325 | 13.727 | VI |
| Castelvecchio Calvisio | Castelvecchio Calvisio | AQ | 42.310 | 13.688 | VI |
| Fontecchio | Fontecchio | AQ | 42.229 | 13.605 | VI |
| Monticchio | L'Aquila | AQ | 42.320 | 13.466 | VI |
| Navelli | Navelli | AQ | 42.236 | 13.730 | VI |
| Ocre (San Panfilo d'Ocre) | Ocre | AQ | 42.285 | 13.475 | VI |
| Pizzoli | Pizzoli | AQ | 42.435 | 13.303 | VI |
| Popoli | Popoli | PE | 42.171 | 13.833 | VI |
| Preturo | L'Aquila | AQ | 42.377 | 13.295 | VI |
| Rocca di Cambio | Rocca di Cambio | AQ | 42.235 | 13.490 | VI |
| Rocca di Mezzo | Rocca di Mezzo | AQ | 42.205 | 13.521 | VI |
| Scoppito | Scoppito | AQ | 42.372 | 13.256 | VI |
| San Pio delle Camere | San Pio delle Camere | AQ | 42.286 | 13.656 | V-VI |

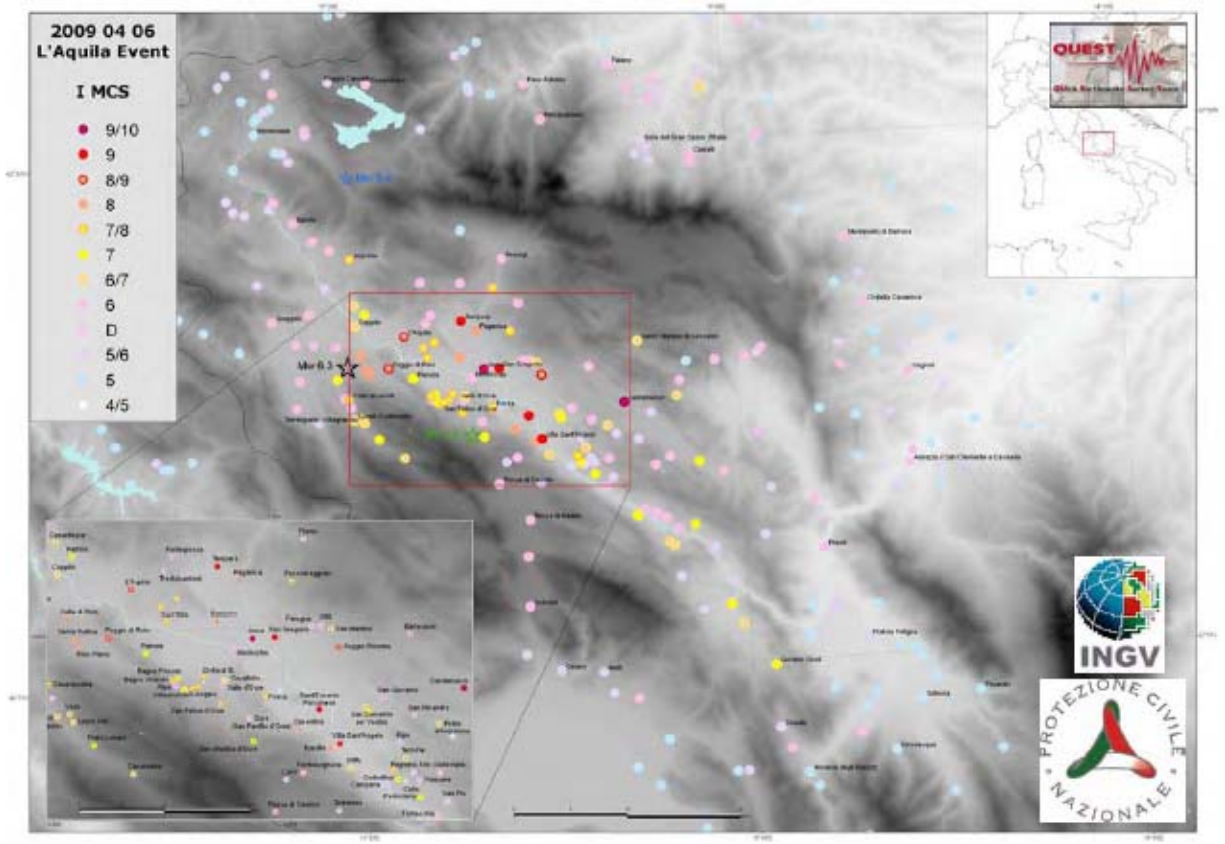



*Figure 21. Result of the QUEST macroseismic survey (http://www.mi.ingv.it/eq/090406/quest.html) for the April 6, 2009 earthquake. The black rectangle indicates the macroseismic box, or the expression of the source fault for this earthquake, based on the distribution of macroseismic intensities.*

**Ground Surface Displacements**

The initial surface deformations associated with the April 6, 2009 L'Aquila Earthquake ($M_w$=6.3) have been evaluated utilizing geodetic methods including Interferometric Synthetic Aperture Radar (InSAR) and Global Positioning System (GPS) measurements. This data provides information about the surface response, activated faults and kinematics. Field surveys were conducted to locate surface fault rupture associated with this event in areas identified by the initial InSAR data. The field observations combined with the processed geodetic data have been used to make a preliminary assessment of the probable source fault for this earthquake. Each data set is discussed individually and the data is then combined to develop a preliminary assessment of the source fault for the April 6, 2009 main shock.

GPS Data

The INGV maintains a GPS network for monitoring crustal deformation associated with both tectonic strain and deformations associated with the numerous active volcanoes within Italy. This network is maintained within the "Rete Integrata Nazionale GPS (RING)" program operated by INGV and integrated with the Central Appennines GPS network resulting in over 100 permanent and non-permanent GPS stations distributed throughout the region (http://ring.gm.ingv.it/). Information related to the sites and instrument clusters and processing methods are available at the referenced web site. Of the stations maintained within RING, 74 are currently located in central Italy and help define the annual deformation rates relative to a stable Eurasian plate (http://ring.gm.ingv.it/velocityfield.php). Figure 22 shows the pre-earthquake GPS velocity field in the region surrounding L'Aquila based on data acquired between 2000 and 2008 (D'Agostino, 2009). This figure shows that the highest interseismic displacement rates are located in the central Apennines and reach magnitudes between 4 mm to 5 mm per year and generally directed in a North, North-East direction. To the Southwest of the April 6, 2009 epicenter, the displacement rates decrease to approximately 1 mm indicating extension strains across the Apennines. A counter-clockwise rotation is observed for the eastern side of the Apennines while a clockwise rotation is observed to the

western side of the Apennines with respect to a rotation pole located in Pianura Padana (http://ring.gm.ingv.it/velocityfield.php). These deformations indicate that in addition to extension, relative lateral deformations must also be accommodated across the Apennine fault systems giving rise to oblique slip on many of the structures in this region. This deformation characteristic was discussed by Galadini and Galli (2000) based on mapped fault patterns in the upper Aterno valley fault system. This is the fault system that was actived by the April 6, 2009 earthquake.

The GPS data was processed in the days following the earthquake to determine the co-seismic displacement field associated with this event. The displacements in the epicentral region between April 5 and April 9 are shown in Figure 23 (D'Agostino, 2009). Additional information is available in Anzidei et al. (2009). The post-earthquake GPS measurements taken on April 6, 7 and 8, 2009, when compared with the data gathered on April 5 and, for a few stations, with measurements taken the previous year, demonstrate "instantaneous" earth surface deformations associated with this earthquake (Figure 23, vectors in yellow). The horizontal movements indicate an area in extension with rotation of displacement vectors within the area of maximum deformation, due to the rebound effect in the NW-SE direction of the area subjected to a SW-NE traction. The vertical movements tend to increase as they move from the city of L'Aquila towards the southeast. The preliminary best fit of the inversion of these data was obtained using movements along a fault plane running NW-SE with normal displacement in a SW direction, which generates an earthquake of $M_w$=6.3 with maximum co-seismic slip of 1.1 m. The location of the fault plain is constrained near Paganica, where co-seismic fractures of the ground were mapped (EMERGEO Working Group, 2009).

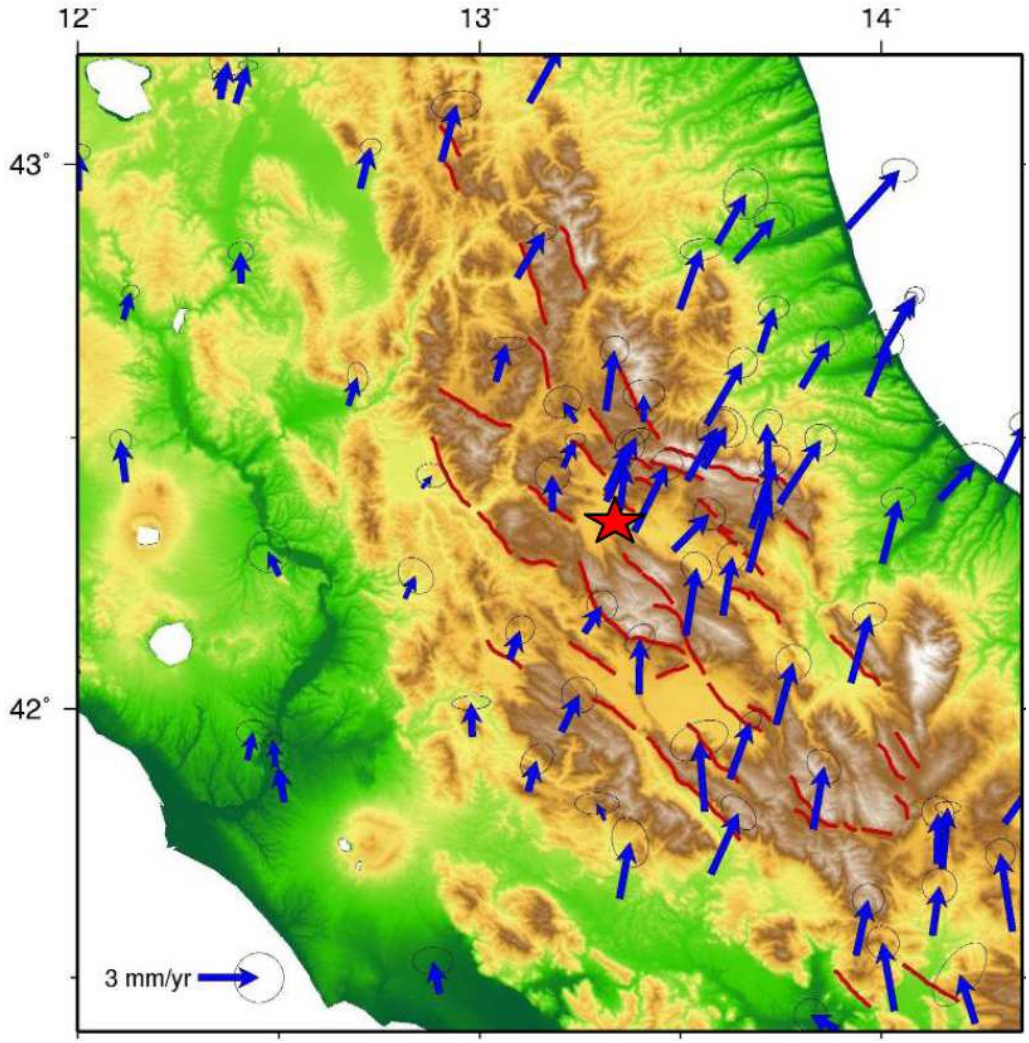



*Figure 22. Annual deformation rates in central Italy determined from GPS data acquired from the RING GPS Network (Modified from D'Agostino, 2009).*

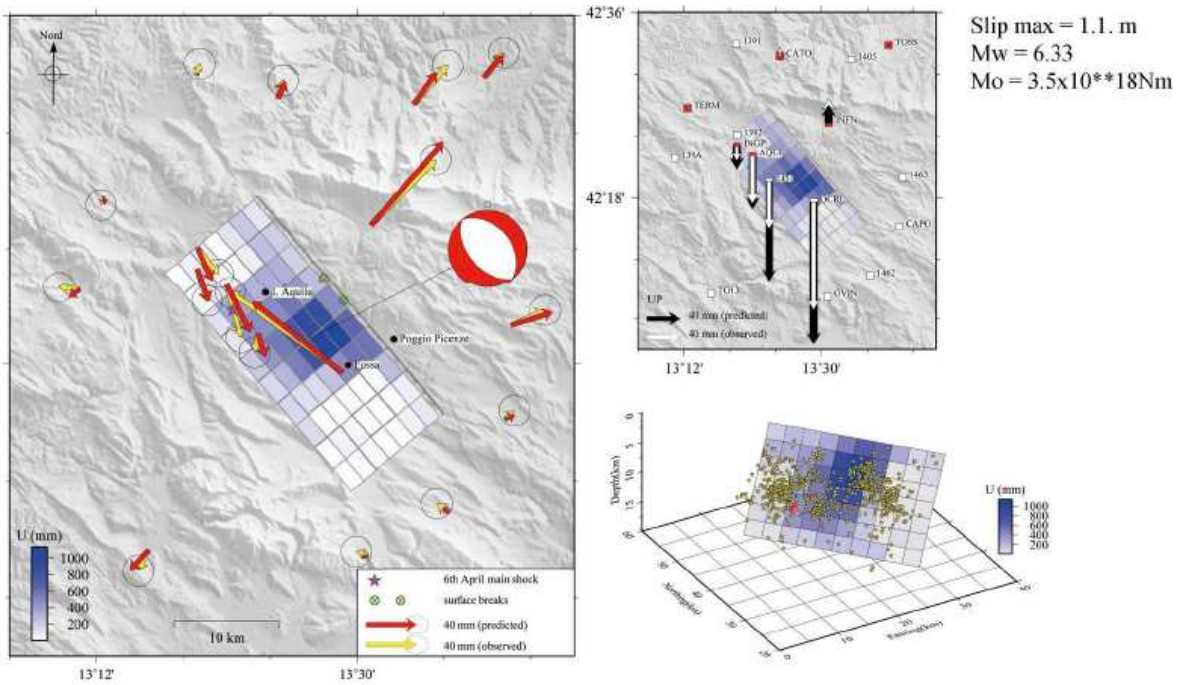



*Figure 23. GPS data inversion: on the left horizontal predicted (red) and observed (yellow) displacements, on the right vertical movements and proposed fault plane solution (Modified from D'Agostino, 2009).*

InSAR Data

Synthetic aperture radar images were acquired by two different satellite systems in the days following the April 6 main shock. The post-seismic acquisitions were combined with compatible images taken previously during routine operations to develop interferometric images.

The first satellite system to acquire a post seismic image was from the COSMO-SkyMED constellation. This constellation is currently composed of three satellites developed and maintained by the Italian Space Agency (Agenzia Spaziale Italiana) in cooperation with the Italian Ministry of Defense. One of the primary goals of COSMO-SkyMED is to provide data for scientific purposes for the prevention and management of environmental disaster and associated relief efforts (earthquakes, volcanoes, floods, etc.). The satellite constellation allows SAR images to be acquired at a specific location with a minimum time difference of 1 day, more typical short term acquisition is 2-3 days between images. This data can be used to assess the temporal surface strains related to this earthquake. More detailed information related to the Sky-Med constellation and the satellite components can be found at http://www.cosmo-skymed.it/en/index.htm.

The second satellite to acquire SAR images after the earthquake was the ENVISAT - Earth Observation Satellite operated by the European Space Agency (ESA). This satellite utilizes an Advanced Synthetic Aperture Radar (ASAR) system to increase the options available for image acquisition based on the needs of different scientific communities. More detailed information about the ENVISAT Earth Observation Satellite can be found at ESA's web site (http://www.esa.int/esaEO/SEMWYN2VQUD_index_0_m.html).

The interferometric analysis is insightful regarding the co-seismic effects of this earthquake. Our primary discussion is based on the work of Salvi et al. (2009), who present the data and detailed analyses. The first interferometric analysis available to the scientific community was developed from the COSMO-SkyMed constellation using images from the February 19 and April 9. This image was processed by INGV researchers and the ISA and was utilized for assisting in the initial field reconnaissance. Figure 24 shows the first interferogram, the epicenter for the $M_w$= 6.3 main shock (large square) and events with a $M_w \geq$ 5.0 (small squares) and the location of ground failures (yellow line). This image shows that the initial surface deformations were concentrated to the north of the main event epicenter and along a line running from L'Aquila past Poggio Picenze. The surface deformation (fringes) are well constrained within different lineaments developed in the surrounding region. Some of these lineaments correspond to identified faults while others do not. Changes in the primary orientation of the fringes can also be observed to change across different lineaments.

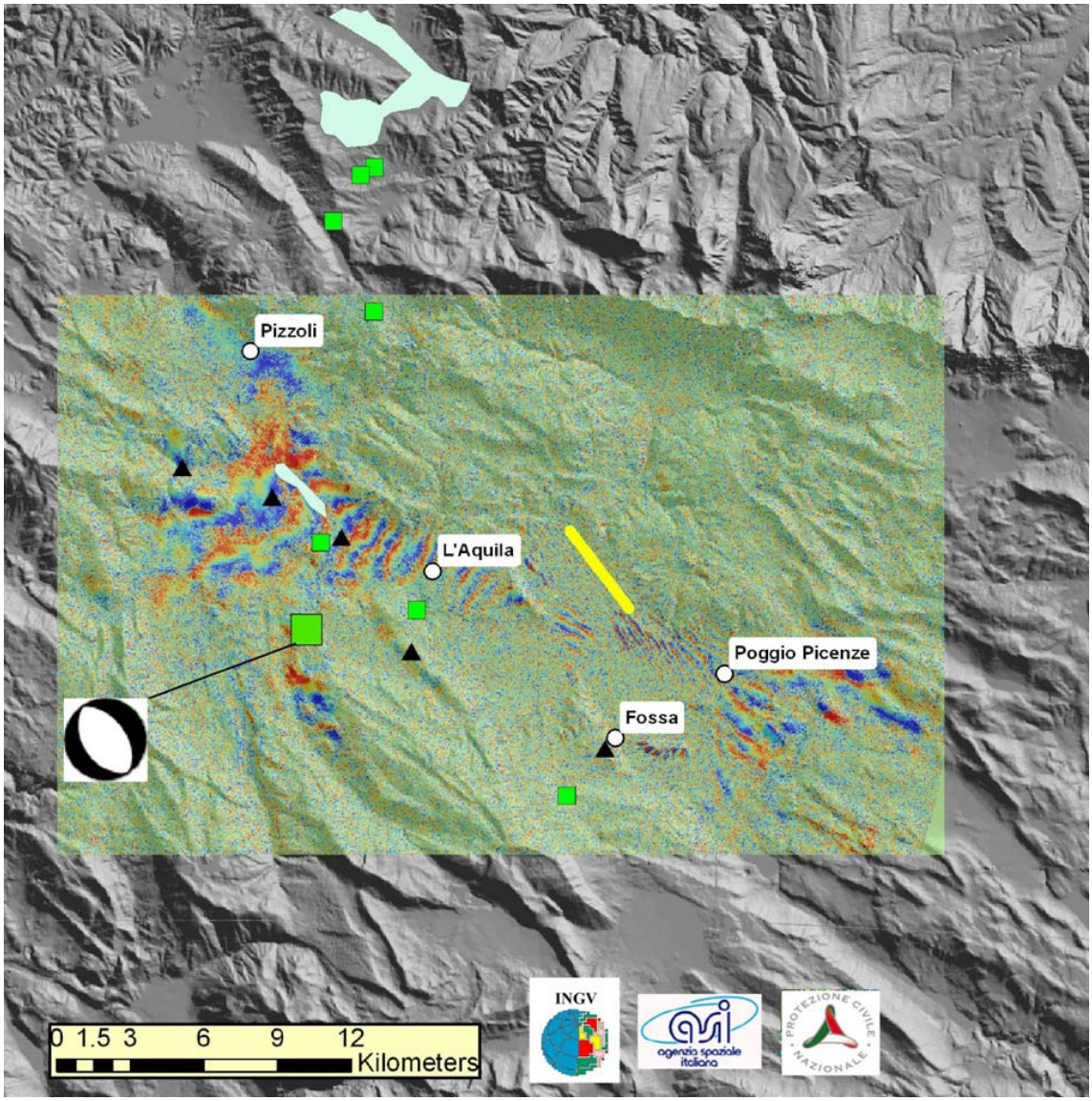



*Figure 24. Interferogram developed from Cosmo-SkyMed images taken on 19 February and 9 April. The $M_w$= 6.3 main event is identified by the large square and focal mechanism. The $M_w \geq$ 5.0 events are marked by the small squares. The yellow line indicates the area of observed ground failures (EMERGEO Working Group, 2009).*

Figure 25 presents one of these analyses showing the interferometric fringes that were created using images downloaded from ENVISAT and COSMO-SkyMed, the earth observation satellite system developed by the Italian space agency Agenzia Spaziale Italiana in cooperation with the Italian Ministry of Defense. Images of the area affected by the earthquake, which were gathered beginning on April 6 by COSMO-SkyMED, were analyzed with the interferometric technique DInSAR (Differential Interferometry Synthetic Aperture Radar). This technique involves taking images from the same geographic area, using the same view angles at different times, for measuring with specific algorithms, the deformations produced on the ground surfaces (http://www.asi.it/it/news/la_faglia_del_terremoto_individuata_grazie_ai_dati_di_cosmoskymed). In Figure 25 each concentric fringe quantifies 1.5 cm of co-seismic vertical deformation. In the same figure, Salvi et al. (2009) also show the trace of the alignment of ground fractures that were observed near the inhabited center of Paganica (EMERGEO Working Group, 2009). The following observations can be made:

1. The maximum negative vertical deformation is about 25 cm (lowering of the topographic surface corresponding to the area of the fault's hanging wall); the maximum positive vertical deformation is about 8 cm (uplift of the topographic surface corresponding to the area of the fault's footwall);

2. The area of maximum negative vertical deformation does not coincide with the outcrop area of the Paganica fault (see black line segment in Figure 25), which several researchers have hypothesized as having generated this earthquake. Rather, the zone of maximum deformation is located about 3-4 km southwest of this tectonic element, a hypothesis supported by the band of fractures observed on the ground (EMERGEO Working Group, 2009). The maximum vertical displacements of the observed fractures are on the order of 10-12 cm;

3. The area of maximum negative vertical deformation coincides with a level zone situated to the Southeast of L'Aquila and Southwest of Bazzano; this zone is next to the plain on which the village of Onna is situated. The plain interrupts the east relief alignment, where the Bazzano Fault is located. The Bazzano fault is reported to have showed superficial evidence of co-seismic reactivation (EMERGEO Working Group, 2009);

4. The interferometric fringes do not abruptly close on the plain of the Paganica Fault, but display two trends at different gradients, one to the northeast and the other to the southwest of the area of maximum vertical deformation. The first group of fringes presents a higher gradient than the second.

5. The interferometric fringes show variations in trend at various points and along several lines associated with active tectonic elements (Pettino Fault, just to the Northwest of L'Aquila and Bazzano-Fossa Fault, between L'Aquila and Paganica) that also had a co-seismic displacement of modest extent. In particular, Figure 25 shows a discontinuity in the interferometric fringes (indicated by the red line) that would correspond to the antithetic Bazzano-Fossa Fault.

6. The preliminary inversion models of co-seismic movement (Figure 26) show that the Paganica Fault would have a limited slip on the surface. This is supported by field observations at several places along the alignment of co-seismic ground fractures, which noted maximum displacements no greater than 10-12 cm, compared to a maximum slip of about 1 m on the fault at depth.

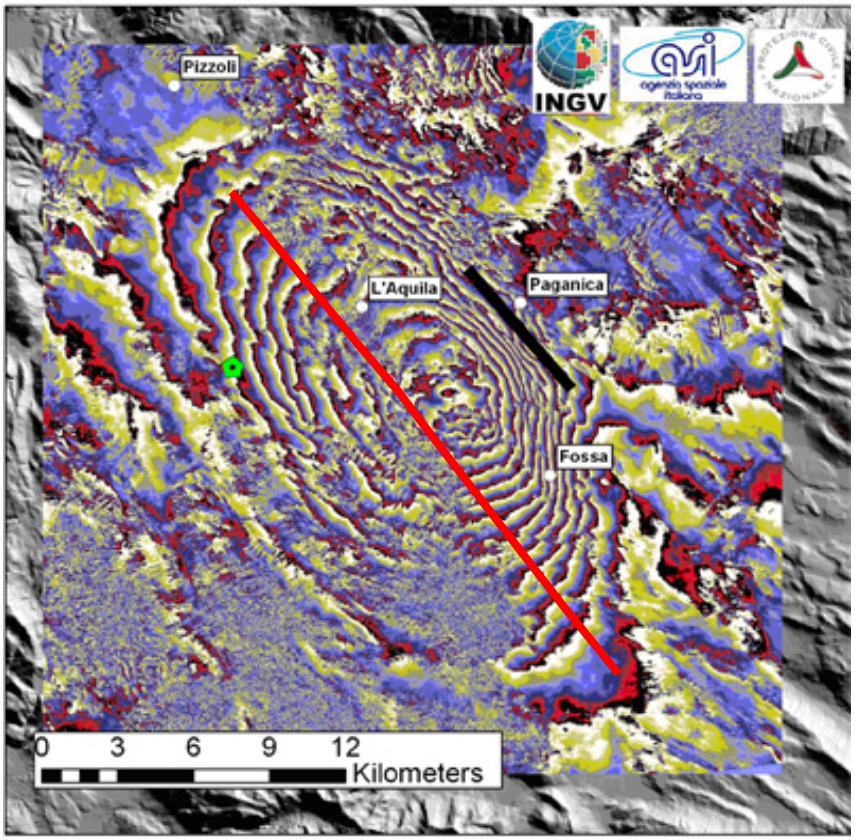



*Figure 25. Interferometric fringes of co-seismic displacements (modified from Salvi et al., 2009). The black line indicates the alignment of ground failures associated to the Paganica Fault. The discontinuity marked by the red line corresponds to the antithetic Bazzano-Fossa Fault.*

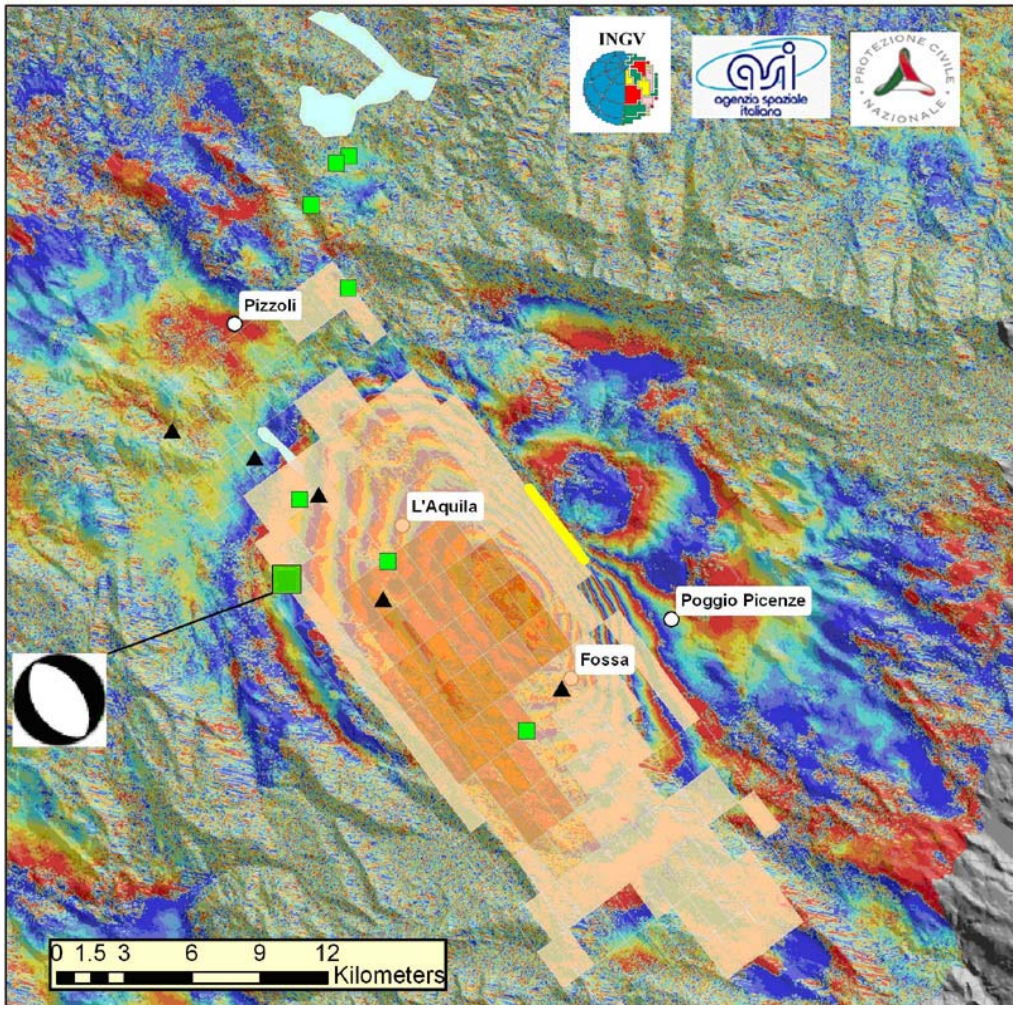



*Figure 26. Fault plane solution by InSAR data inversion (Salvi et al., 2009). The yellow line indicates the alignment of ground failures associated to the Paganica Fault. The maximum slip modeling corresponds to the surface area with maximum vertical displacement. Near the surface, along the Paganica Fault, the vertical displacement is very small.*

Surface Rupture Observations

Several observations of ground cracking have been made in areas near where the fault might be expected to reach the surface. In the hours immediately following the earthquake, the researchers of the EMERGEO Working Group began their reconnaissance of possible co-seismic effects, in collaboration with colleagues from other agencies and institutions. The scope of their activity was to plan numerous investigations spread out over an area of about 900 km$^2$. After that survey came the release of several general observations, which are contained in a report (translated from EMERGEO Working Group, 2009):

*"A preliminary analysis of all the observed co-seismic effects definitely draws attention to the peculiarities of the ruptures observed along the Paganica Fault. In fact, these ruptures, despite being limited in terms of aperture and down-throw, demonstrate a continuity that has no equal in those examined along the other structures where the ruptures, scarps or remobilizations appear sporadically and in correspondence with favorable morphological conditions. Furthermore it was observed that ruptures along the Paganica Fault intersect whether in developed and paved areas or more or less open space, and this occurs independent of the local morphological situation, in some cases (often) forming an angle with the slope. The internal makeup of the structures and microstructures and the total length of approximately 5 km (…), along with other evidence just discussed, lead to ruling out a gravitative origin for these ruptures and to interpreting the set of ruptures along the Paganica Fault as the surface expression of the deeper fault that produced the event of April 6, 2009. It is interesting to note that the location of this set of ruptures is in complete accordance with the seismological, geodetic and*

*remote sensing observations gathered so far. Although limited to a stretch of several hundred meters, even the ruptures along the Bazzano (…) and Monticchio-Fossa (…) faults can represent the surface expression of an antithetic structure reactivated during the event."*

Many observations contained in the EMERGEO report are also confirmed by observations of the GEER Team, which surveyed ground ruptures in areas near the inhabited center of Paganica. In this zone the fracturing lines up for several kilometers and intesects the morphology with a sort of continuity. The area situated to the southwest of the alignment of fracturing sits lower with respect to the sector located northeast of the alignment, although to a very modest degree (a few cm). The ground fractures tend to have an average bearing of 140°.

Near the inhabited center of Paganica, rupture of a water supply line was observed, which some have interpreted as a co-seismic surface expression of the fault (Figure 27). Additional ground fissures were identified at the center of Paganica village as depicted in Figures 28-33. They are concentrated close to a two storey R/C structure built on a slope. Breakage of a water piping system (repaired at the time of GEER reconnaissance) was observed (Figure 28). Movements are generally in the direction of gravity.



*Figure 27. Paganica village: broken major water pipe (repaired) due to co-seismic rupture (Lat. 42,36537N Long. 13,46803E) (Photo by Mylonakis G).*

Additional observations by Ken McCaffrey, Max Wilkinson (University of Durham), Richard Phillips (University of Edinburgh), Gerald Roberts (University of London), and Alessandro Michetti (University of Insubria (personal communication with G. Roberts, 2009) in the Paganica area are strongly suggestive of surface rupture (see also Walters et al., 2009). Figure 34 shows the results of a lidar scan that indicates clear normal slip. The feature shown in the image has a strike and position that aligns with the Paganica fault. The length of the feature is approximately 3-4 km, and the amount of slip is approximately 10 cm.

Based on the consistent observations from numerous groups, surface fault rupture appears to have occurred on the Paganica fault. The slip was consistent with normal faulting and has the length and displacement characteristics described by EMERGEO Working Group and the Durham, London, Edinburgh, Insubria Group.




*Figure 28. Plan view of Paganica site with marked positions of ground fissures, paved walkway cracks and broken water pipes. Directions of photo shots are indicated by yellow signs.*



*Figure 29. Failure of water pipe. (42.359335°N, 13.468954°E).*



*Figure 30. Local settlement close to piping system (42.359335°N, 13.468954°E).*



*Figure 31. Ground fissures at the side of the building (42.359817°N, 13.468649°E).*



*Figure 32. Ground fissures and settlement at the side of the building (42.359817°N, 13.468649°E).*



*Figure 33. Separation cracks at sidewalk on front of building (42.359335°N, 13.468954°E).*

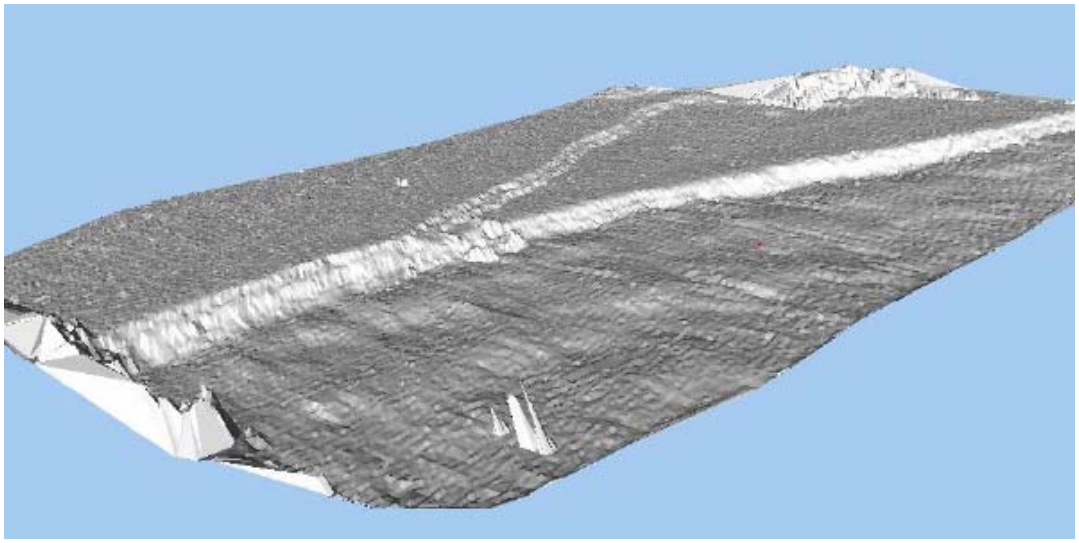


*Figure 34. Lidar scan of normal faulting along Paganica fault (courtesy of G. Roberts, personal communication, 2009).*

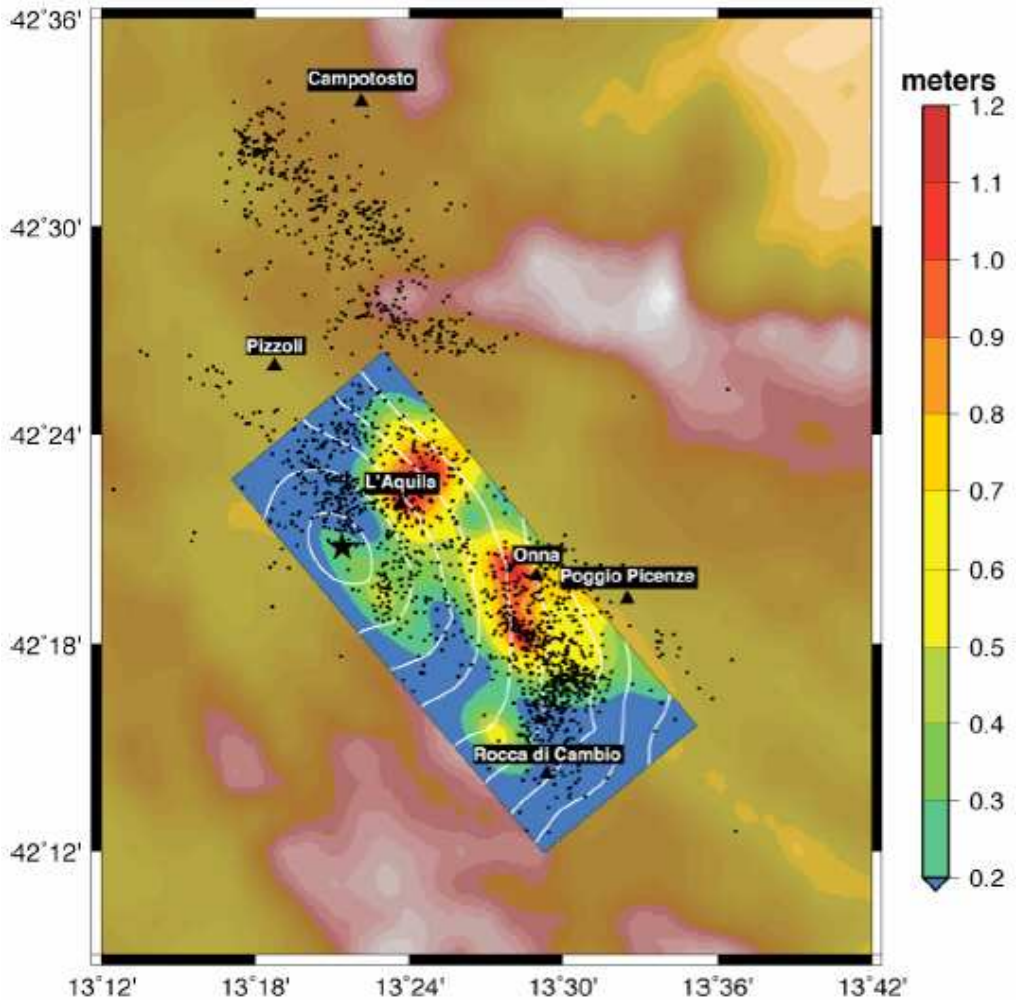



*Figure 35. Inverted rupture model projected on the Earth surface. Colors on the fault plane indicate the slip distribution. White contours represent the position of the propagating rupture at 1 s interval. Black dots are the recorded aftershocks (from Piatanesi and Cirella, 2009).*

**Preliminary Source Fault Proposed for the April 6th, 2009 Earthquake**

Using nonlinear inversion of the accelerometer and GPS data in order to model the rupture process that occurred on the presumed rupture surface that generated the April 6 earthquake, Figure 35 shows the projection of the proposed fault surface, whose characteristics are reported in Table 3 (Piatanesi and Cirella, 2009).

After this preliminary elaboration (originally available two weeks following the April 6 earthquake), additional fault plane solutions have been inverted using different data. Two such inversion results are reported in Figures 36 and 37, respectively by Chiarabba et al. (2009) and Atzori et al. (2009a, 2009b). These solutions have strikes smaller than one given in Table 3. The different source planes have an area approximately between 250 and 280 km$^2$.

*Table 3. Parameters of the source responsible for the April 6, 2009 earthquake (from Piatanesi and Cirella, 2009 and from the focal mechanism: http://earthquake.rm.ingv.it/qrcmt.php).*

| | | |
|---|---|---|
| Coordinates of the corners of the rectangular fault plane | A | Lat. (N): 42°22,71'<br>Lon. (E): 13°17,14' |
| | B | Lat. (N): 42°26,36'<br>Lon. (E): 13°23,00' |
| | C | Lat. (N): 42°15,64'<br>Lon. (E): 13°35,14' |
| | D | Lat. (N): 42°11,90'<br>Lon. (E): 13°29,14' |
| Length | 26 km | |
| Width | 11 km | |
| Strike | 140° | |
| Dip | 43° | |

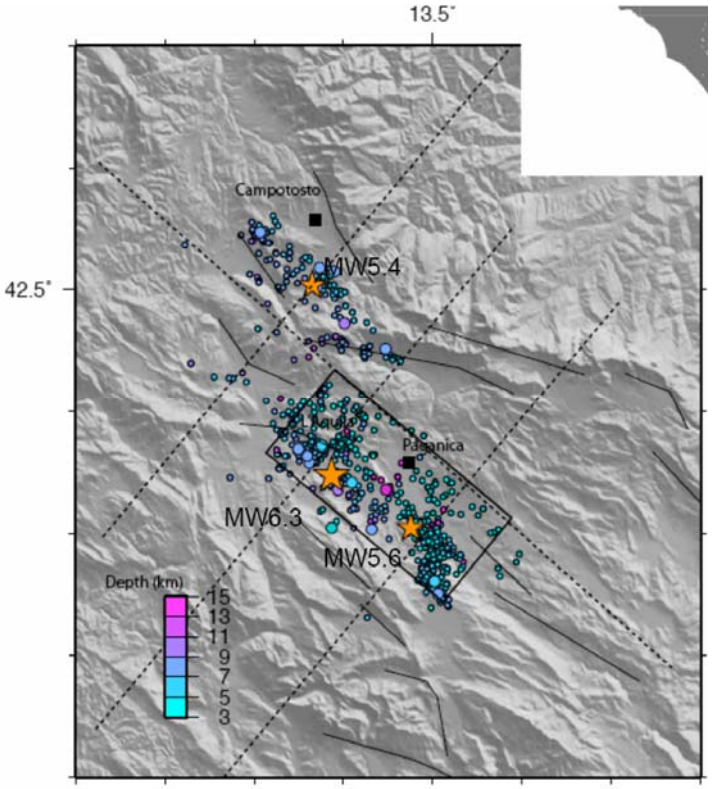
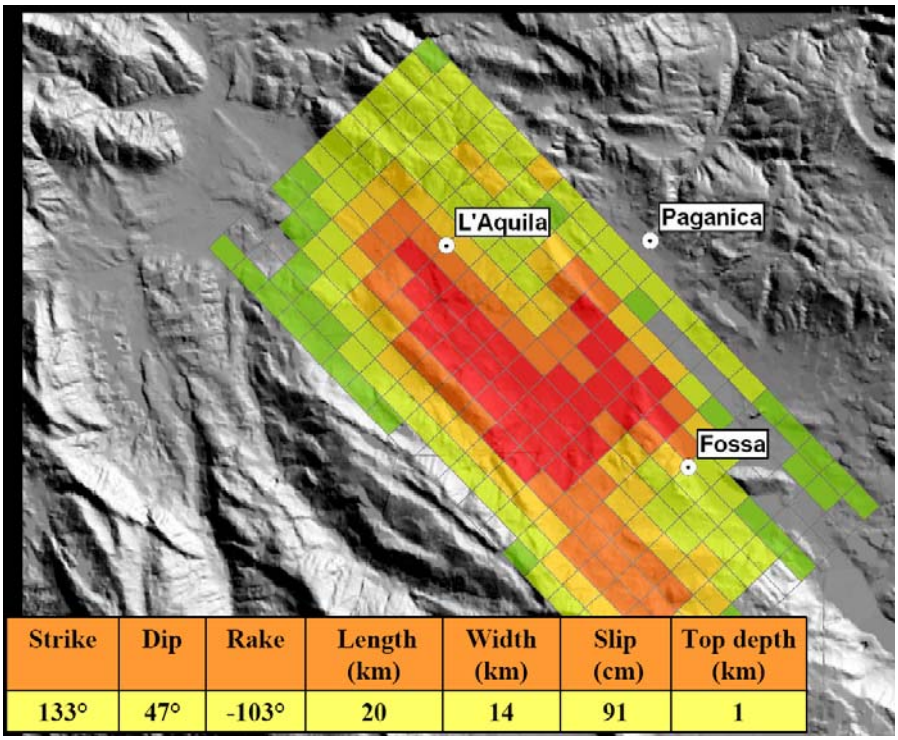



*Figure 36. Proposed source plane (black box) for the April 6 earthquake by inversion using seismological data of about 700 events of 6000 recorded by INGV National Seismic Network. The strike is about 130°. Reproduced from Chiarabba et al. (2009).*




| Strike | Dip | Rake | Length (km) | Width (km) | Slip (cm) | Top depth (km) |
|---|---|---|---|---|---|---|
| 133° | 47° | -103° | 20 | 14 | 91 | 1 |

*Figure 37. Distribution of the slip movements on the source area for the April 6 earthquake by linear inversion of SAR and GPS displacements up to the April 12. Table shows source plane dimensions. Figure from Atzori et al. (2009a,b).*

**Elements for a Scientific Discussion**

At present the various observations and analyses of the data lead to two primary hypotheses about the tectonic structure that generated the April 6 earthquake. One hypothesis is that the Paganica Fault was seismogenic and capable, in other words that it could have generated the April 6 event and displaced far enough to reach the surface (Figure 38) (Salvi et al., 2009). The second hypothesis involves the activation of a low angle fault, which displaced at depths from about 12 km to about 2-3 km, and whose projection towards the surface is represented by the Paganica Fault. The movement observed along this fault would have been caused by passive remobilization (Valensise, 2009), like that of the Bazzano-Fossa Fault, which is antithetic with respect to the Paganica Fault and intersects its plane at a depth of about 2-3 km.

In addition to the two hypotheses currently in discussion, there are other considerations that warrant discussion. The Paganica Fault (which dips to the southwest) and the Bazzano-Fossa Fault (which is antithetic to the Paganica Fault, dipping towards the northeast) have produced the graben where Onna is situated (Figure 39). This area, which suffered strong damage with maximum macroseismic intensity IX-X MCS within Onna, likely experienced an incidental concentration and entrapment of seismic energy inside the graben filled with Quaternary sediments, which are in strong velocity contrast with the rigid substrate composed of Meso-Cenozoic deposits (limestones and marls).

To the west of the graben where Onna is located there is a morphological flat area, depressed with respect to the surrounding zones, that corresponds to the area of maximum negative vertical deformation derived from the SAR data. This area seems to represent the morphological expression of deeper tectonic movements, compared to those that were produced on the surface faults of Paganica and Bazzano-Fossi. The actual morphology of this depressed area suggests that such vertical movements would have previously involved this plane, seemingly without surface expressions of tectonic discontinuities. Another possible explanation arises for the Onna graben, which is the result of coupled movement between the Paganica Fault and the Bazzano Fault. The mobilization of the Paganica Fault would therefore not have been seismogenically significant, in that this tectonic feature would have been involved only in processes of selective remobilization (Valensise, 2009). The Paganica Fault would be rooted at such depth that would render possible and probable a process of channeling incident seismic energy produced on another, deeper fault plane that would not have a surface expression (blind fault) (Valensise, 2009), with a low dip angle like the one suggested by the focal mechanism (http://earthquake.rm.ingv.it/qrcmt.php) of the April 6 earthquake.

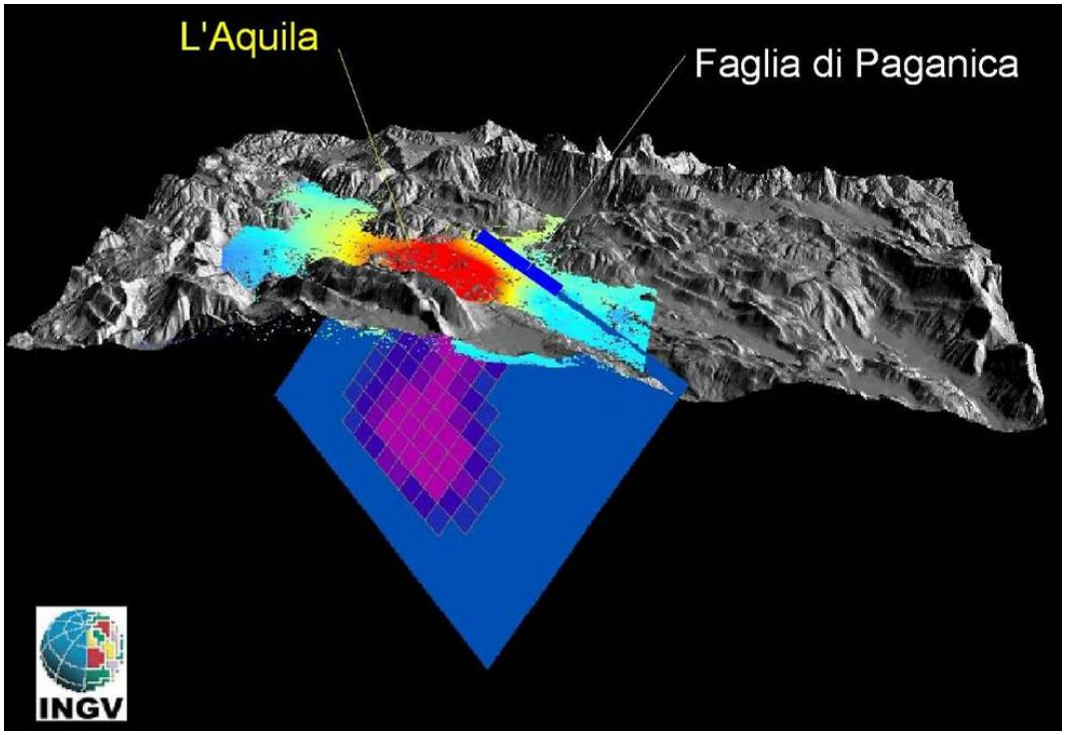



*Figure 38. Fault plane solution by InSAR data inversion, corresponding to the theory of a seismogenic and capable Paganica fault (Salvi et al., 2009). The results of displacement modeling are shown on the fault plane.*

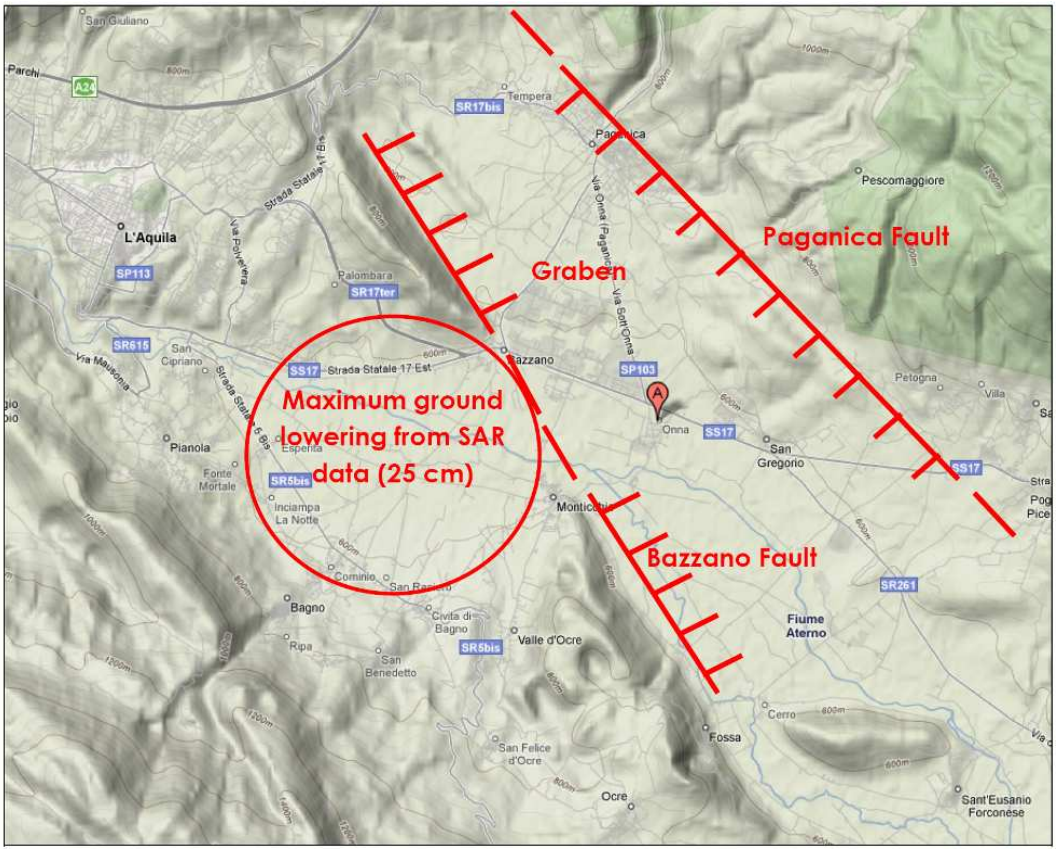



*Figure 39. Relationship between Paganica and Bazzano active faults and topography.*

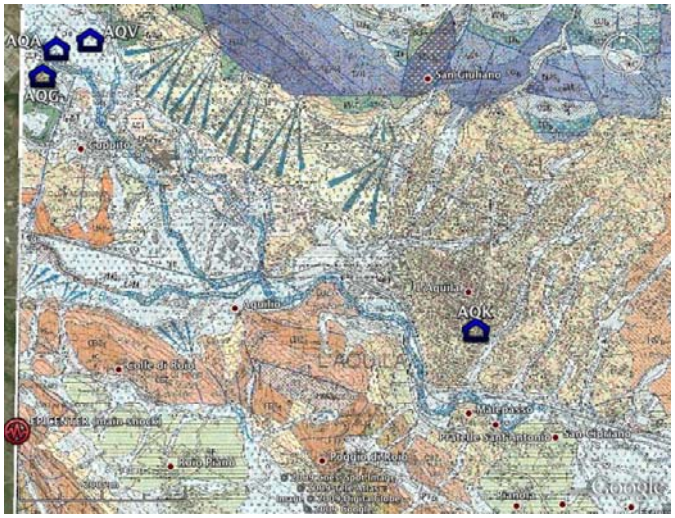
## GROUND MOTION

### Attributes of Recording Stations

The L'Aquila main event of April 6, 2009 was recorded by 56 digital strong motion instruments, 14 of which are in the Abruzzo region as shown in Figure 40a. Figure 40b shows the locations of four instruments located on the hanging wall of the fault near L'Aquila, three NW of the city in an array with one reference rock station (AQG) and two stations on recent alluvium (AQA, AQV) and one instrument near the city center on Pleistocene material (AQK). An additional instrument known as the Moro station recorded the mainshock (AQM), although this data was not released as of this writing. The other 42 instruments that recorded the mainshock are generally located in portions of the Apennines NW and SE of the source region, as shown in Figure 41. These instruments are part of the Italian Accelerometric Network (RAN - Rete Accelerometrica Italliana) that is owned and maintained by Italian Department of Civil Protection (DPC). The entire network is comprised of 388 accelerometers, 199 analogue and 269 digital, distributed across Italy. All stations listed in Table 4 have digital accelerometers, principally Altus Etna and K2 devices with 24-bit A/D converters. It is possible that additional analogue instruments recorded the earthquake and that data from those instruments will become available at a later date.




*Figure 40.(A) Locations of accelerometers in Abruzzo region that recorded the 6 April 2009 main shock. Fault plane surface shown in yellow.*




*(B) Location of instruments on hanging wall near L'Aquila overlayed on 1:50000 scale geology map.*

*Table 4. Characteristics of the 56 digital accelerometer stations that recorded the mainshock.*

| # | Code | Station | | | | Geology | | | | | $V_{s30}$ (m/sec) | | | | Housing (2) |
|---|---|---|---|---|---|---|---|---|---|---|---|---|---|---|---|
| | | Name | Agency | Latitude | Longitude | Age | Description | scale 1/ | Wills-Clahan class. | Scasserra et al. Class. | Source (1) | Type | Measured | Estimated | Preferred | EC8 class | |
| 1 | ant | ANTRODOCO | DPC | 42.418 | 13.079 | Triassic | limestone | 100000 | | MI | D | | | 1000 | 1000 | A | Box |
| 2 | aqk | Aquil PARK ing. | DPC | 42.345 | 13.401 | Pleistocene | conglomerate | 25000 | QT | | D | | | 455 | 455 | B | T |
| 3 | ass | ASSISI | DPC | 43.075 | 12.604 | Cretaceous | limestone and marls | | | MI | D | | | 1000 | 1000 | A | SB |
| 4 | avl | AVELLINO | DPC | 40.923 | 14.787 | Holocene | coarse volcainc material (tufo, piroclastite) | 100000 | Qal,coarse | | D | | | 354 | 354 | C | Box |
| 5 | avz | AVEZZANO | DPC | 42.027 | 13.426 | Quaternary | lacustrine Alluvium | | Qi | | B | CH | 120 | 160 | 120 | C | SB |
| 6 | bdt | BADIA TEDALDA | DPC | 43.707 | 12.188 | Eocene | limestone and sanstone | 100000 | | MI | D | | | 1000 | 1000 | A | SB |
| 7 | bne | BENEVENTO | DPC | 41.128 | 14.785 | Pleistocene | fluvio-lacustrin conglomerate, sand and clayey sand | 25000 | QT | | D | | | 455 | 455 | B | Box |
| 8 | bbn | BIBBIENA | DPC | 43.748 | 11.821 | Miocene | limestone | 100000 | | MI | D | | | 1000 | 1000 | A | Box |
| 9 | boj | BOJANO | DPC | 41.484 | 14.472 | Pleistocene | Fluvial-lacustrin deposit: clayey-sandy silts | 25000 | QT | | A | DH | 495 | 455 | 400 | B | SB |
| 10 | cmb | CAMPOBASSO | DPC | 41.563 | 14.652 | Miocene | limestone | 5000 | | MI | D | | | 1000 | 1000 | A | Box |
| 11 | cso1 | CARSOLI 1 | DPC | 42.10 | 13.088 | Mesiniano | sandstone | 25000 | Tss | | D | | | 515 | 515 | B | Box |
| 12 | cnm | CASALNUOVO MONTEROTARO | DPC | 41.618 | 15.105 | Miocene | breccias | 100000 | | Pc | D | | | 1000 | 1000 | A | Box |
| 13 | css | CASSINO | DPC | 41.486 | 13.823 | Eocene | limestone | 100000 | | MI | D | | | 1000 | 1000 | A | Box |
| 14 | cds | CASTEL DI SANGRO | DPC | 41.787 | 14.112 | Miocene | sandstone with clay | 100000 | Tss | | D | | | 515 | 515 | B | Box |
| 15 | cmr | CASTELMAURO | DPC | 41.833 | 14.712 | Miocene | limestone and marls | 100000 | | MI | D | | | 1000 | 1000 | A | Box |
| 16 | ctl | CATTOLICA | DPC | 43.955 | 12.736 | Pleistocene | gravel and sands | 100000 | QT | | D | | | 455 | 455 | B | – |
| 17 | cln | CELANO | DPC | 42.085 | 13.521 | Cretaceous | limestone | 25000 | | MI | D | | | 1000 | 1000 | A | Box |
| 18 | cer | CERIGNOLA | DPC | 41.260 | 15.910 | Pleistocene | sands | 100000 | QT | | D | | | 455 | 455 | B | Box |
| 19 | cht | CHIETI | DPC | 42.37 | 14.148 | Quaternary | gray clay and marls | 25000 | Qoa | | D | | | 387 | 387 | B | SB |
| 20 | fmg | FIAMIGNANO | DPC | 42.268 | 13.117 | Miocene | Breccias | 100000 | | Pc | D | | | 1000 | 1000 | A | SB |
| 21 | for | FORLI' | DPC | 44.199 | 12.042 | Pleistocene | sand, gravels, and clay | 100000 | QT | | D | | | 455 | 455 | B | Box |
| 22 | gnl | GENZANO DI LUCANIA | DPC | 40.843 | 16.033 | Pleistocene | sand and conglomerates | 100000 | QT | | D | | | 455 | 455 | B | Box |
| 23 | gsa | GRAN SASSO (Assergi) | DPC | 42.421 | 13.519 | Eocene | limestone | 100000 | | MI | D | | | 1000 | 1000 | A | SR |
| 24 | gsg | GRAN SASSO (Lab. INFN galleria) | DPC | 42.46 | 13.55 | Eocene | limestone | 100000 | | MI | D | | | 1000 | 1000 | A | T |
| 25 | isr | ISERNIA | DPC | 41.611 | 14.236 | Pleistocene | Fluvial-lacustrin deposit silt and clay with gravel | 5000 | QT | | D | | | 455 | 455 | B | – |
| 26 | aqv | L'Aquila - V. Aterno - Centro Valle | DPC | 42.377 | 13.344 | Holocene | fluvial alluvium coarse | 25000 | Qal,coarse | | A | CH | 475 | 354 | 475 | B | Box |
| 27 | aqg | L'Aquila - V. Aterno -Colle Grilli | DPC | 42.373 | 13.337 | Cretaceous | limestone | 25000 | | MI | C | | | 1000 | 1000 | A | Box |
| 28 | aqa | L'Aquila - V. Aterno -F. Aterno | DPC | 42.376 | 13.339 | Holocene | fluvial alluvium coarse | 25000 | Qal,coarse | | B | CH | 475 | 354 | 475 | B | Box |
| 29 | lss | LEONESSA | DPC | 42.558 | 12.969 | Jurassic | marly limestone | 100000 | | MI | D | | | 1000 | 1000 | A | Box |
| 30 | mnn | MANFREDONIA | DPC | 41.634 | 15.911 | Jurassic | limestone | 100000 | | MI | D | | | 1000 | 1000 | A | – |
| 31 | mmp1 | MOMPEO 1 | DPC | 42.249 | 12.748 | Jurassic | limestone | 25000 | | MI | D | | | 1000 | 1000 | A | SB |
| 32 | mng | MONTE S. ANGELO | DPC | 41.704 | 15.958 | Jurassic | limestone | 100000 | | MI | D | | | 1000 | 1000 | A | – |
| 33 | mtr | MONTEREALE | DPC | 42.524 | 13.245 | Miocene | sandstone | 100000 | Tss | | D | | | 515 | 515 | B | Box |
| 34 | nap | NAPOLI Ovest | DPC | 40.799 | 14.18 | Holocene | sand and silt | 100000 | Qal,coarse | | D | | | 354 | 354 | C | Box |
| 35 | orc | ORTUCCHIO | DPC | 41.954 | 13.642 | Holocene | sandy-clayely recent alluvium, locally gravely | 100000 | Qal,coarse | | D | | | 354 | 354 | C | SB |
| 36 | ptf | PETRELLA TIFERNINA | DPC | 41.696 | 14.702 | Cretaceous | clay and marly calys (argille scagliose) | 25000 | | Tm | C | | | 660 | 660 | B | Box |
| 37 | pic | PIANCASTAGNAIO | DPC | 42.85 | 11.685 | Pliocene | volcanic rock (ignimbrite) | 100000 | | Mv | D | | | 1000 | 1000 | A | Box |
| 38 | pdm | PIEDIMONTE MATESE | DPC | 41.355 | 14.385 | Holocene | debris poorly cemented | 100000 | Qal,coarse | | D | | | 354 | 354 | C | – |
| 39 | ric | RICCIA | DPC | 41.483 | 14.838 | – | limestone and marly limestone | 100000 | | MI | D | | | 1000 | 1000 | A | – |
| 40 | scm | S. CROCE DI MAGLIANO | DPC | 41.711 | 14.984 | Holocene | debris | 100000 | Qal,coarse | | D | | | 354 | 354 | C | Box |
| 41 | sep | S. ELIA A PIANISI | DPC | 41.625 | 14.88 | Miocene | sandstone | 5000 | Tss | | D | | | 515 | 515 | B | Box |
| 42 | sdg | S. GIOVANNI ROTONDO | DPC | 41.709 | 15.733 | Jurassic | limestone | 100000 | | MI | D | | | 1000 | 1000 | A | – |
| 43 | ssr | S. SEVERO | DPC | 41.691 | 15.374 | Pliocene | sandy silt and silty sand | 25000 | QT | | B | CH | 412 | 455 | 412 | B | – |
| 44 | snm | SAN MARINO | DPC | 43.934 | 12.449 | Miocene | limestone | 100000 | | MI | D | | | 1000 | 1000 | A | SB |
| 45 | sns | SANSEPOLCRO | DPC | 40.243 | 15.550 | Pleistocene | alluvium | 100000 | Qoa | | D | | | 387 | 387 | B | Box |
| 46 | stl | SATRIANO DI LUCANIA | DPC | 40.541 | 15.642 | Cretaceous | limestone, marls and siliceous deposits | 100000 | | MI | D | | | 1000 | 1000 | A | Box |
| 47 | scp | SERRACAPRIOLA | DPC | 41.807 | 15.165 | Pleistocene | Serracapriola sands | 100000 | QT | | D | | | 455 | 455 | B | Box |
| 48 | spo | SPOLETO | DPC | 42.734 | 12.741 | Pleistocene | conglomerate | | | Pc | D | | | 1000 | 1000 | A | – |
| 49 | spc | SPOLETO (cantina) | DPC | 42.743 | 12.74 | Pleistocene | lacustrin deposit | 100000 | QT | | D | | | 455 | 455 | B | – |
| 50 | stn | STURNO | DPC | 41.018 | 15.112 | Oligocene | clay and marls | 2000 | | Tm | A | CH | 382 | 660 | 382 | B | Box |
| 51 | sbc | SUBIACO | DPC | 41.913 | 13.106 | Miocene | limestone | 100000 | | MI | D | | | 1000 | 1000 | A | Box |
| 52 | sul | SULMONA | DPC | 42.089 | 13.934 | Cretaceous | limestone | 25000 | | MI | D | | | 1000 | 1000 | A | Box |
| 53 | tls | TELESE TERME | DPC | 41.222 | 14.53 | Cretaceous | limestone | 100000 | | MI | D | | | 1000 | 1000 | A | Box |
| 54 | tmo | TERMOLI | DPC | 41.989 | 14.975 | Pleistocene | Gravels and conglomerates | 100000 | QT | | D | | | 455 | 455 | B | Box |
| 55 | vrp | VAIRANO PATENORA | DPC | 41.333 | 14.132 | Pleistocene | conglomerates | 100000 | | Pc | D | | | 1000 | 1000 | A | Box |
| 56 | vie | VIESTE | DPC | 41.877 | 16.165 | Miocene | limestone | 100000 | | MI | D | | | 1000 | 1000 | A | – |

Table 4 lists attributes of the 56 digital accelerometer stations that recorded the mainshock, including location, surface geology, $V_{s30}$ (average shear wave velocity in upper 30 m), and instrument housing type. Surface geologic descriptions are preliminary in many cases, being based on relatively large-scale maps (1:100.000) by Servizio Geologico d'Italia. We generally prefer to classify surface geology using relatively local smaller-scale maps, which will take additional time to locate for most of the stations. However, some sites have been previously classified by Scasserra et al. (2009a) using 1:25000 and 1:5000 scale maps, and those results are shown in Table 3.1 where available. Furthermore, relatively local 1:25000 maps have been retrieved for the near-source region (unpublished INGV and DPC internal files), and classifications for instruments in those areas are derived using the local maps.

A site parameter commonly used in many modern ground motion prediction equations is $V_{s30}$. We evaluate $V_{s30}$ values following the protocols of Scasserra et al. (2009a), which can be summarized as:

- Data Source Type A: On-site measurements of velocity using established geophysical techniques (downhole, cross-hole, SASW, etc.). As shown in Table 4, there are three such mainshock stations for the L'Aquila earthquake (BOJ, AQV, STN).

- Type B: Velocity measurements are available at nearby sites having the same surface geology as the subject station, as confirmed by on-site observations by a geologist. Three such stations are listed in Table 4 (AVZ, AQA, SSR).

- Type C: Velocity estimated based on measurements from the same geologic unit as that present at the site (based on local geologic map, but no site visit by a geologist).

- Type D: Velocity estimated based on general (non-local) correlation relationships between mean shear wave velocity and surface geology.



*Figure 41. Locations of instruments that recorded 6 April 2009 main shock.*

For Type C and D sites, Scasserra et al. (2009a) developed relationships between surface geology and $V_{s30}$ for a number of surface geologic categories relevant to the subject region: Quaternary alluvium categories segregated by sediment depth and material texture (Qal,thin; Qal,deep; Qal,coarse), older Quaternary alluvium (Qoa), Quaternary to Tertiary alluvial deposits (QT), Tertiary sandstone formations (Tss), Pleistocene to Pliocene conglomerate (Pc), and Mesozoic limestone and volcanic rocks (Ml and Mv, respectively).

Table 4 lists for each of the 56 digital stations that recorded the earthquake the Data Source Type (A-D), the local geology as inferred from the smallest scale map currently available, the closest-related geologic category of Scasserra et al. (2009a), and the corresponding $V_{s30}$ value (as measured or estimated, depending on the data source type). Based on those $V_{s30}$ values, Eurocode 8 (EC8) classifications are also listed.

**Attributes and Preliminary Processing of Recordings**

Uncorrected digital accelerograms were downloaded from the Department of Civil Protection website (www.protezionecivile.it) approximately one week after the earthquake. Those motions were forwarded to the USGS National Engineering Strong Motion Project Data Center (Chris Stephens) and Pacific Engineering and Analysis (Walt Silva) for processing. Preliminary processing in which consistent high-pass and low-pass corner frequencies are applied to all records has been completed by the USGS group (Stephens, personal communication, 2009) and was also performed separately by Working Group ITACA (2009). Pacific Engineering and Analysis processed the data following PEER/NGA protocols, which include selection of record-specific corner frequencies to optimize the usable range of the recordings. Note that this processing reduced the number of recordings from 56 to 47 due to the noisy nature of recordings more than 200 km from the source. Specialized baseline correction has not yet been performed of near-fault stations (the AQ* stations) to draw out downward baseline shift, which is evident in those recordings.

The ground motion intensity measures of Peak Horizontal Acceleration (PHA) and Peak Horizontal Velocity (PHV) for the three components are shown in Table 5. Note that according to RAN standard installation procedures (Milana, personal communication, 2009), horizontal azimuths for all of the digital instruments are 000 for the 'north' component and 090 for the 'east' component. Positive vertical is upward. Also shown in Table 5 are closest distances to the fault plane ($R_{rup}$) and closest distances to the surface projection of the fault plane ($R_{jb}$). The fault plane that is the basis for these distances is modified from that in previous section by removing edge areas that were subject to low slip.

*Table 5. Peak Horizontal Acceleration (PHA) and Peak Horizontal Velocity (PHV) recorded at RAN stations during the mainshock.*

| | Station | | | | Azimuth 000 | | Azimuth 090 | | Vertical | |
|---|---|---|---|---|---|---|---|---|---|---|
| # | code | Station Name | $R_{epi}$ (km) | $R_{JB}$ (km) | PHA (g) | PHV (cm/s) | PHA (g) | PHV (cm/s) | PVA (g) | PVV (cm/s) |
| 1 | ANT | ANTRODOCO | 23.1 | 16.2 | 0.026 | 2.550 | 0.020 | 1.790 | 0.012 | 1.170 |
| 2 | AQA | L'Aquila - V. Aterno -F. Aterno | 5.8 | 0.0 | 0.443 | 27.100 | 0.402 | 31.900 | 0.496 | 9.700 |
| 3 | AQG | L'Aquila - V. Aterno -Colle Grilli | 4.3 | 0.0 | 0.515 | 36.000 | 0.482 | 31.100 | 0.273 | 10.700 |
| 4 | AQK | Aquil PARK ing. | 5.6 | 0.0 | 0.383 | 36.500 | 0.341 | 32.400 | 0.361 | 21.600 |
| 5 | AQV | L'Aquila - V. Aterno - Centro Valle | 4.8 | 0.0 | 0.554 | 43.100 | 0.669 | 40.400 | 0.525 | 12.100 |
| 6 | ASS | ASSISI | 101.7 | 94.8 | 0.003 | 0.393 | 0.006 | 0.438 | 0.002 | 0.300 |
| 7 | AVL | AVELLINO | 198.1 | 179.5 | 0.001 | 0.418 | 0.001 | 0.360 | 0.001 | 0.347 |
| 8 | AVZ | AVEZZANO | 34.9 | 17.5 | 0.069 | 11.400 | 0.056 | 10.900 | 0.027 | 3.750 |
| 9 | BBN | BIBBIENA | 199.6 | 192.5 | 0.001 | 0.256 | 0.001 | 0.270 | 0.001 | 0.267 |
| 10 | BDT | BADIA TEDALDA | 178.8 | 171.5 | 0.002 | 0.384 | 0.002 | 0.293 | 0.001 | 0.372 |
| 11 | BNE | BENEVENTO | 180.4 | 160.7 | 0.002 | 0.701 | 0.002 | 0.453 | 0.002 | 0.415 |
| 12 | BOJ | BOJANO | 133.5 | 113.7 | 0.014 | 3.340 | 0.013 | 3.240 | 0.005 | 1.440 |
| 13 | CDS | CASTEL DI SANGRO | 88.5 | 68.9 | 0.009 | 1.720 | 0.010 | 1.720 | 0.007 | 1.650 |
| 14 | CER | CERIGNOLA | 245.2 | 224.5 | 0.001 | 0.358 | 0.002 | 0.452 | 0.001 | 0.197 |
| 15 | CHT | CHIETI | 67.1 | 51.8 | 0.030 | 6.850 | 0.028 | 7.900 | 0.017 | 3.900 |
| 16 | CLN | CELANO | 31.6 | 12.8 | 0.091 | 6.650 | 0.083 | 4.890 | 0.046 | 7.080 |
| 17 | CMB | CAMPOBASSO | 138.9 | 116.3 | 0.003 | 0.862 | 0.003 | 1.330 | 0.002 | 0.847 |
| 18 | CMR | CASTELMAURO | 126.9 | 106.6 | 0.004 | 0.836 | 0.005 | 0.854 | 0.003 | 0.670 |
| 19 | CNM | CASALNUOVO MONTEROTARO | 166.9 | 146.4 | 0.002 | 0.726 | 0.002 | 0.829 | 0.002 | 0.523 |
| 20 | CSO1 | CARSOLI 1 | 33.0 | 29.2 | 0.018 | 1.480 | 0.019 | 2.350 | 0.016 | 1.720 |
| 21 | CSS | CASSINO | 102.7 | 83.8 | 0.010 | 1.390 | 0.008 | 1.590 | 0.003 | 0.783 |
| 22 | CTL | CATTOLICA | 186.6 | 177.3 | 0.003 | 0.736 | 0.004 | 0.731 | 0.001 | 0.314 |
| 23 | FMG | FIAMIGNANO | 19.3 | 16.7 | 0.027 | 1.690 | 0.024 | 2.860 | 0.020 | 1.310 |
| 24 | FOR | FORLI' | 232.3 | 224.2 | 0.002 | 0.668 | 0.002 | 0.593 | 0.001 | 0.298 |
| 25 | GNL | GENZANO DI LUCANIA | 279.4 | 255.7 | 0.002 | 0.543 | 0.002 | 0.569 | 0.001 | 0.249 |
| 26 | GSA | GRAN SASSO (Assergi) | 18.0 | 9.7 | 0.150 | 7.970 | 0.152 | 9.990 | 0.118 | 4.320 |
| 27 | GSG | GRAN SASSO (Lab. INFN galleria) | 22.6 | 14.3 | 0.030 | 3.330 | 0.021 | 3.310 | 0.019 | 3.260 |
| 28 | ISR | ISERNIA | 109.7 | 90.2 | 0.006 | 0.737 | 0.007 | 0.864 | 0.003 | 0.476 |
| 29 | LSS | LEONESSA | 39.1 | 31.8 | 0.008 | 0.801 | 0.010 | 0.671 | 0.006 | 0.738 |
| 30 | MMP1 | MOMPEO 1 | 49.2 | 44.9 | 0.007 | 0.624 | 0.009 | 0.866 | 0.005 | 0.506 |
| 31 | MNG | MONTE S. ANGELO | 228.4 | 208.5 | 0.002 | 0.311 | 0.002 | 0.349 | 0.001 | 0.186 |
| 32 | MNN | MANFREDONIA | 227.3 | 207.2 | 0.001 | 0.247 | 0.002 | 0.291 | 0.001 | 0.198 |
| 33 | MTR | MONTEREALE | 22.4 | 14.5 | 0.063 | 2.890 | 0.044 | 3.530 | 0.023 | 3.280 |
| 34 | NAP | NAPOLI Ovest | 184.5 | 165.7 | 0.003 | 0.938 | 0.002 | 0.817 | 0.001 | 0.352 |
| 35 | ORC | ORTUCCHIO | 49.4 | 30.6 | 0.041 | 3.300 | 0.066 | 5.890 | 0.031 | 3.730 |
| 36 | PDM | PIEDIMONTE MATESE | 139.4 | 120.2 | 0.001 | 0.339 | 0.002 | 0.324 | 0.001 | 0.356 |

**Preliminary Comparisons to GMPEs**

Figure 42 shows geometric mean PHA and PHV, as computed using the GMRotI50 parameter (Boore et al., 2006), as a function of $R_{jb}$ for EC8 subsoil classes A (rock), B (weathered rock and stiff soil), and C (medium-stiff soils). Four stations (AQA, AQK, AQG, AQV) are on the hanging wall and hence have $R_{jb}$=0. Those are plotted at $R_{jb}$=1 km in the figure. Also shown in Figure 42 are medians (μ) and medians ± one standard deviation (σ) for the Boore and Atkinson (BA) 2008 GMPE as modified for faster attenuation in Italy by Scasserra et al. (2009b) for PHA (no modification for PHV). The BA GMPE was plotted for $V_{s30}$=360 m/s. The red curve in the figure is the original BA 2008 median. Note that the modification for faster distance attenuation better captures the data trends.

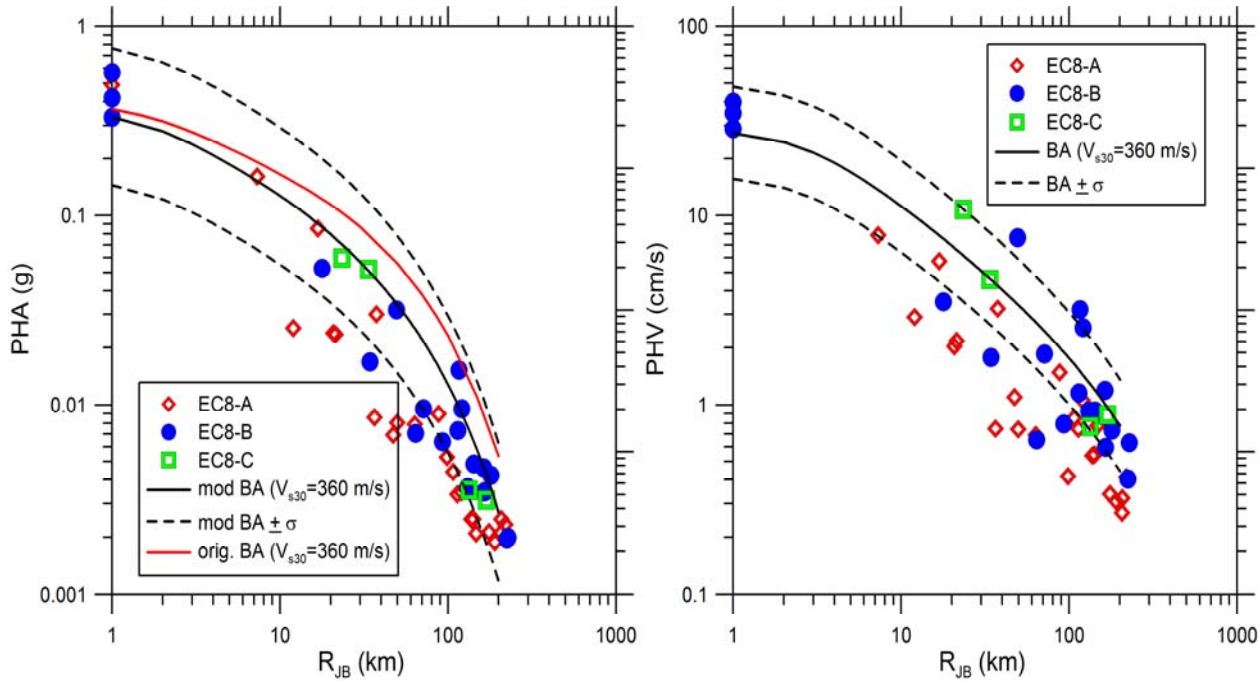



*Figure 42. Variation of orientation-independent geometric mean (GMRotI50) PHA and geometric mean PHV with $R_{jb}$ for EC8 site categories A, B, and C.*

Data for EC8 categories A and B are numerous and allow approximate inference of site effects. At large distance ($R_{jb}$ > ~50 km) B sites appear to be higher-amplitude than A sites, whereas the difference is not distinguishable for the relatively few stations at closer distance ($R_{jb}$ < ~30 km). These apparent trends will be evaluated through statistical analysis in subsequent work.

Actual site conditions at the recording stations vary as shown in Table 4. To more accurately evaluate the performance of the GMPEs relative to the data, we calculate residuals for each data point considering the appropriate source distance and site condition as follows:

$$R_i = \ln\left(IM_i\right)_{rec} - \ln\left(IM_i\right)_{GMPE} \quad (1)$$

where $(IM_i)_{rec}$ = value of ground motion intensity measure from recording i and $(IM_i)_{GMPE}$ = median value of that same IM from a ground motion prediction equation. The intensity measures used here are PHA and $S_a$ at 0.2, 0.5, 1.0, and 2.0 sec. We used the BA GMPE as modified by Scasserra et al. (2009b) for T ≤ 1.0 sec, the Sabetta and Pugliese (1996) GMPE, and the Ambrasseys et al. (2005) GMPE. Results of those calculations are shown in Figure 43 for the IMs of PGA and 1.0 sec $S_a$.

The results shown in Figure 43 indicate that the distance attenuation for the modified BA relation is consistent with the data, as indicated by the nearly horizontal trend lines. The other GMPEs have what appears to be a significantly non-

horizontal trend line for PHA, suggesting that the actual distance attenuation is faster than that predicted by the models. These trends will be more formally evaluated in subsequent work.

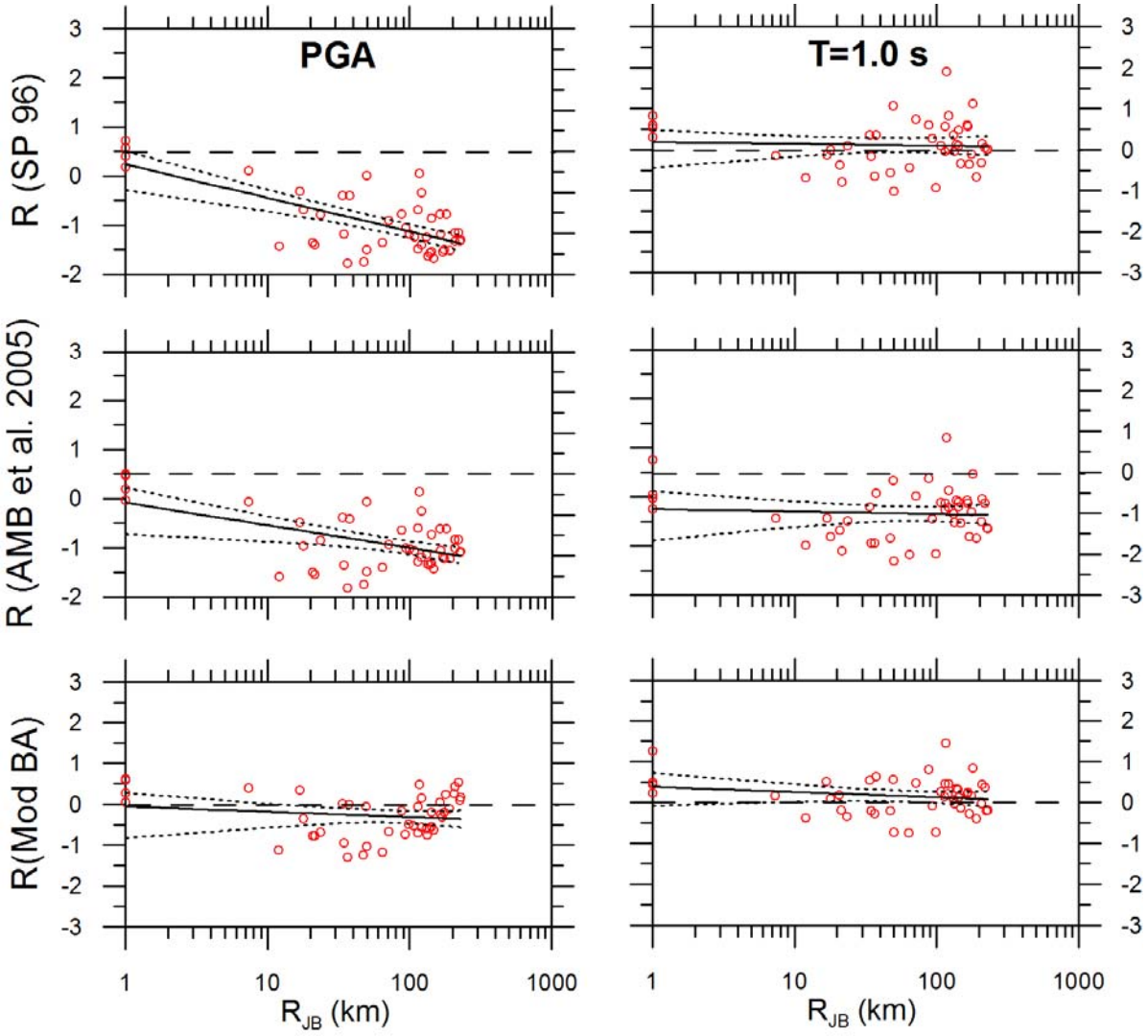



*Figure 43. Residuals of intensity measures from recorded ground motions (GMRotI50) relative to predictions of the modified Sabetta and Pugliese (SP) (1996) GMPE, the Ambrasseys et al. (AMB) (2005) GMPE, and the modified BA GMPE (Scasserra et al., 2009b). Log-linear trend line shown with 95% confidence limits.*

Although nearly horizontal, the modified BA trend line is not at zero ordinate. This indicates a systematic bias of the model relative to the data. Since this event is well recorded, this bias is nearly equal to an event term as would be calculated from a mixed-effects regression (e.g., Abrahamson and Youngs, 1992). Non-zero event terms are typical; what is of interest is to see if the event terms for the L'Aquila mainshock are consistent with event-to-event scatter as observed from previous earthquakes. This is typically represented by event term dispersion $\tau$. Figure 44 shows the L'Aquila mainshock event terms at the aforementioned periods along with the $\pm \tau$ model from the modified BA GMPE (the $\tau$ terms are identidical in the original and modified GMPEs). The L'Aquila event terms are seen to be unusually low at short periods but nearly zero at longer periods.

In Figure 45 we show V/H ratios for the mainshock peak accelerations and velocities, where H is taken as the geometric mean of the recorded motions. For peak acceleration, V/H is high in the near field and drops with distance in a manner consistent with empirical relationships (Bozorgnia and Campbell, 2004). For peak velocity, V/H increases with distance.

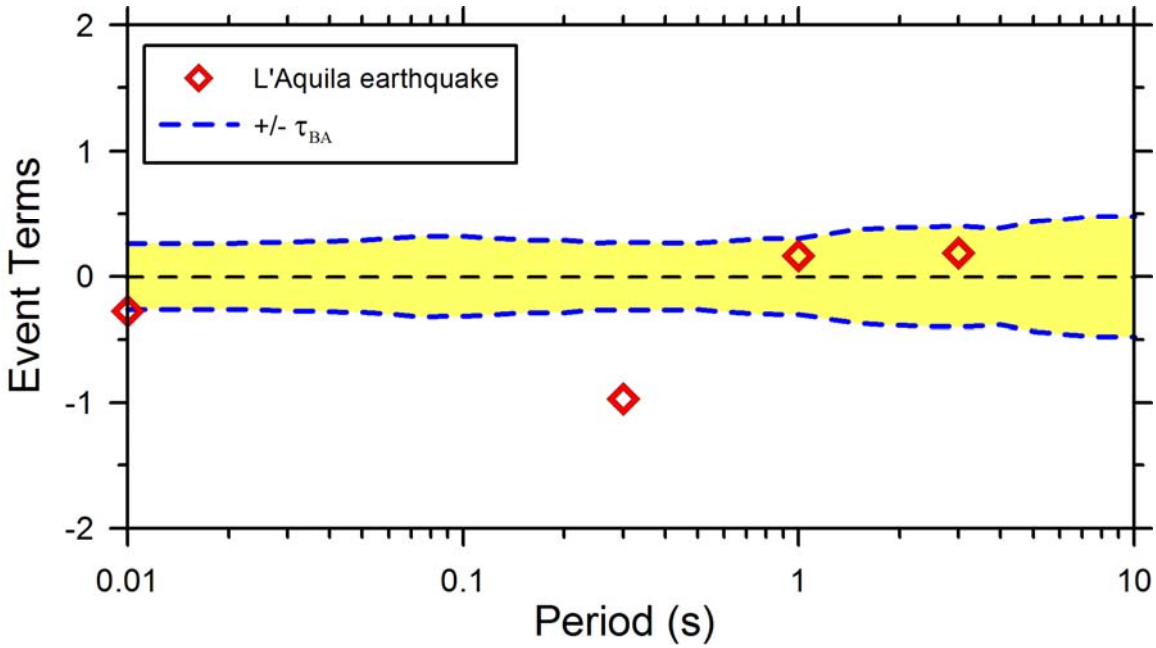



*Figure 44. L'Aquila earthquake event terms versus standard deviation of event terms (τ) from the BA (2008) GMPE.*

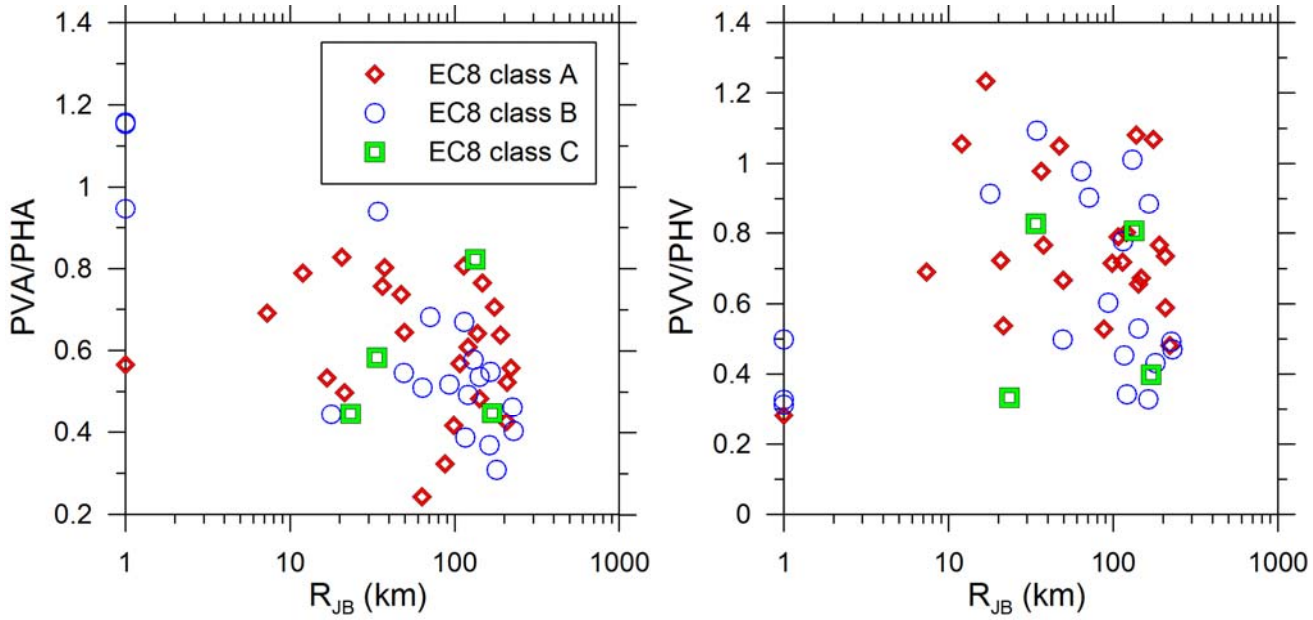



*Figure 45. L'Aquila earthquake V/H ratios for peak acceleration and velocity.*

**Spectra of near-Fault Recordings**

Figure 46 shows 5% damped pseudo-acceleration response spectra for four stations on the hanging wall of the fault. Before calculating spectra, the motions were rotated into fault normal and fault parallel directions, based on the 147 degree strike reported in the Earthquake setting and source characteristics section. The results are not suggestive of significant polarization of ground motion in the fault normal direction, which is an indicator of rupture directivity.

A notable feature of these motions is significant energy content at high frequencies for which motions in California have often saturated to the peak acceleration. In the 0.3-1.0 sec period range, the two motions from relative soft site conditions (AQA and AQV) appear to be relatively more energetic than those for firmer site conditions (AQG and AQK).

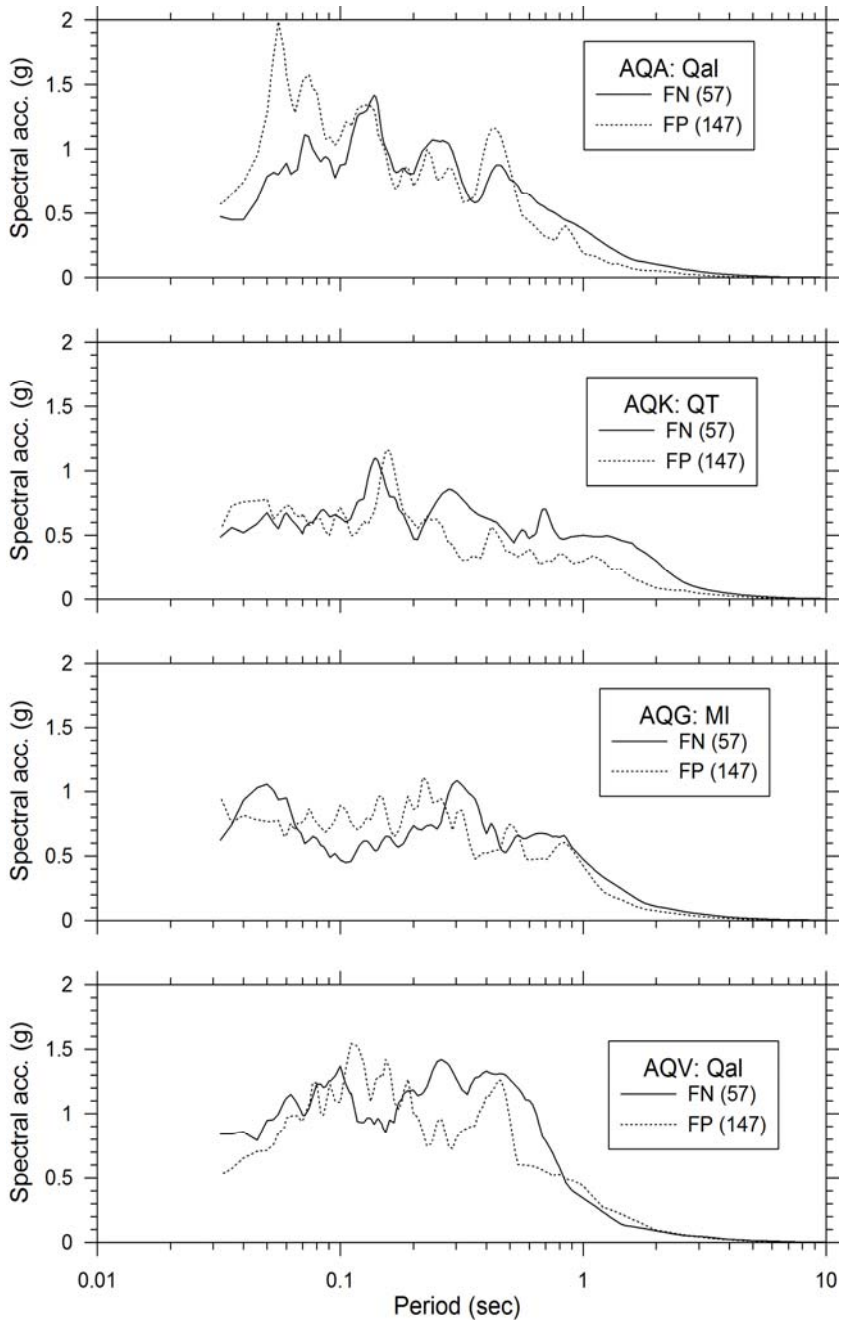



*Figure 46. Pseudo acceleration response spectra (5% damping) for four motions recorded on hanging wall of fault.*

**Observations of Rigid Bodies Providing Insight into Ground Motion Characteristics**

Rotation of Monumental Stone Block in Paganica

The response of massive block-type monuments to strong ground shaking can provide insight into ground motion characteristics (Yegian et al., 1994, Athanasopoulos, 1995). An interesting case of response of a stone monument to the main shock of April 6, 2009 was observed in Paganica (42.358616°N, 13.471250°E), within 1 km of the surface expression of the fault.

The monument consists of a block of porous stone with dimensions 0.75 m x 0.75 m x 1.12 m, sitting on a level stone pedestal made of similar material (Figure 47). As a result of the main shock, the block rotated about 14° counter-clockwise

(Figure 48) leading to a maximum sliding at the edge of the stone of approximately 20 cm. The final position of the block was almost aligned with NS direction. As the coefficient of friction is not less than 0.4, peak ground acceleration at the site may have been higher than 0.4g. More analysis is needed to back calculate additional ground motion parameters.



*Figure 47. Rotated monument in Paganica.*

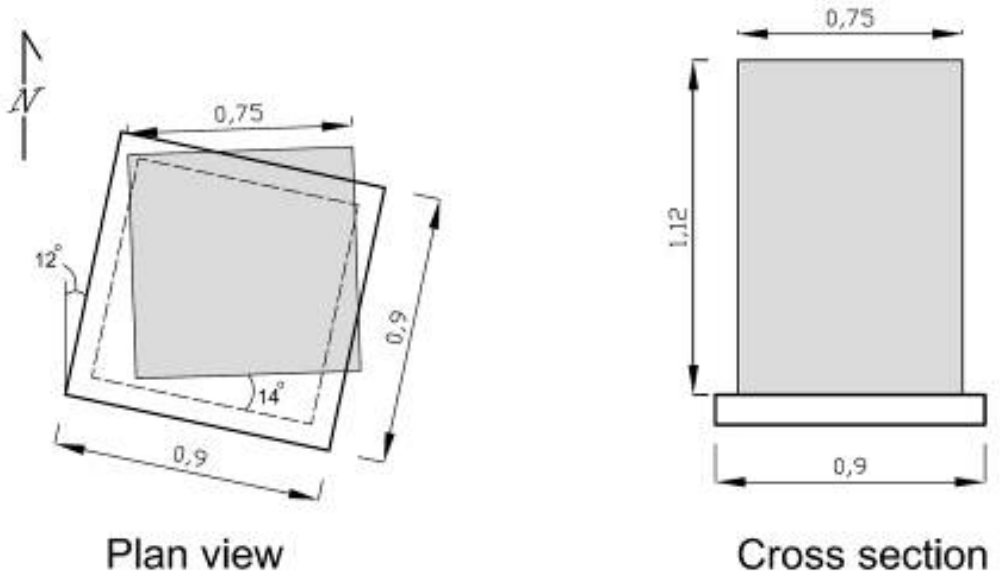



*Figure 48. Plan view and cross section of stone monument showing initial and aftershock positions.*

L'Aquila Cemetery – Response of Tombs and Structures

The L' Aquila cemetery (42.351515°N, 13.412318°E) was visited on April 15, 2009. Only a very small portion of grave markers were found damaged as a result of rotation, toppling, or falling (Figure 49-51). A number of facade ornaments of tombs were broken after falling to the ground. An example is shown in Figure 52. The observations in the cemetery seem to

indicate that the direction of toppling, breakage and falls is approximately North-South (with deviations of the order of 20°).

An interesting example of earthquake response was observed at the mortuary (Camera Mortuaria) of the cemetery shown in Figure 53. An ornamental masonry block originally placed at the top of the front facade detached and fell on the ground in S20°W direction. The block fell from a height of about 8 m and hit the ground at a horizontal distance of 2.50 m from the building, as shown in Figure 53.

An approximate formula, neglecting air resistance, for back calculating peak horizontal velocity of the fallen object at the time of separation, $V_{ox}$, is given by the following equation:

$$V_{ox} = \frac{s - u_g}{\frac{V_{oz}}{g} + \sqrt{\left(\frac{V_{oz}}{g}\right)^2 + 2\left(\frac{h}{g}\right)}} \tag{2}$$

where $h$ = height of fall, $s$ = horizontal distance travelled, $V_{oz}$ = vertical velocity at time of separation, $u_g$ = ground movement during fall, $g$ = acceleration of gravity. Using $h$ = 8m, $s$ = 2.5m, $g$ = 10m/s$^2$, and assuming $V_{oz}$ on the order of 0.1 to 0.2cm/$s$, $u_g$ = 0.05m, one obtains the estimate

$V_{ox}$ = 1.9 to 2.0 m/$s$ (3)

which is more than five times the maximum recorded PGV in the meizoseismal area. Note that neglecting initial vertical velocity and ground movement, equation (2) simplifies to $V_{ox} = s/(2\,h/\,g)^{0..5}$, which leads to the almost identical prediction of 1.98 m/$s$. Evidently, the response of the structure, including rocking of the foundation, may have influenced significantly the horizontal velocity of the object. More analyses are required to come up with realistic inversions. Preliminary hand calculations indicate that the amplification due to building response is unlikely to have exceeded 4. This suggests that the peak ground velocity at the site may be higher than those recorded at the accelerographic locations.



*Figure 49. Grave markers breakage.*



*Figure 50. Grave marker rotation.*



*Figure 51. Grave markers toppling.*



*Figure 52. Breakage and fall of ornamental objects from a tomb roof.*




*Figure 53. Fall of facade object at mortuary building.*

**DAMAGE PATTERNS**

Site effects were investigated in the form of variable building damage intensities from one region to another having similar styles of construction. The investigations occurred at multiple scales. Within the region's largest urban center (L'Aquila), damage patterns were investigated in detail in a structure-by-structure manner. In that case, the intent was to investigate damage localization within particular geologic units or near particular geologic structures. In the relatively small villages outside of L'Aquila, our intent was to document general intensities of damage so that village-to-village comparisons could be made. To the extent that adjacent villages might have different underlying geologic conditions and different topographies, village-to-village damage variations could be taken as indicators of site effects. We have also documented damage at a number of additional villages without immediate neighbours from which site effects are inferred.

For both the local and relatively regional damage mapping, we used a common description of damage intensity, which is shown in Table 6. The marker color shown in the figure is used subsequently. Table 7 summarizes damage observations in villages.

*Table 6. Definition of damage categories (adapted from Bray and Stewart, 2000).*

| Damage Level | Description | Marker Color |
|---|---|---|
| D0 | No damage | |
| D1 | Cracking of non-structural elements, such as dry walls, brick or stucco external cladding | |
| D2 | Major damage to the non-structural elements, such as collapse of a whole masonry infill wall; minor damage to load bearing elements | |
| D3 | Significant damage to load-bearing elements, but no collapse | |
| D4 | Partial structural collapse (individual floor or portion of building) | |
| D5 | Full collapse | |

*Table 7. Selected sites affected by the earthquake and surveyed macroseismic intensities (Galli and Camassi, 2009).*

| Locality | Municipality | Province | Lat. (N) | Lon. (E) | I (MCS) |
|---|---|---|---|---|---|
| Castelnuovo | San Pio delle Camere | AQ | 42.295 | 13.628 | IX-X |
| Onna | L'Aquila | AQ | 42.327 | 13.48 | IX-X |
| San Gregorio | L'Aquila | AQ | 42.327 | 13.496 | IX |
| Sant'Eusanio Forconese | Sant'Eusanio Forconese | AQ | 42.288 | 13.525 | IX |
| Tempera | L'Aquila | AQ | 42.366 | 13.458 | IX |
| Villa Sant'Angelo | Villa Sant'Angelo | AQ | 42.269 | 13.538 | IX |
| L'Aquila (city centre) | L'Aquila | AQ | 42.356 | 13.396 | VIII-IX |
| Poggio Picenze | Poggio Picenze | AQ | 42.32 | 13.541 | VIII-IX |
| Bazzano | L'Aquila | AQ | 42.337 | 13.455 | VIII |
| Casentino | Sant'Eusanio Forconese | AQ | 42.278 | 13.51 | VIII |
| Paganica | L'Aquila | AQ | 42.358 | 13.473 | VIII |
| Roio Piano | L'Aquila | AQ | 42.327 | 13.357 | VIII |
| Tussillo | Villa Sant'Angelo | AQ | 42.267 | 13.531 | VIII |
| Fossa | Fossa | AQ | 42.296 | 13.487 | VII-VIII |
| Castelvecchio Subequo | Castelvecchio Subequo | AQ | 42.13 | 13.731 | VII |
| Goriano Sicoli | Goriano Sicoli | AQ | 42.08 | 13.775 | VII |
| Pettino | L'Aquila | AQ | 42.375 | 13.355 | VII |
| Pianola | L'Aquila | AQ | 42.322 | 13.404 | VII |
| Carapelle Calvisio | Carapelle Calvisio | AQ | 42.298 | 13.684 | VI-VII |
| Coppito | L'Aquila | AQ | 42.366 | 13.344 | VI-VII |
| Prata d'Ansidonia | Prata d'Ansidonia | AQ | 42.277 | 13.609 | VI-VII |
| San Demetrio ne' Vestini | San Demetrio ne' Vestini | AQ | 42.288 | 13.558 | VI-VII |
| Santo Stefano di Sessanio | Santo Stefano di Sessanio | AQ | 42.343 | 13.645 | VI-VII |
| Stiffe | San Demetrio ne' Vestini | AQ | 42.256 | 13.545 | VI-VII |
| Assergi | L'Aquila | AQ | 42.414 | 13.505 | VI |
| Barete | Barete | AQ | 42.45 | 13.283 | VI |
| Barisciano | Barisciano | AQ | 42.325 | 13.592 | VI |
| Bominaco | Caporciano | AQ | 42.244 | 13.658 | VI |
| Bussi sul Tirino | Bussi sul Tirino | PE | 42.21 | 13.826 | VI |
| Campotosto | Campotosto | AQ | 42.558 | 13.369 | VI |
| Capestrano | Capestrano | AQ | 42.266 | 13.769 | VI |
| Caporciano | Caporciano | AQ | 42.25 | 13.674 | VI |
| Castel del Monte | Castel del Monte | AQ | 42.325 | 13.727 | VI |
| Castelvecchio Calvisio | Castelvecchio Calvisio | AQ | 42.31 | 13.688 | VI |
| Fontecchio | Fontecchio | AQ | 42.229 | 13.605 | VI |
| Monticchio | L'Aquila | AQ | 42.32 | 13.466 | VI |
| Navelli | Navelli | AQ | 42.236 | 13.73 | VI |
| Ocre (San Panfilo d'Ocre) | Ocre | AQ | 42.285 | 13.475 | VI |
| Pizzoli | Pizzoli | AQ | 42.435 | 13.303 | VI |
| Popoli | Popoli | PE | 42.171 | 13.833 | VI |
| Preturo | L'Aquila | AQ | 42.377 | 13.295 | VI |
| Rocca di Cambio | Rocca di Cambio | AQ | 42.235 | 13.49 | VI |
| Rocca di Mezzo | Rocca di Mezzo | AQ | 42.205 | 13.521 | VI |
| Scoppito | Scoppito | AQ | 42.372 | 13.256 | VI |
| San Pio delle Camere | San Pio delle Camere | AQ | 42.286 | 13.656 | V-VI |

**Damage to Villages in the Eastern Aterno Valley**

Site amplification on soil deposits is evident in the towns and villages east of L'Aquila, down the axis of the Aterno River valley. A map of the Valley can be seen in Figure 54 and includes the heavily damaged towns of Castelnuovo, Onna, San Gregorio, and Poggio Picenze. Other, less damaged, towns found in this valley are Monticchio, Fossa, Tussio, San Pio delle Camere, and Barisciano. Site effects are evident from relative damage between nearby villages in the Aterno Valley. Near Castelnuovo are the towns of San Pio delle Camere, San Demetrio, and Tussio, and near the town of Onna are the villages of San Gregorio and Monticchio.

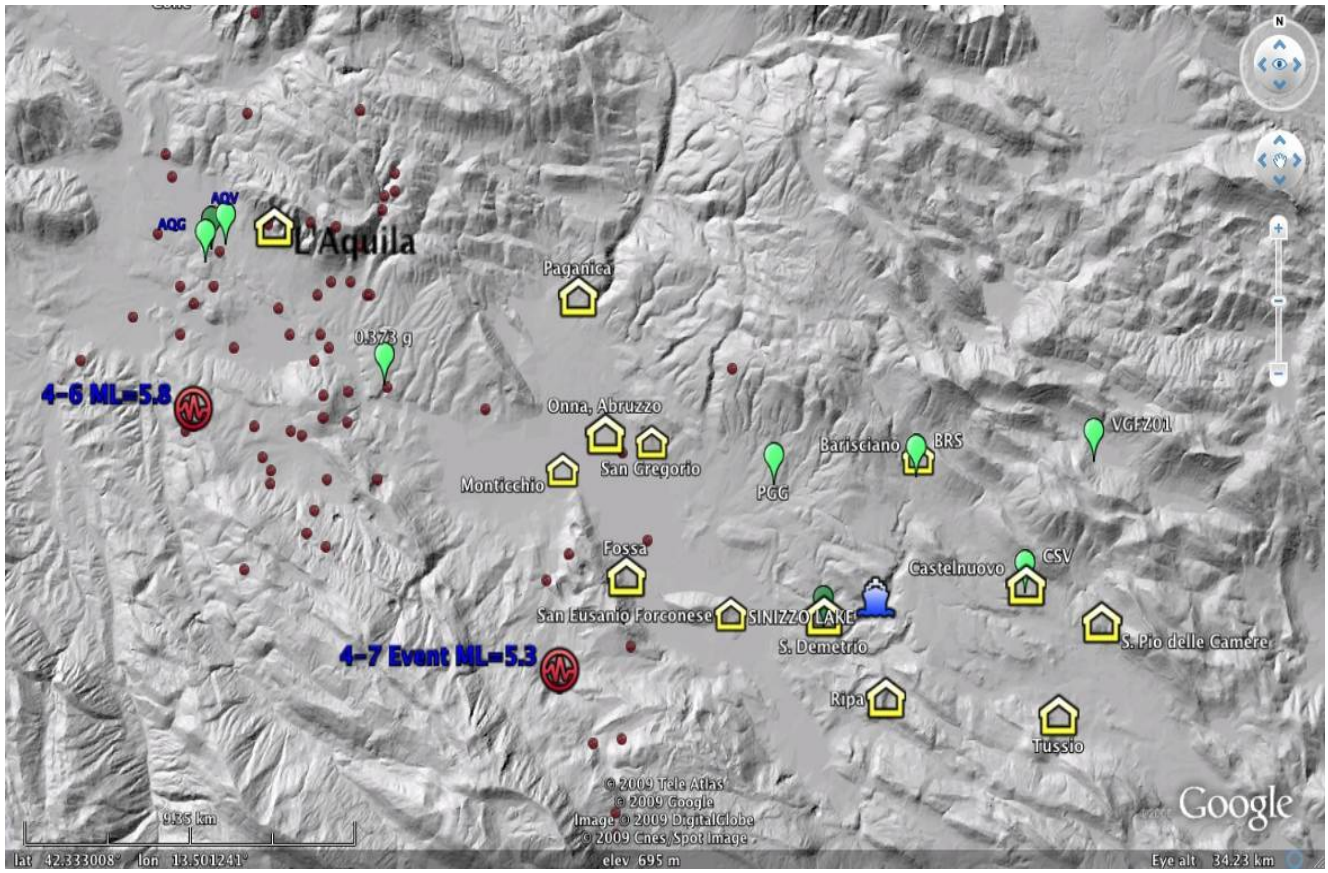



*Figure 54. Map of Central Abruzzo and the central Aterno valley with the main shock fault plane and epicenters of April 6 and April 7 events. The villages of the Aterno valley are south east of the capital city of L'Aquila.*

Damage to Castelnuovo and Surrounding Villages

Castelnuovo

The village of Castelnuovo is located on a hilltop 10-70 m above the surrounding alluvial plain. The village (810-860 m elevation) is settled on an elliptical hill, consisting of fluvio-lacustrine deposits of lower to medium Pleistocene age. The village top is an eroded Pleistocene unit of weakly cemented sand with inter-collated gravel and conglomerate (Bosi and Bertini, 1970; Bertini et al., 1989). This unit lies on top of a soft erodable carbonate silt of the San Nicandro formation that was incised by the Aterno river during Pleistocene time. Holocene fluvial and alluvial deposits fill-in the topographic lows and surround the eastern and southern sides of the village (Figures 55 and 56). The site is located 5 km away from the surface projection of the fault plane depicted in Figure 35. During the reconnaissance, we observed outcrops of the weakly cemented sandstone near the top of the village in a sinkhole that formed among D5 collapsed structures. On the north side of the village at the base of the hill is an abandoned masonry ENEL seismograph station that was badly damaged during the earthquake (Figure 57).

The village consists of un-reinforced masonry structures 2-3 stories in height. Some of the structures were retrofitted with through-going iron bars. Shaking was strong enough to significantly damage (D2 or greater) almost the entire village, with most of the structures in the upper half of the hill either collapsed or teetering on collapse (D3-D5). Figure 58 shows a D2 structure near the base of the village, where the D4-D5 Ratio was approximately 25%. In this area most structures survived the event. Figure 59 shows a series of collapsed structures near the top of the hill, where the D4-D5 ratio was 80-90%. Figure 60 shows a sinkhole apparently associated with erosion from a water pipe break at this same location near the top of the hill. The village of Castelnuovo was previously almost completely destroyed during the earthquake of 1461 (Rovida et al. 2009).

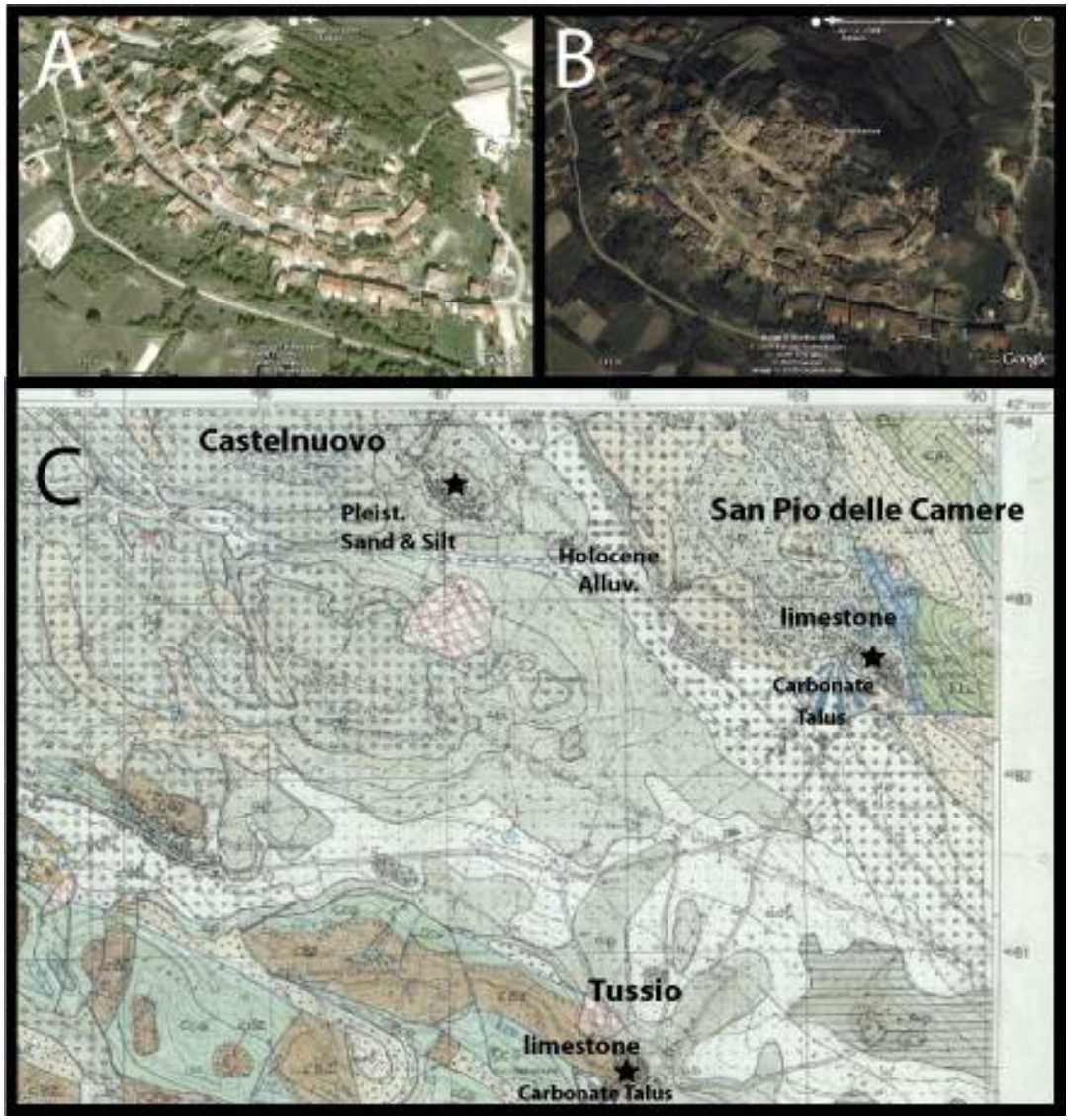



*Figure 55. Castelnuovo village before the earthquake. (A) The village after the earthquake, (B) Geologic map of the eastern Aterno Valley region, (C) Geologic map of the region (Courtesy of INGV).*

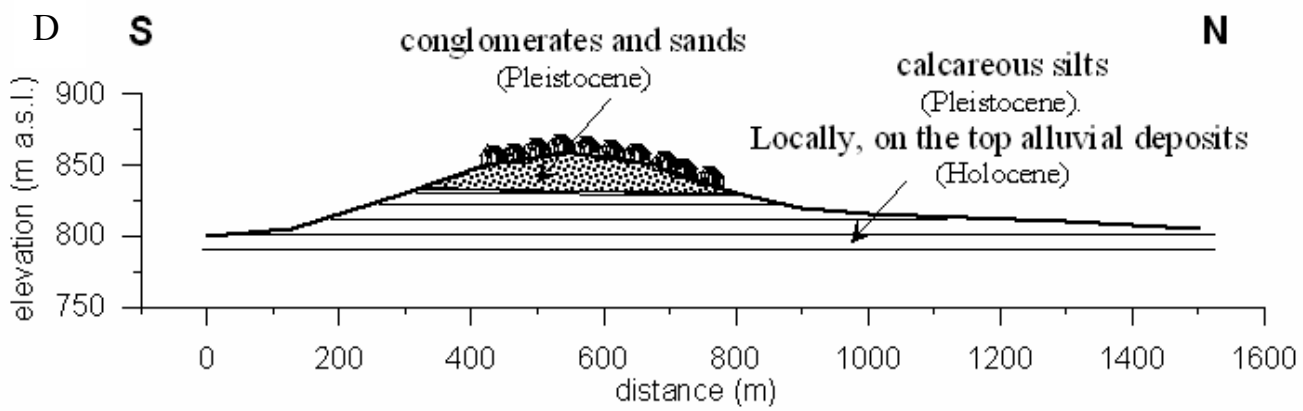
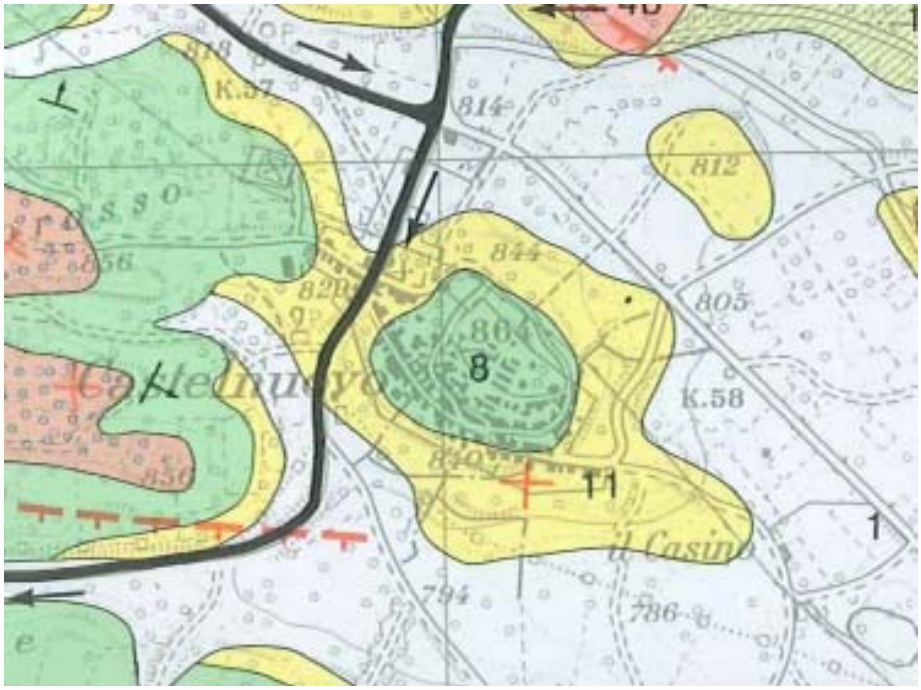



*Figure 55. (D) Geologic section through the hill. Castelnuovo is built on Pleistocene sand and silt deposits, whereas nearby villages with the same building stock are located on Mesozoic carbonate Bedrock, and limestone talus.*




| | |
|---|---|
| 1 | Alluvial and colluvial sediments (Holocene) |
| 8 | Gravel and conglomerates interbedded with cemented sand (medium Pleistocene) |
| 11 | Carbonate silts with thin sand lenses (lower Pleistocene) |

*Figure 56. Geological map of Castelnuovo (modified after Bertini et al., 1989).*



*Figure 57. Heavily damaged seismometer station box (not in use at the time of the earthquake, no recording) on the northeast valley beneath the town of Castelnuovo. (42.2982°, 13.6295°).*



*Figure 58. A typical heavily damaged structure in the lower elevation of Castelnuovo. Many structures in the lower elevation neighborhood had less observable damage. (42.2956°, 13.6274°).*



*Figure 59. At the highest elevation of the hilltop town of Castelnuovo, almost all of the structures collapsed (D5) or were near collapse (D4). (42.2947°, 13.629°).*



*Figure 60. In the foreground of Figure 59 at the top of the hill in the center of Castelnuovo, a large sinkhole formed beneath the road exposing the weakly cemented Pleistocene sandstone that underlies the village. Water draining through the sinkhole was actively eroding a large void approximately 3-5 m in diameter and at least 6 m in depth. Cementation was strong enough to support small overhangs, at least temporarily (42.2947°, 13.629°).*

San Pio delle Camere

Castelnuovo is located 2 km northeast of the village of San Pio delle Camere, a hill slope village built on carbonate bedrock. This village is at a similar elevation above the valley floor and approximately 7 km from the fault plane. The housing stock of the village is similar to Castelnuovo. This village had no observable significant damage to any of the structures. Several fine cracks were observed in the exterior walls of some of the two-story and three-story residences, as shown in Figures 61 and 62.




*Figure 61. (A) The village of San Pio delle Camere built on Mesozoic limestone. This picture was taken from the lower flanks of Castelnuovo (from location 42.2898°, 13.6297° looking southeast).*

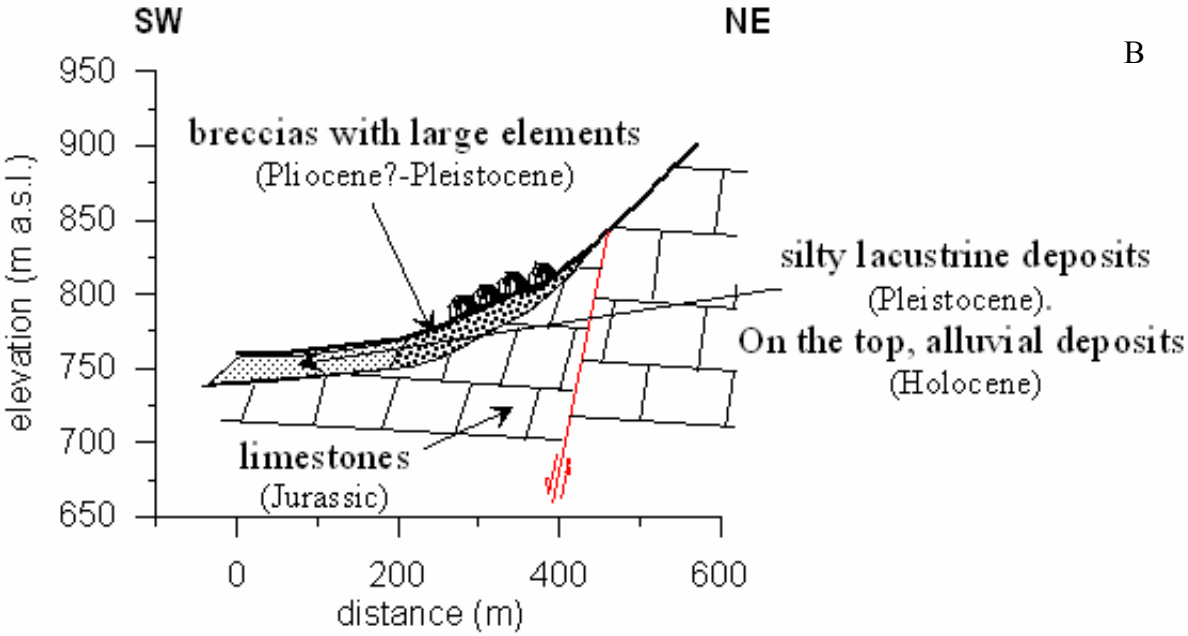



*Figure 61. (B) Geologic cross section through the village.*



*Figure 62. Typical unreinforced masonry structures in the village of San Pio delle Camere suffered no damage (D0), or slight cracking (D1). Structures in this village are similar to those in Castelnuovo. San Pio delle Camere is built on limestone bedrock.*

Tussio

The village of Tussio is located 3.4 km south southeast of Castelnuovo and was built on limestone bedrock and carbonate alluvial fan debris. It is similar to San Pio delle Camere in that it was also built on the side of a hillslope on carbonate bedrock, and coarse debris. Tussio also suffered essentially no significant structural damage during the earthquake, as shown in Figure 63.

Based on the response of the structures, the shaking intensity at Castelnuovo was significantly greater than at San Pio delle Camere or Tussio. It is also noteworthy that the damage to the top of the village of Castelnuovo was considerably worse than at the base. Accordingly, Castelnuovo is a good candidate for a dense array of seismometer instruments to characterize the relative amplification of aftershock motions as compared with the surrounding villages, and also to characterize the difference between motions at the lower elevations of the town relative to the town center at the top of the hill. Some element of topographic amplification may have contributed to the strong shaking at the highest elevations of the village. However, there is no indication of damaging topographic amplification at San Pio delle Camere or Tussio.



*Figure 63. The reconnaissance team observed no damage to the town of Tussio. The town is built on Mesozoic calcareous bedrock (42.2657°, 13.6414°).*

Damage to Onna and Surrounding Villages

Onna

The hardest hit village near the city of L'Aquila was Onna (Figure 64), an old village on the floor of the Aterno valley built on Holocene calcareous alluvial and fluvial deposits of sand and gravel, and inter-bedded clay and silt, some more than 5 m thick (Figures 65 and 66). The village is in the valley thalweg on the left bank of the Aterno river. The village is similar to Castelnuovo in that it is composed mainly of 2-3 story unreinforced masonry structures, with a minority of retrofitted structures. Unlike Castelnuovo, this village has a small number of newer reinforced concrete residential structures (Figure 64). The village is on the hanging wall of the fault above a region of high slip ($R_{jb}$=0, see Figure 35) at an average elevation of 580 m elevation. Unreinforced masonry structures in Onna suffered a collapse (D5) rate of about 80% (Figure 67a). Reinforced concrete structures suffered minor or no damage. The intensity degree attributed by QUEST team was IX-X.




*Figure 64. The village of Onna suffered D4—D5 damage in most of the unreinforced masonry structures. Reinforced concrete structures at the margins of the village performed well with only minor damage (D0-D2).*

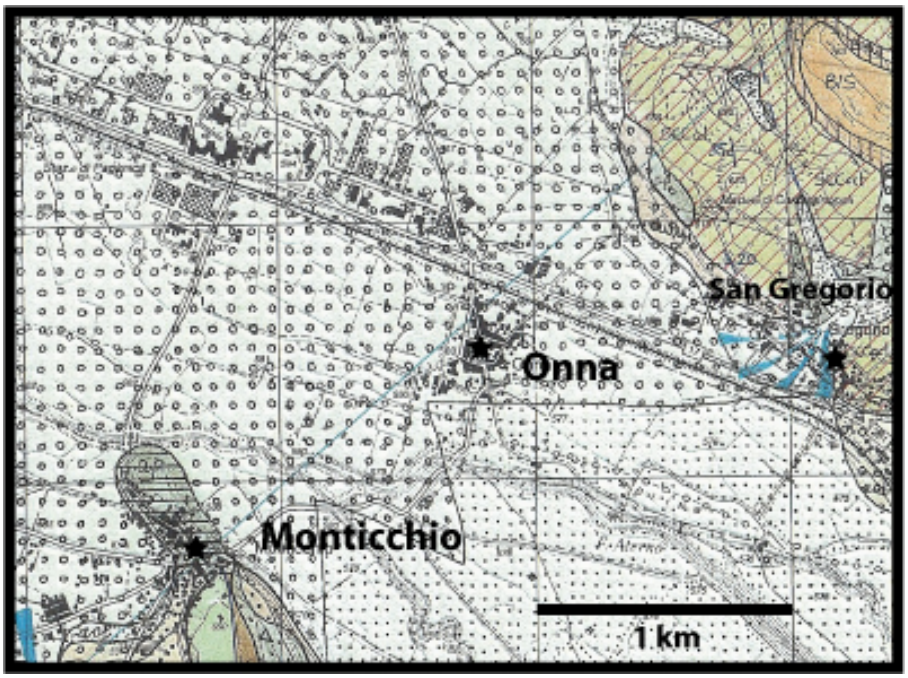



*Figure 65. L'Aquila geologic map close-up of Onna, San Gregorio, and Monticchio. Onna is built on Quarternary alluvium and suffered mostly D4-D5 damage in the masonry structures. Monticchio is built on Mesozoic limestone, and Quaternary breccia and suffered mostly D0-D1 damage. San Gregorio is built on Miocene limestone, Pleistocene Fluvial and lacustrine deposits, and Holocene alluvium. Damage was high in the historic center of town (mostly D4-D5). Damage was considerably lower on the limestone deposits (D0-D2).*




*Figure 66. Geological map of Monticchio, Onna and San Gregorio (modified after Bosi and Bertini, 1970).*




*Figure 67. Onna. (A) D5 damage level on masonry building structures, (B) D0 damage on a RC building (except for the tilting of the chimney).*




*Figure 68. Onna. (A) Collapse (D5).*




*Figure 68. Omna. (B) Intense damage (D4) of RC bridges on the Aterno river.*

The town was previously destroyed by the historical earthquake in 1461 (Rovida et al., 2009). During that event, the village was reported to have suffered X MCS, and an eighteenth century chronicler Anton Ludovico Antinori reported that 'Nella Villa di Onda né tampoco restò casa impiedi' ('In the Onda village no house remained standing').

Onna is surrounded by a number of villages on various geologic units (Figure 65 and 66). One village on a similar setting is a portion of San Gregorio, 1.2 km to the east. Portions of San Gregorio that were built on Holocene alluvial deposits, or fluvial lacustrian deposits of Pleistocene age, suffered high ratios of D4-D5 damage. In the historic center of the village, the D4-D5 ratios approach 100%, whereas portions of the village built on Miocene limestone suffered lower levels of damage. The village of Monticchio, 1.3 km southwest of Onna, is founded on Mesozoic limestone and Pleistocene breccia. This village suffered almost no damage in its unreinforced 2-3 story masonry residences nor any damage to reinforced concrete residential structures. The apparent elevated shaking intensity at Onna, as compared with the surrounding villages built on bedrock or stiffer alluvial debris, make it a good candidate for installation of a dense seismometer array to characterize site amplification effects of the valley fill relative to surrounding bedrock.

Heavy damage (D4 to D5) was also observed on two bridges crossing the Aterno river near Onna (Figure 68). The first bridge (Figure 68a) appears to have collapsed when the displacement exceeded the limit of the bridge bearings. The second bridge failed due to associated to ground failure at the abutment (Figure 68b).

Monticchio

The village on Monticchio is 1.5 km southwest of Onna ($R_{jb}$=0) on the right side of the Aterno river valley at an elevation around 600 m. It was built on a gentle slope at the toe of the northern part of Cavalletto mountain. In the south-western part of the village, Jurassic limestone outcrops (Figure 69). In other areas of Monticchio, this bedrock formation is covered by carbonate breccia of Pleistocene age, with thicknesses of 100 m and more.



*Figure 69. Monticchio: outcrop of the Jurassic limestone formation.*

The town is mostly 2-3 story masonry buildings and to a lesser extent RC buildings. The intensity assigned by QUEST team was VI. A D0-D1 damage was detected on both structure types throughout the village (Figure 70).

After the main shock, an accelerometer station was installed on a stiff formation by AMRA-CIMA to record aftershocks. Due to its position relative to Onna, and the relatively low intensity of shaking on bedrock and stiff carbonate breccia, this town is a good reference site for evaluating site amplification effects at Onna where another mobile station was installed by INGV Milan.

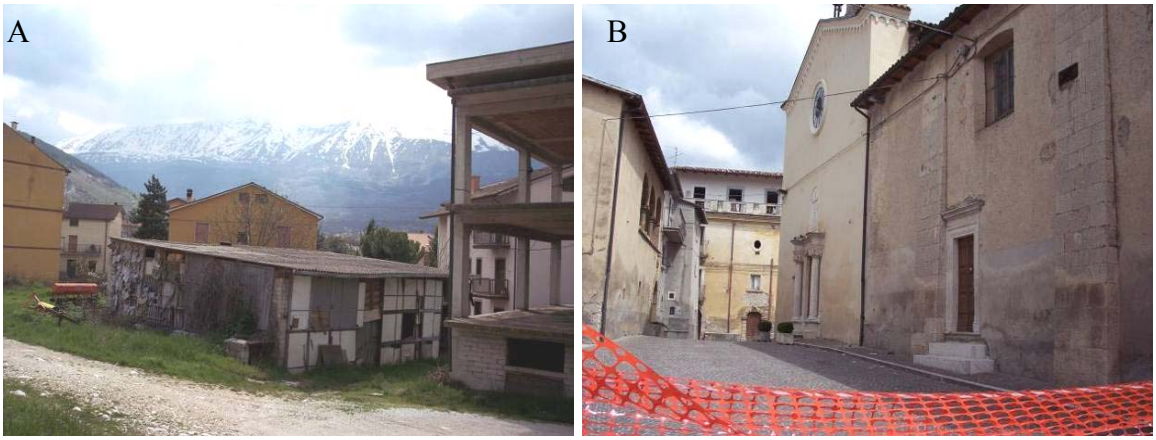



*Figure 70. Monticchio. (A) D0 damage level on different building structures, (B) D0 damage on monumental masonry buildings.*




*Figure 70. Monticchio. (C) D1 damage (fall of the cornice) on a masonry building.*

San Gregorio

The village of San Gregorio is on the western flank of the Aterno valley at 600 m elevation. The village extends over different geological formations (Figure 71): the western part is founded on fluvio-lacustrine deposits (lower to medium Pleistocene) consisting of gravels and conglomerates (this part of the village is not shown in the Bosi and Bertini, 1970, geological map, below); the historic center was built on top of alluvial deposits; Miocene limestone outcrops in the eastern part of the village.

The MCS intensity at San Gregorio reached IX and damage was mainly concentrated in the historic center founded on alluvium. At the town center, the majority of the buildings were constructed with poor quality masonry and most collapsed including the church (D5=75% and D4=25%) (Figure 72). The western part of the village was built on Pleistocene gravels and conglomerates (Figure 73) and did not have significant damage (50% D2, 25% D1 and 25% D0); the eastern part, largely consisting of RC buildings (Figure 74 and 75), founded on either alluvium and limestone showed different levels of damage (30% D4, 40% D3, 30% D2, 10% D1). San Gregorio is a good candidate for assessing site amplification effects in the same town over short baselines because of the different geologic units crossing the urbanized portions of the town. The limestone area in the eastern portion of the town would be an obvious candidate for a rock site to normalize the response of the alluvial section at the town's historic center.

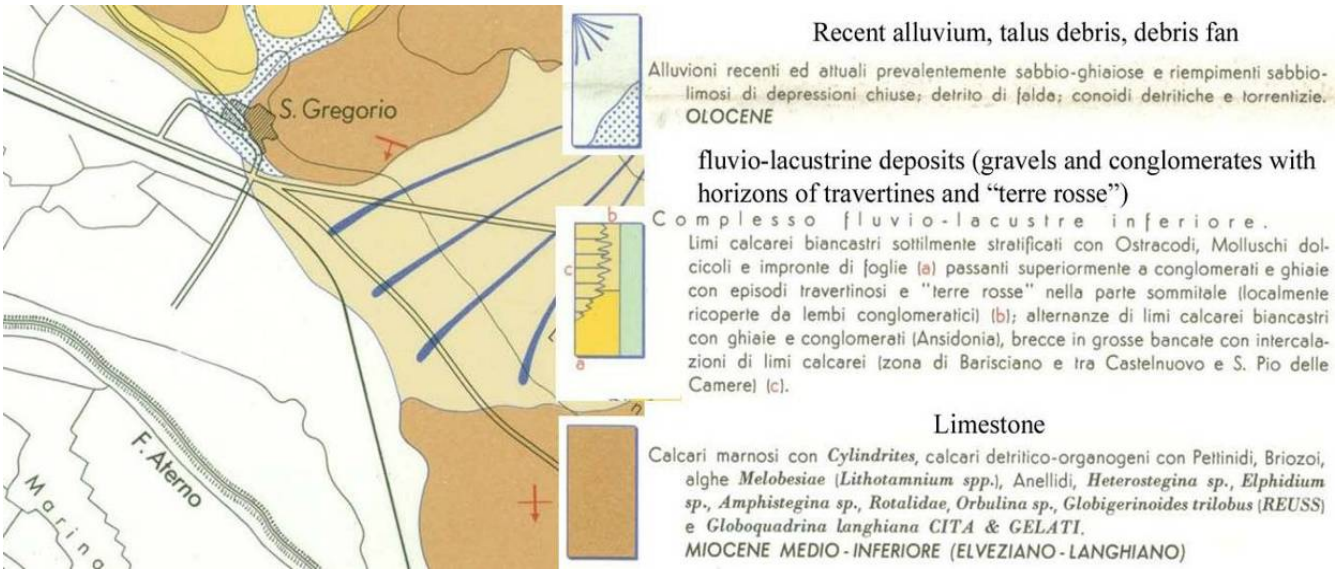



*Figure 71. Geological map of San Gregorio (after Bosi and Bertini, 1970).*




*Figure 72. San Gregorio. (A) View of the historic center with collapsed masonry buildings.*




*Figure 72. San Gregorio. (B) Remains of the church.*






*Figure 73. San Gregorio western part: masonry buildings with minor damages.*




*Figure 74. San Gregorio eastern part. (A) RC building "pancake" collapse, (B) Detail of sheared pillars.*




*Figure 75. San Gregorio eastern part. (A) RC building with structural damage, (B) Detail of the damage to the beam-column connection.*

**Other Towns and Villages in the Aterno Valley Region**

Fossa

The village of Fossa was built on the eastern flank of the Aterno valley (600-650 m elevation) along the slopes of Cavalletto mountain. It is on the hanging wall of the fault ($R_{jb}$=0), and the estimated MCS intensity was VII-VIII. Most of the village is built on talus debris from a ridge of Mesozoic limestone (Figure 76). The historic center is comprised principally of 2-3 story masonry buildings, whereas in the newer part of the village around the perimeter of the historic center is typically 2-3 story RC buildings. Heavy damage (D3/D4) was mostly concentrated in the historic part of the village, where masonry buildings of poor and irregular brickwork had vertical cracks in the walls. The rest of the village, composed of RC buildings and retrofitted masonry, had lower damage (D1-D2) (Figure 77). The church of Santa Maria ad Criptas built in the middle-ages was heavily damaged (D3).




*Figure 76. Geological map of Fossa (after Bosi and Bertini, 1970).*

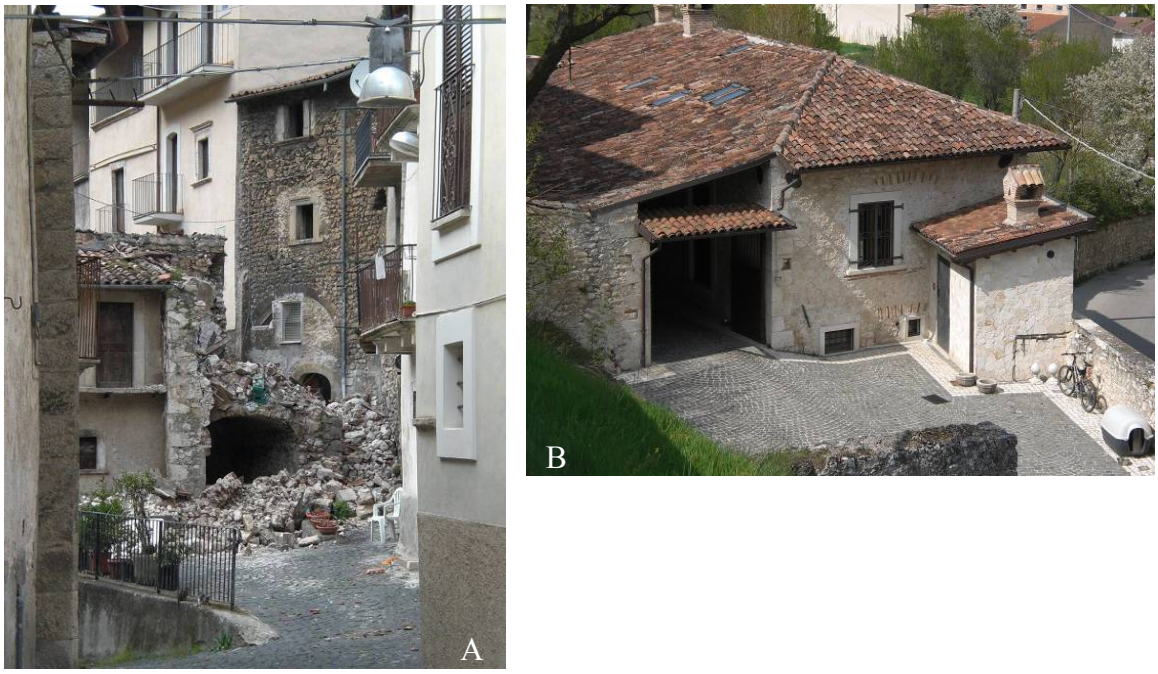



*Figure 77. Fossa. (A) Collapse of masonry constructions in the historic center, (B) Sstrengthened masonry construction with no damage.*

San Eusanio Forconese & Casentino

The villages of San Eusanio Forconese and Casentino are built on the eastern flank of the Aterno valley at 590 m and 630 m elevation, respectively. Both towns are on the hanging wall of the fault ($R_{jb}$=0). S. Eusanio village is built on fluvio-lacustrine deposits (medium Pleistocene) of sand and gravel with interbedded silts and clays. Casentino is built on talus debris (Figure 78).

The village of S. Eusanio is primarily composed of 2-3 story masonry buildings and, to a lesser extent, 2-3 story RC buildings. The MCS intensity was IX and the level of damage was high for the URM buildings (D4-D5~50%), whereas, low damage (D1) was observed in the RC buildings (Figures 79-81).

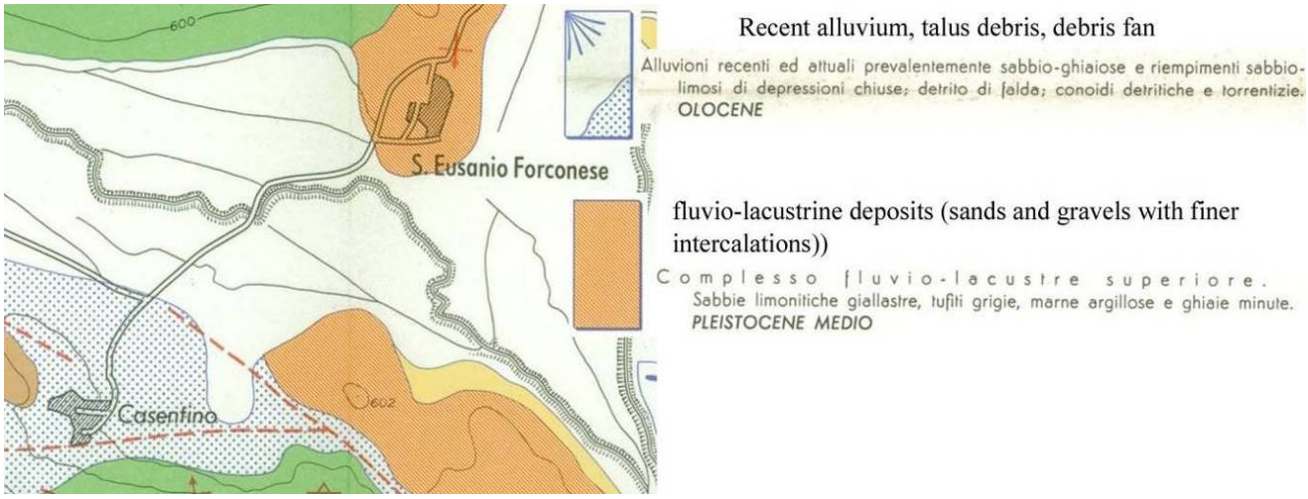



*Figure 78. Geological map of S. Eusanio Forconese and Casentino (Bosi and Bertini, 1970).*




*Figure 79. S. Eusanio Forconese village. (A) Partial collapse of masonry building (D4), (B) Slight damage to a RC building nearby (D1).*




*Figure 80. S. Eusanio Forconese. (A) Collapse of old masonry building (D5), (B) Partial collapse of masonry building (D4).*



*Figure 81. S. Eusanio Forconese: partial collapse of the masonry church (D4).*

In Casentino the MCS intensity was VIII. It was not possible to survey the inside of the village, but from the access road we observed a high level of damage (D4-D5) for the masonry buildings, and low damage (D1) for the few RC buildings (Figures 82 and 83).




*Figure 82. Casentino. (A) Partial collapse of the masonry building at the entrance of the village, (B) Collapse of old poor quality masonry buildings in the historic center.*



*Figure 83. Casentino masonry buildings with some wall cracks.*

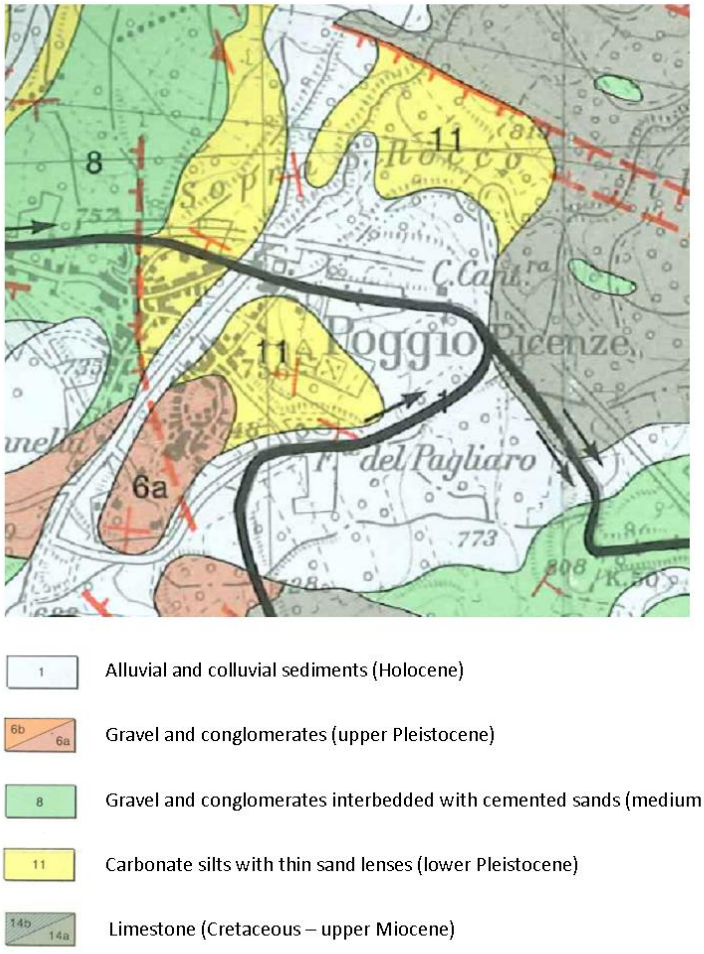



*Figure 84. Geological map of Poggio Picenze (modified after Bertini et al., 1989).*

Poggio Picenze

This town (695-760 m elevation) lies along a slope located on the north side of the river Aterno valley, very close to the surface projection of the fault plane ($R_{jb}$=1.5 km). The western side of the town is settled on a Pleistocene gravel and conglomerate (Figure 84); most of the historical center is on softer colluvium and the carbonate silt of the San Nicandro formation (Figure 85), locally covered by Pleistocene gravel. The MCS intensity degree at Poggio Picenze was VIII-IX. The 1461 earthquake produced an MCS intensity of X. The buildings are an approximately equal number of masonry and RC houses, mostly 2-3 stories tall. Both irregular stone and higher quality regular stone masonry houses are found throughout the town: The irregular stone houses were more heavily damaged (Figure 86a). In the historic center of the town, the masonry buildings including a monumental church (Figure 86c) were heavily damaged (typically, D3-D4), whereas, nearby RC buildings were almost unaffected by the shaking (Figure 86b). Minor damage was detected in the western and downhill parts of the town, where the soil is Pleistocene gravel and conglomerate.




*Figure 85. Outcrop of (A) San Nicandro carbonate silts (note the gravel cover).*




*Figure 85. Outcrop of (B) Pleistocene conglomerate.*




*Figure 86. Poggio Picenze. (A) Variable damage (D3-D4) on masonry buildings of different style.*




*Figure 86. Poggio Picenze. (B) Undamaged RC house (D0) close to the (C) monumental church (D3).*




*Figure 86. Poggio Picenze. (C) monumental church (D3).*

Villa Sant'Angelo

The village of Villa Sant'Angelo is at 560 m elevation on the east side of the Aterno river, on the hanging wall of the fault ($R_{jb}$=0). The MCS intensity was IX. The village is built on fluvio-lacustrine deposits of lower to medium Pleistocene age. These deposits are alternating beds of calcareous silt and coarse gravel-conglomerate (Figure 87). The historic center with mostly 2-3 stories poor quality masonry buildings suffered high damage levels (30% D5, 40% D4, and 30% D3). The perimeter of the village has numerous 2-3 stories RC buildings that had minor damage of D1-D2. Retrofitted old masonry buildings performed well and had only minor cracks (Figures 88 and 89).

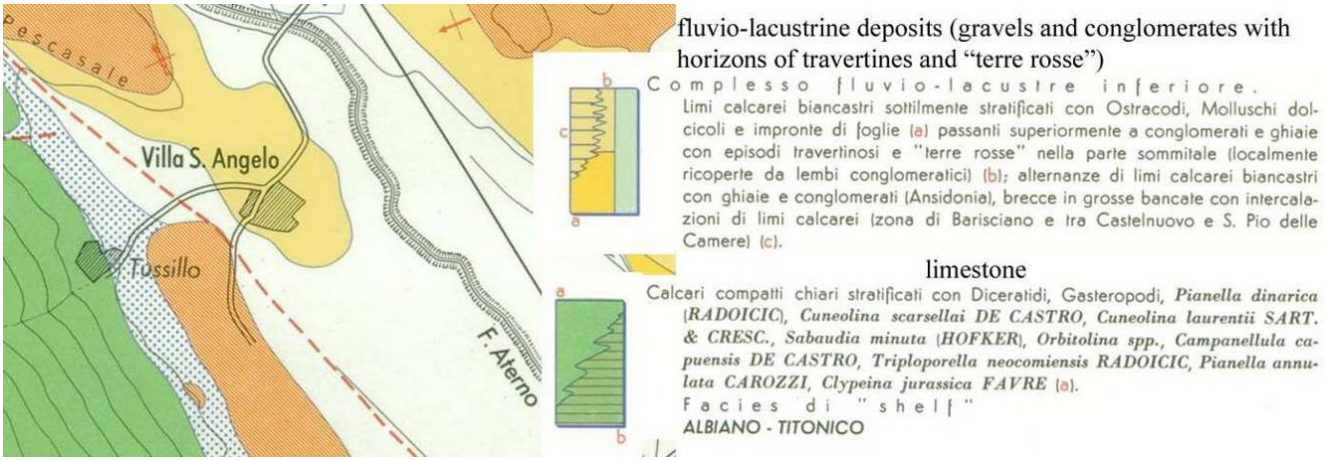



*Figure 87. Geological map of Villa S. Angelo (after Bosi and Bertini, 1970).*




*Figure 88. Villa S. Angel. (A) Collapsed masonry buildings (D5) in the historic center.*




*Figure 88. Villa S. Angel. (B) Reinforced masonry in the historic center with minor cracks in the highest story (D2).*




*Figure 89. Villa S. Angelo, historic center with (A) masonry building crack,; (B) partly collapsed church.*

Tussillo

The village of Tussillo rises on the eastern flank of the Aterno valley at 600 m elevation and is very close to Villa S. Angelo. Unlike Villa S. Angelo, the intensity felt at Tussillo was VII-VIII. The village is built on limestone (Figure 90). Buildings are of 2-3 stories masonry or reinforced concrete. The level of damage was D4-D5 for some of the older construction in the historic center, though no survey inside the village was allowed. Generally, the level of damage was lower than that observed in Villa S. Angelo.

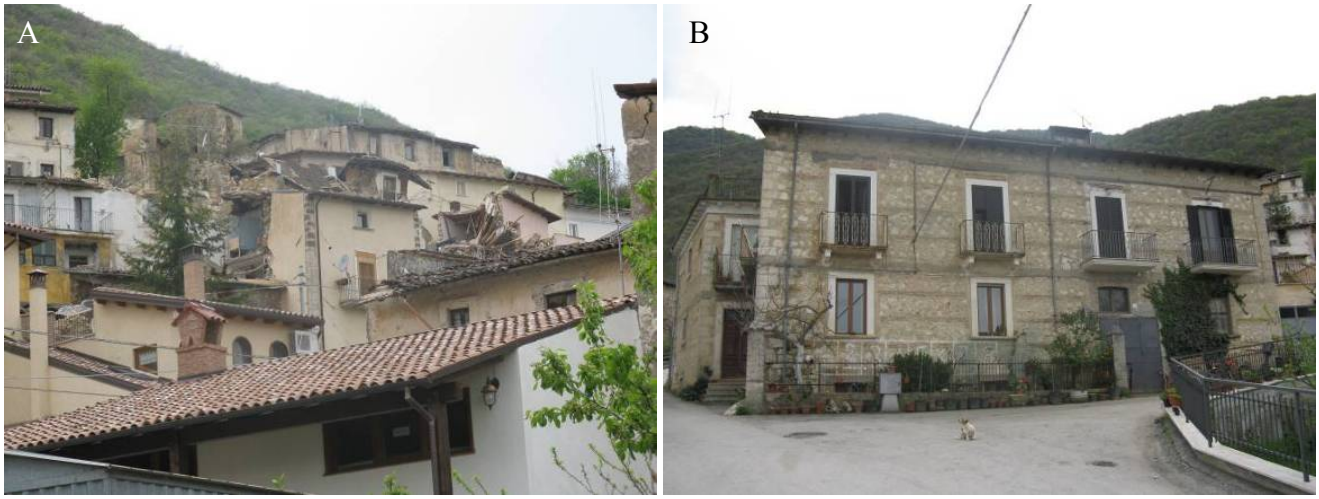



*Figure 90. Tussillo. (A) View of the historic center with some collapsed masonry buildings on the background, (B) Masonry building at the entrance of the village showing no damage.*

San Demetrio ne' Vestini

The village of San Demetrio ne' Vestini is on the western flank of the Aterno valley, between 670 and 700 m elevation, very close to the surface projection of the fault plane ($R_{jb}$=0.3 km). The village sits on Pleistocene gravels and conglomerates (Valle dell'Inferno unit), and partly on gravel and sand (San Giovanni unit) (Figure 91). The older part of the village mainly consists of 2-3 story masonry buildings of generally higher quality to those of the surrounding villages. Modern 2-3 story RC buildings form the town perimeter. The MCS intensity felt was VI-VII. The level of damage was low for masonry as well as RC buildings (30% D0, 60% D1 and 10% D2) (Figures 92 and 93). A few very old buildings, such as the "Madonna dei Raccomandati" church, were severely damaged (D4). The damage to the uppermost "Via Crucis" stations along a slope close to the village might indicate evidence of topographic amplification (Figure 94).

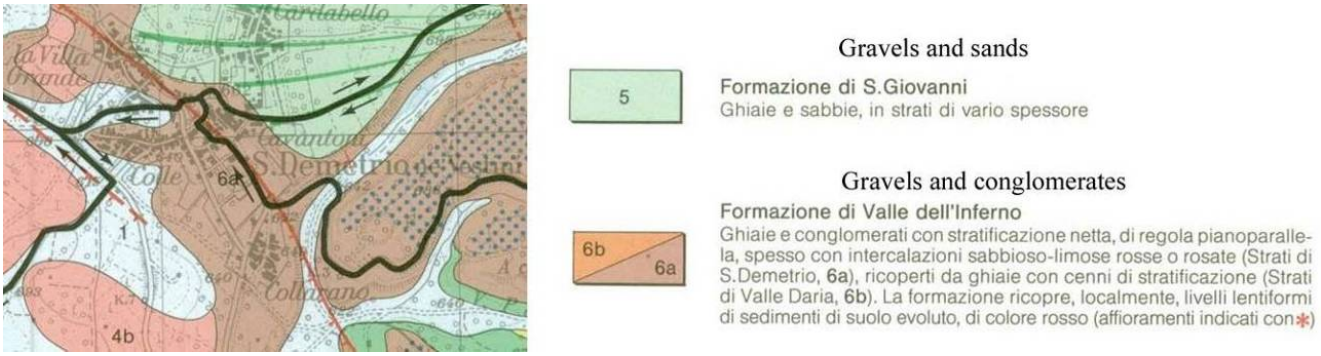



*Figure 91. Geological map of S. Demetrio ne' Vestini (Bertini et al., 1989).*

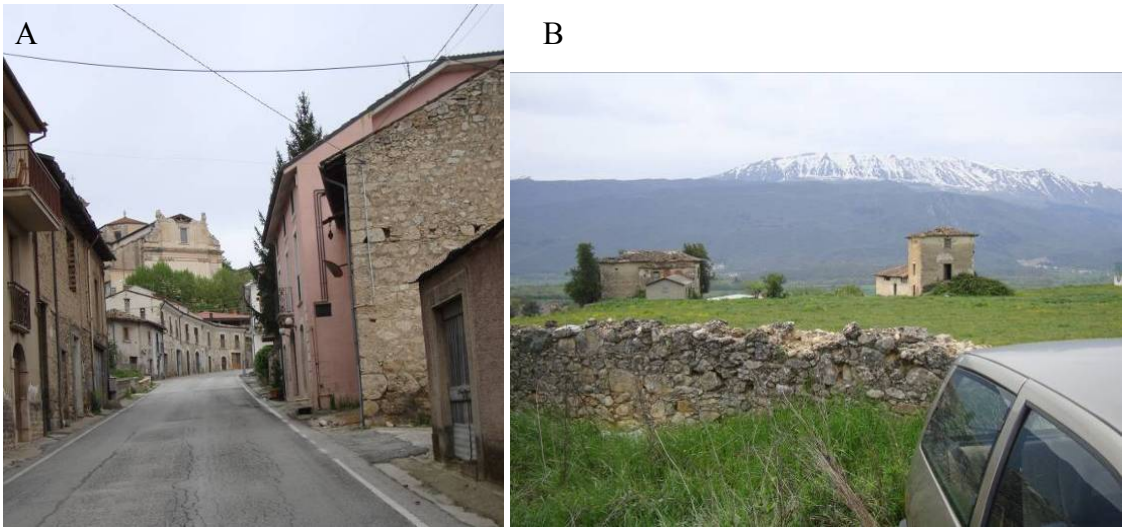



*Figure 92. San Demetrio ne' Vestini (A) access road to the village showing mostly masonry buildings with no damage, (B) old masonry buildings with no damages.*

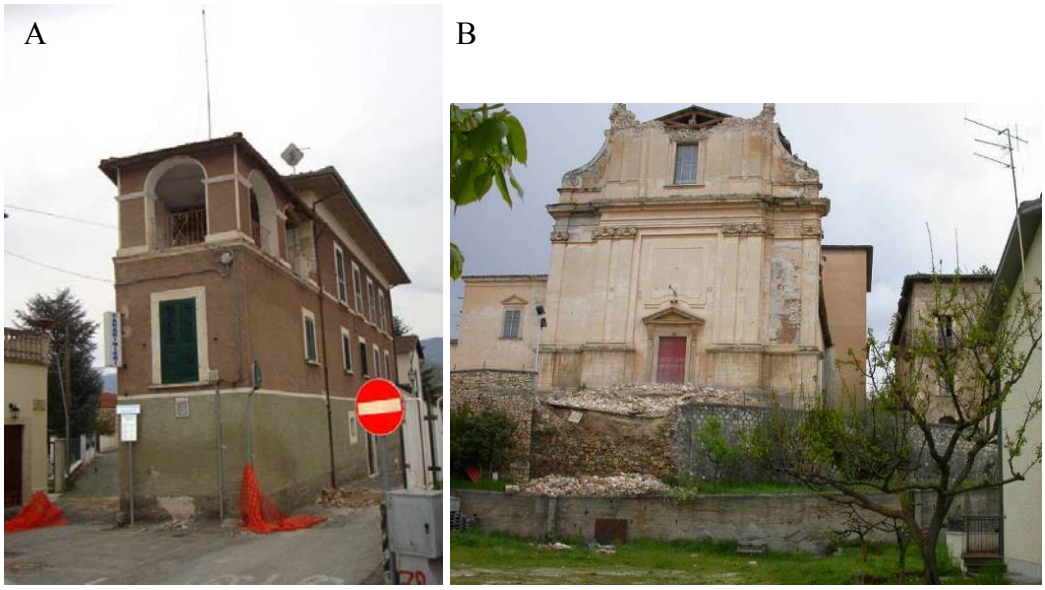



*Figure 93. San Demetrio ne' Vestin. (A) "Caserma dei Carabinieri" with cracks (not evident in the picture) and falls from the highest story, (B) Partial collapse of the tympanum of the facade of the Madonna dei Raccomandati church.*

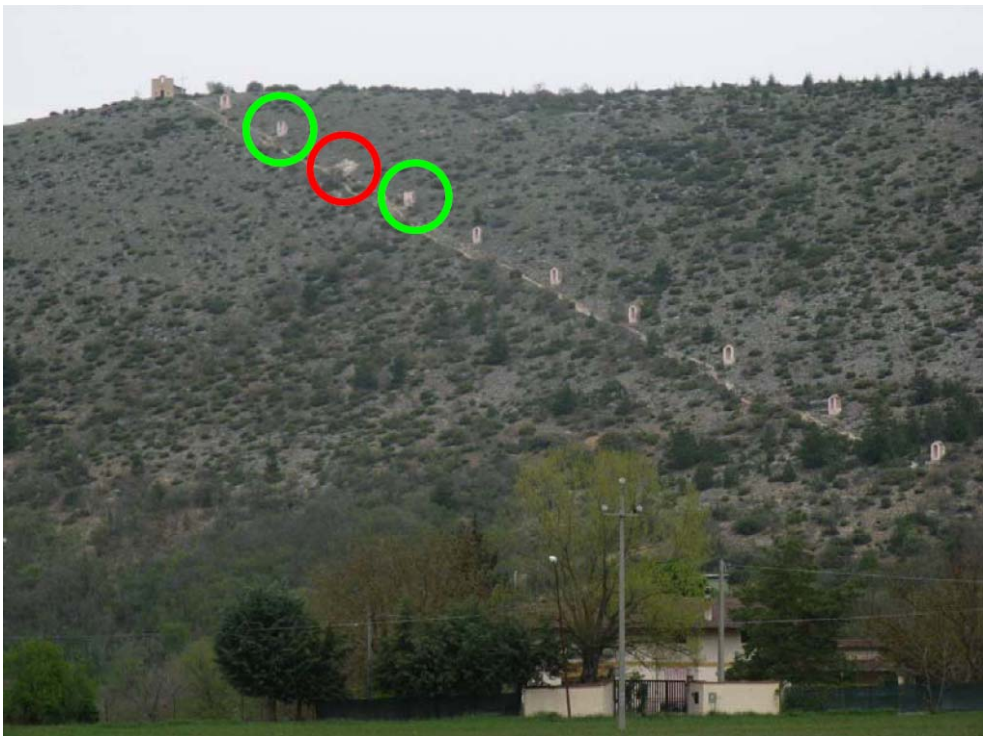


*Figure 94. San Demetrio ne' Vestini: damages at the "Via Crucis" stations constructed along the slope.*

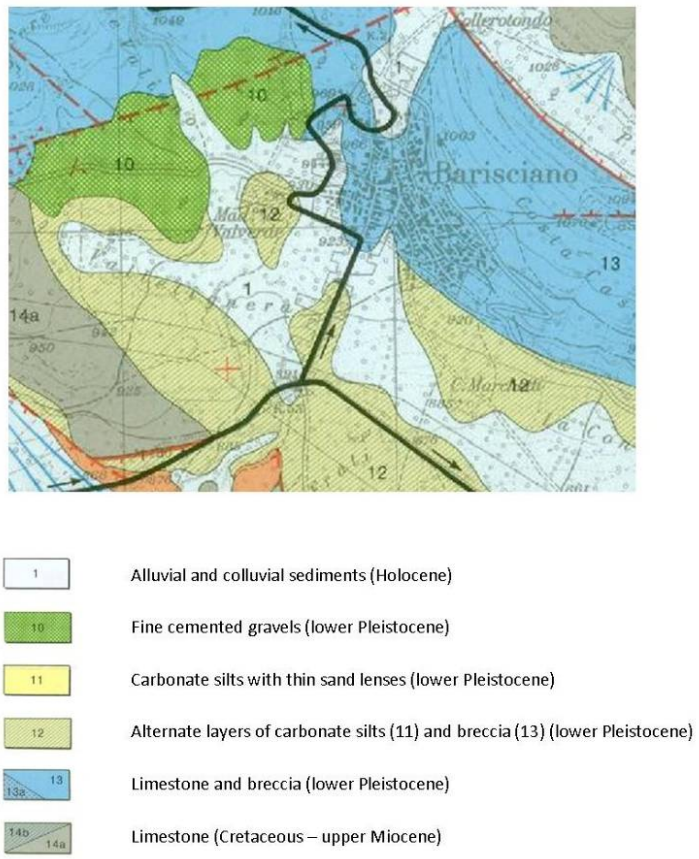



*Figure 95. Geological map of Barisciano (modified after Bertini et al., 1989).*

Barisciano

The village of Barisciano is at 900 and 1000 m elevation and is 5 km from the surface projection of the fault. It lies along a slope to the north of the Aterno river valley. It sits on a middle-lower Cretaceous-upper Miocene carbonate ridge (grey in Figure 95). The town center rests upon coarse calcareous Pleistocene breccia (light blue in Figure 95). The town center midway up the slope is mostly 2-3 story masonry construction, and more recent 2-3 story reinforced concrete structures are present uphill and downhill of the center. The MCS intensity was VI, but, there was some damage at D4/D5 level for some old masonry buildings (Figure 96a). Most structures were damaged at D1 levels (Figure 96b).




*Figure 96. Barisciano. (A) Collapse (D5) of an old masonry building in background, (B) Damages (D1/D2) to RC buildings.*

Goriano Sicoli

The village of Goriano Sicoli rises on the eastern flank of the Aterno valley at 720 m elevation and is 25 km from the surface projection of the fault. The village lies partly on limestone bedrock, and partly on talus debris and alluvial fan (Figure 97). The majority of the buildings are 2-3 story masonry buildings and RC buildings. The MCS intensity was VII. The damage was generally low (D1) in the part of the village founded on the bedrock, while significant damage (D3-D4) was observed in the western part of the village founded on talus debris and alluvial deposits (Figure 98). San Gemma church was also significantly damaged (D3).

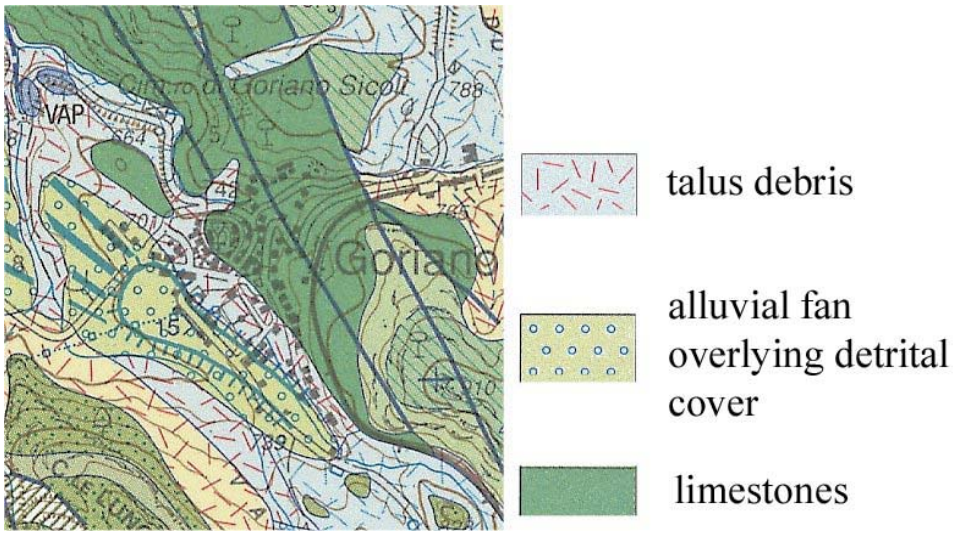



*Figure 97. Geological map of Goriano Sicoli (Carta Geologica d'Italia 1:50000).*




*Figure 98. Goriano Sicoli. (A) Diagonal cracks in a masonry building (D3, (B) Partially collapsed masonry school (D4).*

**Damage Patterns within L'Aquila**

Pettino Fault Region

The Pettino fault daylights NW of the L'Aquila city center with a NW-SE trend, as shown in Figure 99. West of the A24 highway, the fault marks the boundary between hills steeply dipping towards the southwest and sloped Pleistocene sediments, as shown in Figure 99. In this area there is almost no construction on the northeast side of the fault, as shown in Figure 100. The fault continues as a concealed trace on the east side of the A24 highway as shown by the red line in Figure 99. A survey of damage patterns in the vicinity of the fault was performed. The specific areas investigated are marked in yellow in Figure 101.

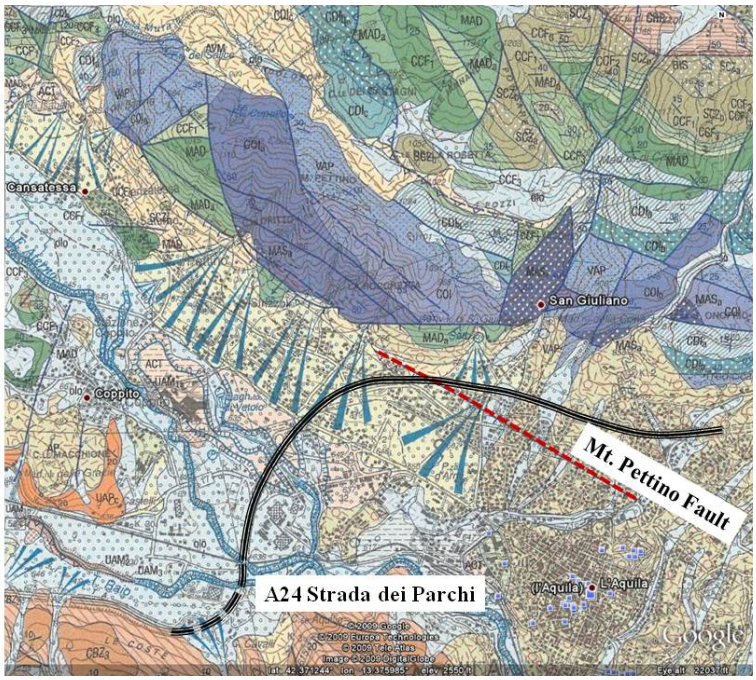



*Figure 99. Geology of the L'Aquila region (modified from INGV).*

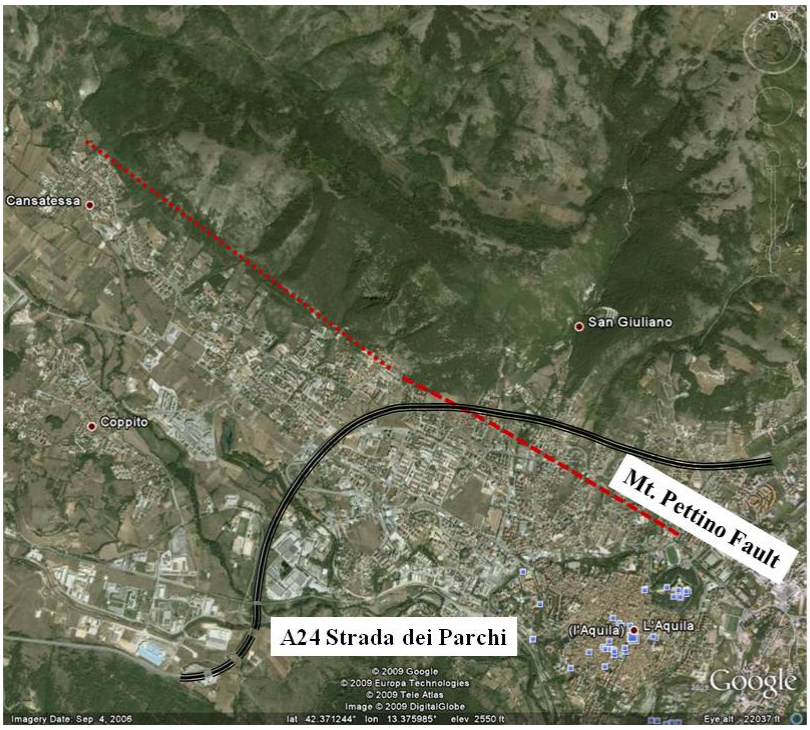



*Figure 100. (A) Geology of the L'Aquila region and (B) Satellite photo (from Google Earth) showing the Mt. Pettino Fault and its extension towards northwest.*

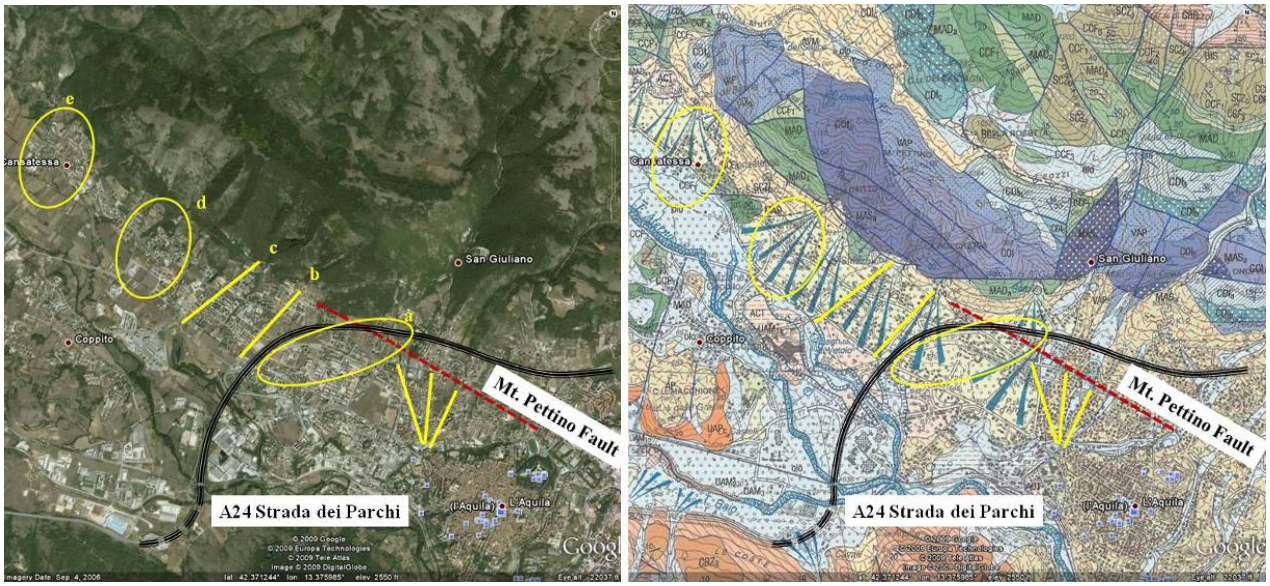



*Figure 101. Satellite photo from Google Earth of the L'Aquila showing the traces of the building damage survey lines in yellow.*

Within the zones marked in Figure 101, structure-by-structure damage surveys were performed in which structural performance was mapped according to the categories shown in Table 6. These relatively rapid structural assessments were based on the exterior appearance of the buildings from the street. Each damage level was assigned a colored marker in the map, as defined in Table 6. Figure 102 shows a general view of the damage survey results. This is a recently developed suburban area of L'Aquila, therefore most buildings are relatively modern reinforced concrete frame structures with masonry infill on exterior walls. Most residential buildings are two to four-stories high, with apartment buildings closer to the city center reaching 5 or 6 stories. The few collapses observed in the damage survey were of four-story reinforced

concrete buildings, typically at the ground floor level. Many structures in this area were not damaged, and where damage occurred, it generally involved relatively minor cracking (D1) to relatively severe cracking or collapse (D2) of the masonry infill walls. Incidents of serious structural damage in categories D3 or greater was relatively rare. It is possible the survey was not detailed enough to capture damage at the level of the single structural element from the outside; however, whenever D2 damage was visible, we took particular care to examine the structural elements that were visible.

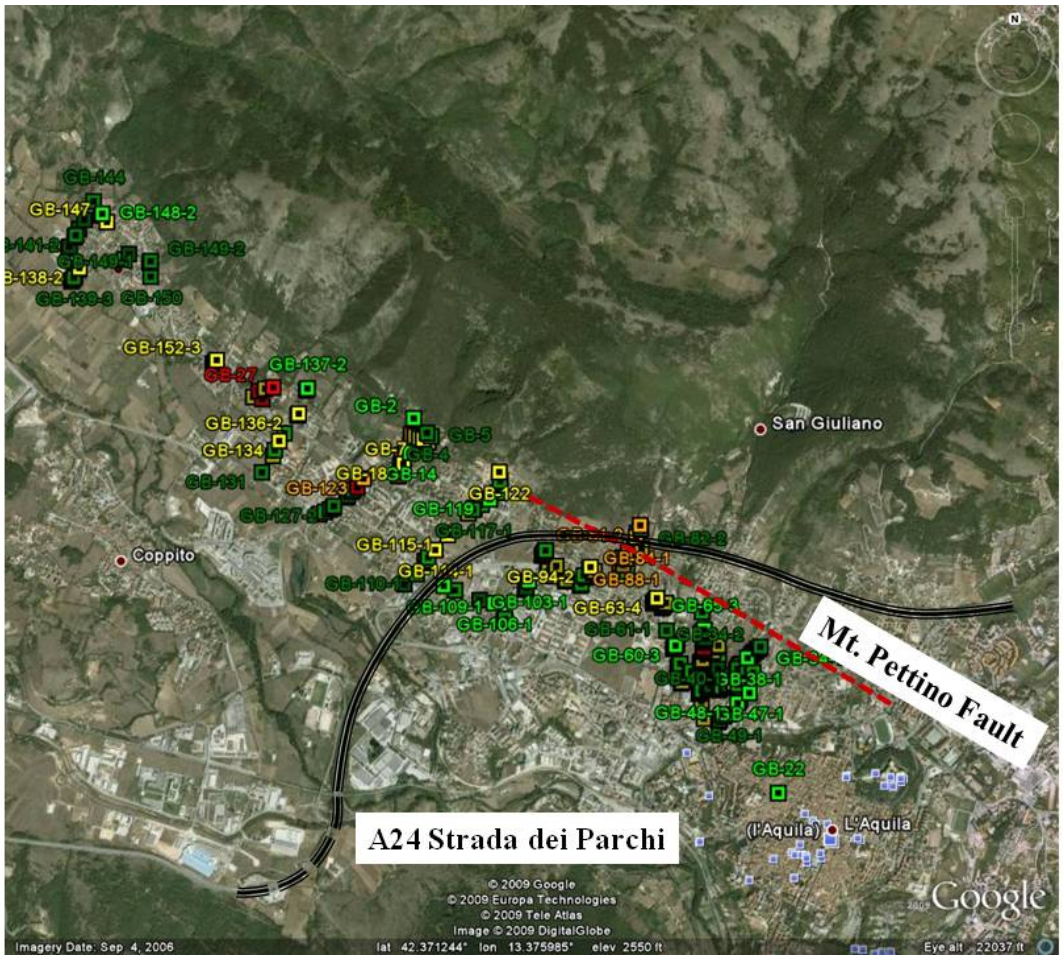


*Figure 102. Satellite photo from Google Earth of the L'Aquila with a general view of the building damage survey.*

Figures 103 and 107 show close-up views of the mapped zones marked (a) to (e) in Figure 101. Zone (a) is the easternmost mapped area. The concentration of structures with damage level D3 is higher in this area than anywhere else along the Mt. Pettino Fault. Waypoints GB-80-1 and GB-82-1 are both masonry structures (Figure 104a and b). The first one is an older and abandoned building, while the second was a family residence (Figure 105). The remaining waypoints are reinforced concrete structures with masonry infill ranging between 2 and 5 stories. Of the five structures in this zone with damage classified at the D3 level, four are 3-stories, and the fifth is a 4-story building. An example of D3 damage (from the building at waypoint GB-88-1) is shown in Figure 105. Another area with a number of collapsed buildings is located in zone (a). These are all reinforced concrete structures, 3- to 4-story high in which the ground floor columns collapsed, causing it to pancake (Figure 106). Although high levels of damage are concentrated in this small area, similar buildings on adjacent streets show D2-level damage. Damage in zone (b) of the survey was generally lower, with only a few structures suffering D2 levels (Figure 107). Moving northwest, damage levels increase in zone (c), with a higher concentration of apartment buildings with minor structural damage (D3). Many of these buildings are actually the same design oriented differently. The area of collapsed buildings in zone (d) is isolated. Figure 107 shows in detail the location of the buildings in the damage cluster and Figures 108-110 show examples of damage in this area. The ground floor collapsed in the structures at waypoints GB-23-1 and GB-24-1. From conversations with the owners of units in the lightly damaged building, structures at waypoint GB-22-1 (D1) and GB-24-1 (D5) were built by the same construction company, but GB-

24-1 was built a year before the other. Similarly, GB-23-1 (D5) was constructed by the same company as GB-25-1 (D2). All buildings were constructed in the mid-1980s. New construction to the southeast of GB-26-1 (D2) showed no damage at all (D0) in spite of the rigid external brick cladding. In zone (e) at the northwest end of the surveyed zone, the damage falls to D0 and D1 levels (Figure 107).

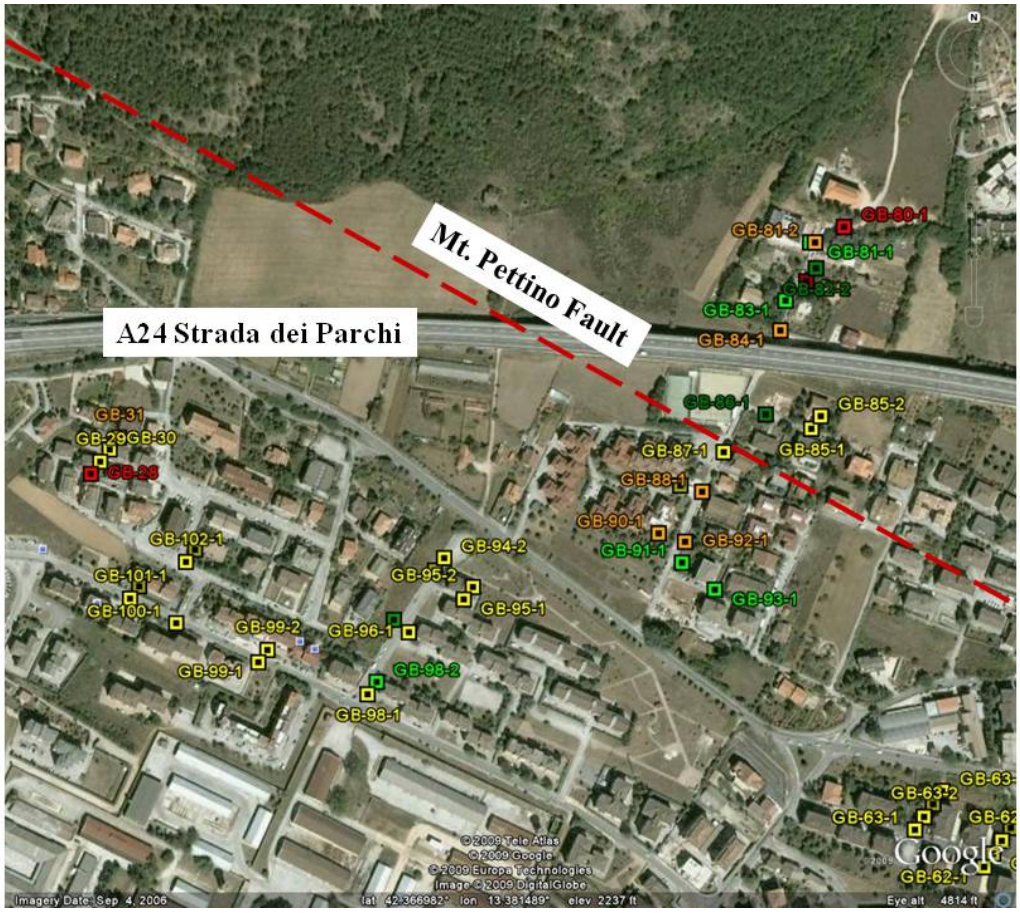


*Figure 103. Zone (a) of the building damage survey along the Mt. Pettino Fault.*


*Figure 104. Masonry structure at waypoint GB-82-1.*



*Figure 105. Example of D3 damage in the building at waypoint GB-88-1.*



*Figure 106. Example of D5 damage in the building at waypoints GB-27-1 and GB-28-1.*






*Figure 107. Results of the building damage survey along the Mt. Pettino Fault: Zones b, c, d, and e.*




*Figure 108. Cluster of damage in zone (d).*




*Figure 109. Damage on the structures in the cluster in zone (d). (A) Waypoint GB-22-1 (D1), (B) Waypoint GB-23-1 (D5).*




*Figure 110. Damage on the structures in the cluster in zone (d). (A) Waypoint GB-24-1 (D5).*




*Figure 110. Damage on the structures in the cluster in zone (d). (B) Waypoint GB-25-1 (D2).*




*Figure 110. Damage on the structures in the cluster in zone (d). (C) Waypoint GB-26-1 (D2).*

As shown in Figure 111, north and west of the L'Aquila town center, the Pleistocene terrace deposits on which most of L'Aquila sets are eroded, and the resulting channels are partially filled with Holocene sediments. Some of those channels are developed with similar styles of construction to those on the adjoining terrace deposits. The type of construction is generally similar to that described in the previous section (Pettino fault region) – mostly RC structures of 3-6 story height, although there are some masonry buildings as well. Where we have adjoining this terrace/channel deposits, we typically found higher damage levels in the swales.

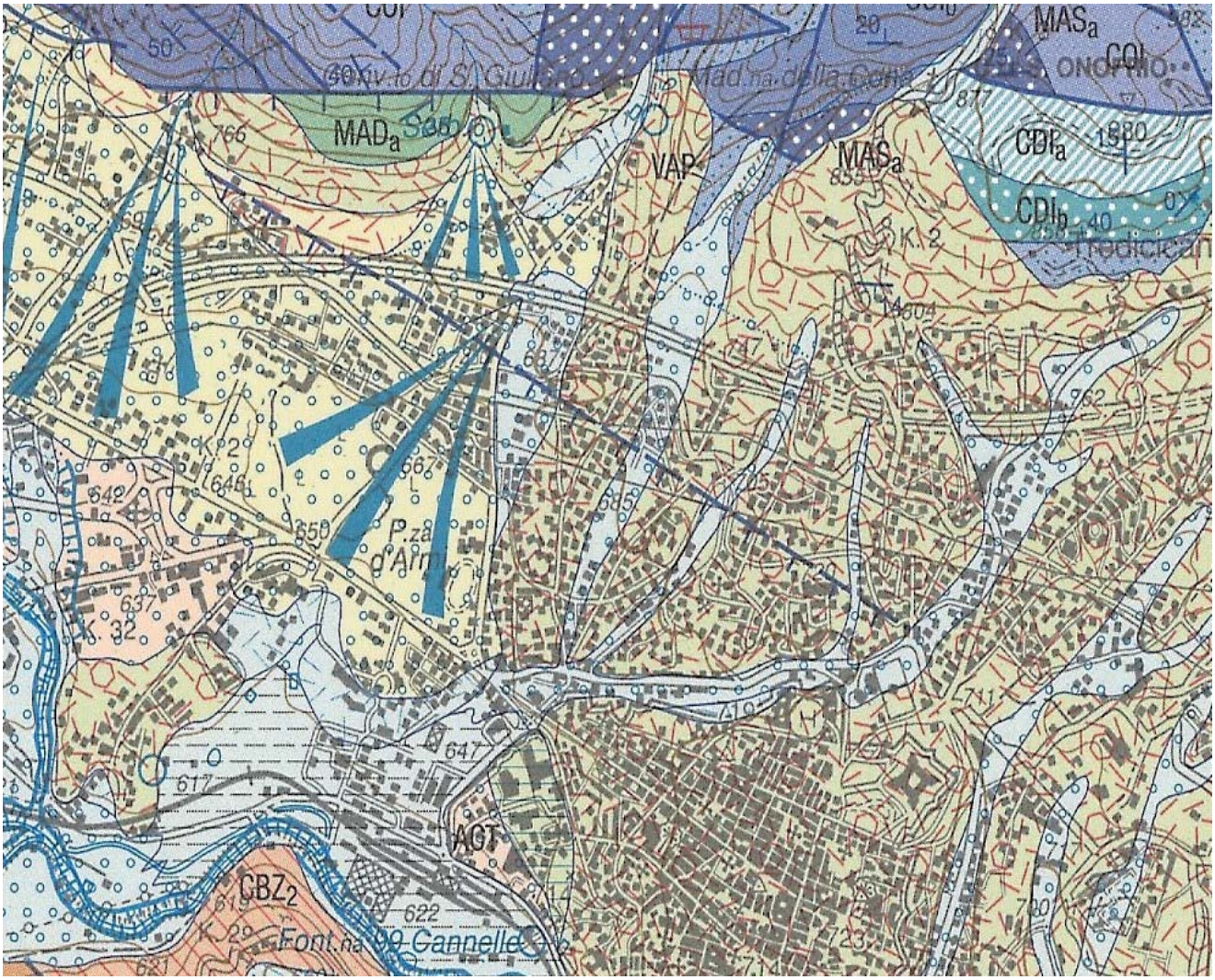



*Figure 111. Geological map of the area north of L'Aquila old center.*

**GROUND FAILURE**

**Introduction**

Observed ground failures, defined as permanent ground deformations induced by the earthquake, were for the most part relatively minor. Observed ground failures were related mainly to slope instability, localized incidents of lateral spreading, collapse of some underground cavities, and seismic compression of unsaturated soils. Figure 112 is a reference map with the locations of specific sites discussed subsequently. This section does not include discussion of ground failure near the Paganica fault, which was interpreted as surface fault rupture.

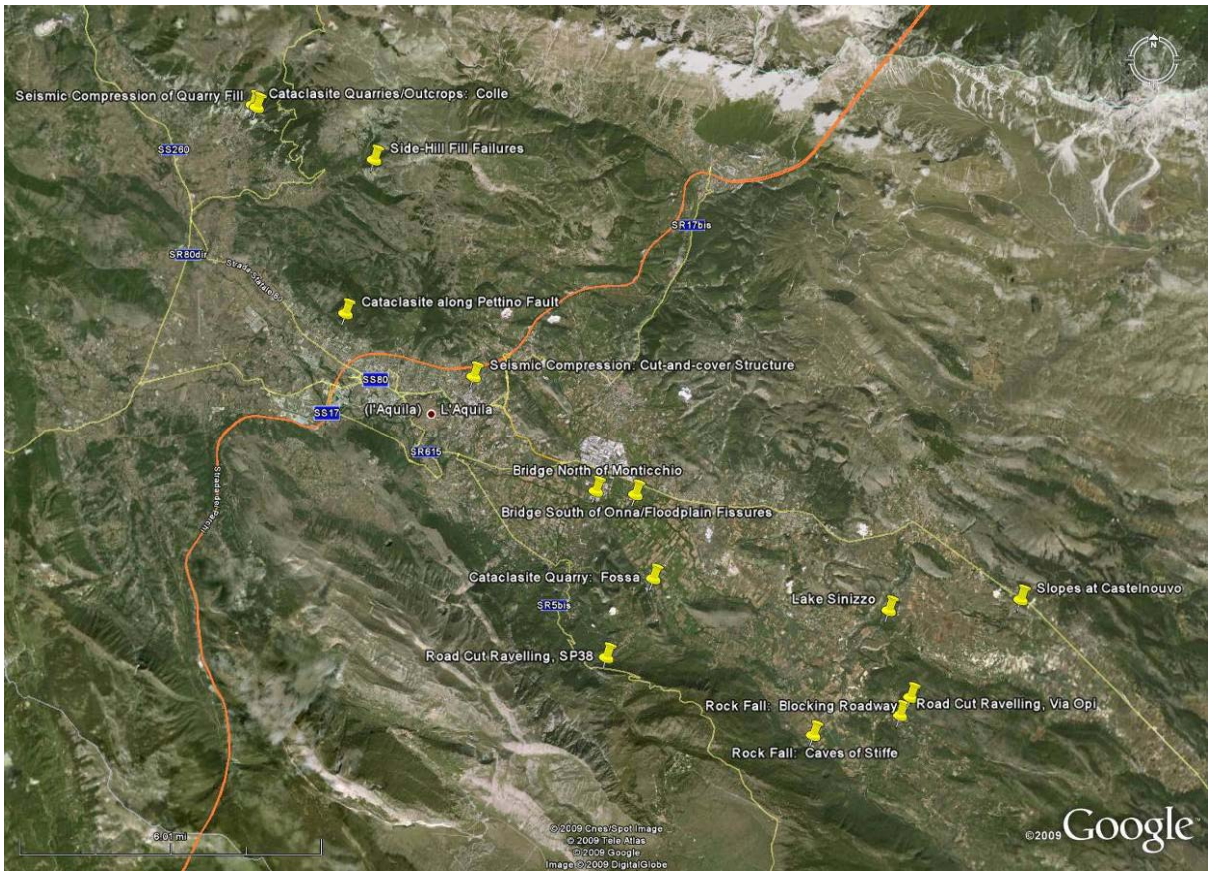



*Figure 112. Reference map with locations of specific sites.*

**Slope Instability**

Mountains surrounding the L'Aquila area are rugged; however, only limited occurrences of significant slope instability were observed. Typically, the failures were localized and minor, with modes including ravelling and sloughing of road cuts, quarries, and natural outcrops, permanent displacement of fill embankments, and rock falls. Examples of typical slope failures are summarized below, together with an interesting case of permanent displacement of saturated sediments around the margin of Lake Sinizzo.

The areas investigated by the GEER team for landslide occurrences include the middle Aterno valley south of L'Aquila between two SW-NE sections passing through Paganica (north) and Stiffe (south) and the SW flank of the Aterno valley north of L'Aquila. Our work focused on the southern Aterno valley and in the plateau located to the SW of the Aterno valley (i.e. Altopiano delle Rocche).

The geology of the subject region is described in the Earthquake Setting and Source Characteristics section above. Non-seismic landslides are relatively rare in the region due to favourable geologic conditions. Slope failures induced by the earthquake generally occurred in bedrock and in cemented layers within the continental deposits (conglomerates, travertines, breccias). The failures were local features confined within the shallower portions of the outcrops. The instabilities generally fall into three categories:

(a) Rock falls in limestone and marly-sandstone formations, including single blocks (a1), ravelling of intensely fractured rock masses of modest (a2) to large (a3) volume.
(b) Small slumps/slides and minor ravelling/sloughing on cut slopes (road cuts, quarries) in colluvium, cataclastic limestones, slightly cemented breccias/conglomerates, or debris;
(c) Debris flow/avalanches.

Our observations of instabilities are organized into subsections consistent with the above categories.

Ground shaking was sufficient to destabilize loose (and perhaps somewhat precarious) surficial rock blocks that subsequently travelled downhill as rock falls. Falls of this type were observed:

1. To the south-east of L'Aquila along both flanks of the Aterno valley in the limestone bedrock (example shown in Figure 113a):

(a) within Fossa village and on the cliffs overlooking the road between Monticchio and Fossa;
(b) between Paganica and Camarda, see Figure 113b from ISPRA (2009a,b);
(c) at Stiffe village at cave entrance and road above the village (discussed further below);
(d) along a road from Caporciano to Opi in the southern Aterno valley (see Figure 113c from ISPRA (2009a,b)).

2. To the south-east of L'Aquila in sound conglomerate or breccia layers of the continental deposits at S.Demetrio, Poggio Picenze, and Barisciano.

3. To the south-west of L'Aquila in the limestone bedrock:

(a) along the Raio valley (Lucoli, Casamaina);
(b) on the Altopiano delle Rocche plateau, on top of the right flank of the Aterno valley (Terranera, Ovindoli);
(c) along the Eastern flank of Mt. Ocre;
(d) at Goriano Sicoli.

Relatively detailed investigation and mapping was performed for a rock fall event at the Caves of Stiffe (Grotte di Stiffe). In this case, a large block was liberated from the slope high above this popular tourist area and impacted a concession building (Figure 114). The last impact mark of the block prior to impacting a building is at a distance from the building of about 15 m (Figure 115), indicating high velocity of the block. Additional impact marks are indicated by an alignment of fresh scars progressing up the hillside (Figure 116).




*Figure 113. (A) Large block of a rock fall event (42.266N, 13.585E).*

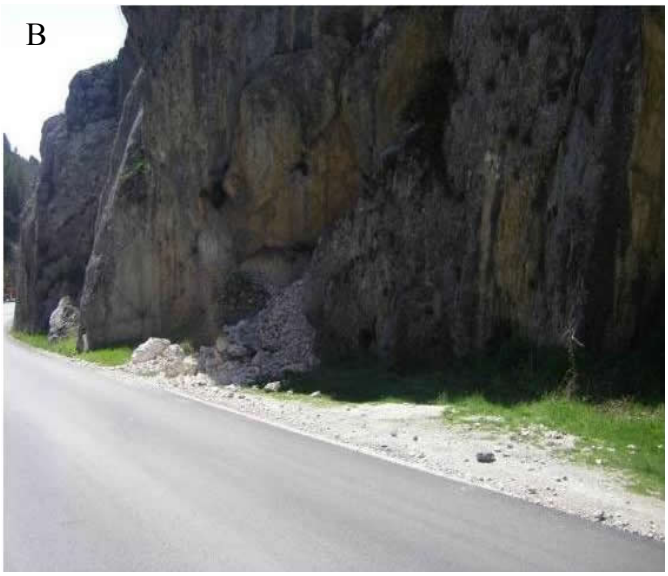



*Figure 113. (B) Rock fall between Paganica and Camarda, (from ISPRA, 2009a,b).*




*Figure 113. (C) Rock fall along a road from Caporciano to Opi in the southern Aterno valley (from ISPRA, 2009a,b).*



*Figure 114. Rock fall impact at the Caves of Stiffe (42.255N 13.547E).*



*Figure 115. Last impact mark prior to impacting building at the Caves of Stiffe; the block trajectory was above the small tree (42.255N 13.547E).*



*Figure 116. Additional impact marks as indicated by an alignment of fresh scars (42.255N 13.547E).*

Ravelling of Modest Volume on Intensely Fractured Rock Slopes (a3)

Typical ravelling-type failures of cut slopes made into the strong and fractured limestone bedrock dominating the local geology are shown in Figures 117 and 118. The failures involved the uppermost weathered blocks that are bounded by soil-filled joints. These examples are located along SP38 approximately 9.5 km south of L'Aquila. In general, the performance of cut slopes into the limestone bedrock was excellent, and minor surficial failures were not widespread.



*Figure 117. Shallow ravelling-type failure of weathered limestone blocks (42.278N, 13.467E).*



*Figure 118. Shallow ravelling-type failure of weathered limestone blocks (42.278N, 13.468E).*



*Figure 119. View of Fossa from Mt. Di Cerro. The detachment area of the rock failure that generated the rock avalanche is circled (42.29274N,13.48575E).*



*Figure 120. View of the cliff overlooking the northeastern side of Lake Sinizzo. Two failures in the overhanging thick layers of conglomerates are apparent with the related rock avalanches (42.292N, 13.580E).*

Ravelling of Large Volume on Intensely Fractured Rock Slopes (a3)

Relatively large-volume rock falls occurred above Fossa and Lake Sinizzo (S.Demetrio). As shown in Figure 119, the former involved the southern part of a steep limestone cliff and generated a small rock avalanche onto a road. Some outrunner blocks threatened the outermost buildings of Fossa. Figure 120 shows the rock cliff above Lake Sinizzo, formed by alterations of gravel and conglomerate layers with intercalations of finer horizons. Differences in strength and erodibility between the materials cause some conglomerate layers to overhang. Shear or tensile failure of the rock layers occurred and generated rock avalanches. The lake is on the prolongation of the Paganica fault and its sides were affected by apparent ground ruptures.

Quarry and road cut faces in these materials were found to be affected by ravelling, slides and slumps. Minor ravelling of weakly cemented sand and gravel, as depicted in Figure 121 and 122, occurred locally but significant or deep-seated failures in such deposits were not observed.



*Figure 121. Minor ravelling of weakly cemented sand and gravel; dashed lines indicate the extent of freshly deposited talus along the base of road cut (Via Opi N42.261, E13.581).*



*Figure 122. Ravelling along the road from S. Demetrio to Lake Sinizzo (42.28845N,13.56442E).*

Cuts made into silty clayey colluvium also generally performed well, and only minor instances of shallow sloughing as shown in Figure 123 was observed. A larger failure affected a road cut excavated in breccias on the road from Barisciano to S. Stefano di Sessanio (Figure 124). Besides the collapsed material the presence of stepped ground surfaces with apparent tension cracks was observed behind the top of slope. Small slides and ravelling occurred also in pervasively jointed limestones (Scaglia formation) on the eastern flank of the hill of Bazzano, which overlooks the SS17 highway (Figure 125). Slides did not exceed few tens of $m^3$ but were widespread over the whole slope.

Several quarries in the region surrounding L'Aquila have been developed in cataclastic geologic units formed along the base of the bounding mountain ranges. Cataclasites are created by the mechanical breakdown of bedrock materials resulting from past major fault activity. In the region they are typically white to light gray, cemented, with strongly interlocked clasts ranging from fines to boulder sizes. Typical characteristics of the cataclasite, as exposed along the Pettino fault approximately 4.0 km northwest of L'Aquila, are depicted in Figure 126. Quarries in the cataclasite were also observed in Fossa (Figure 127) and northeast of the town of Colle (Figures 128 and 129). These quarries performed very well, with only localized and insignificant minor ravelling. Small slides on cut faces of abandoned quarries in pervasively fractured/cataclastic limestones were observed on the SS80 State highway uphill from Arischia (Figures 130 and 131).

Approximately 300 m east of the quarry depicted in Figure 127, and continuing along the base of the northwest-trending mountain range, are natural outcrops of the cataclasite. The outcrops are recognizable by their characteristic white to light gray erosional scars (Figure 132). Although the natural slopes also experienced only minor and localized ravelling-type failures, their occurrence (Figure 133) is greater than observed in the nearby cataclasite quarries. This is potentially attributable to the relative absence of weak and weathered near-surface material in the quarries, having already been removed by mining operations. In the same area, failures were observed on the road from Fossa to the S. Angelo D'Ocre convent (Figure 134).

Near the convent, ravelling was observed at the base of a natural rock spur (Figure 135), which is affected by persistent subvertical fractures isolating large prisms that are backward tilted by a larger block slump. This area is reported as a landslide area in the 1:50000 geological map (sheet 359). Therefore except for the ravelling (that was surely caused by the earthquake), re-activation or triggering of larger phenomena is to be clarified through aerial photo interpretation and direct surveys that were not possible due to road closure.



*Figure 123. Shallow sloughing of regolith along road cut (southern flank of Castelnuovo N42.294, E13.628).*



*Figure 124. Slides and topples along the road from Barisciano to S.Stefano.(DC-11-1; 42.3349N, 13.5796E).*

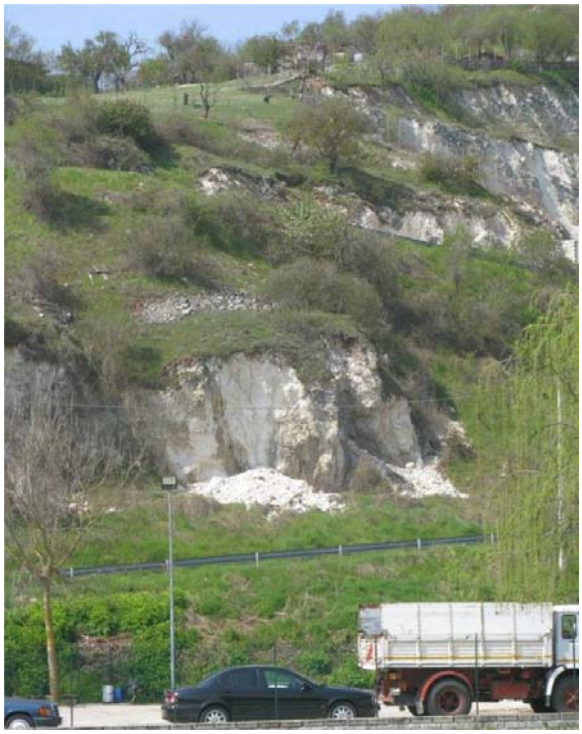


*Figure 125. Slides on the eastern flank of the Bazzano hill (in the foreground SS17 highway) (42.34005N, 13.45560E).*



*Figure 126. Cataclasite exposed along the Pettino Fault (left) and detail of cemented and interlocked particulate structure (right) (42.376N, 13.365E).*



*Figure 127. Quarry in Cataclasite with estimated 60° slopes up to approximately 35 m high, located in Fossa (42.300N, 13.485E).*



*Figure 128. Quarry in Cataclasite with near vertical slopes segments up to approximately 15 m high, located northeast of Colle (42.435N, 13.330E).*



*Figure 129. Quarry in Cataclasite with estimated 50° slopes up to approximately 60 m high, located northeast of Colle (42.437N, 13.328E).*



*Fig. 130. Slide of a small wedge in cataclastic limestones on the SS80 at km 16.5, uphill from Arischia (42.41973N, 13.34926E).*



*Figure 131. Ravelling in pervasively fractured/cataclastic limestones on a road cut retained by steel-net protections on SS80 at km 18.2: (DC-18-1) (42.4281N, 13.3460E).*



*Figure 132. Characteristic erosional scars developed in cataclasite (42.434N, 13.334E).*



*Figure 133. Characteristic ravelling-type failure in natural outcrops of cataclasite; partially buried pine trees evidence recent movement (42.434N, 13.334E).*



*Figure 134. Slides in cataclasites along the road from Fossa to S.Angelo d'Ocre. Detail of the spur on the right is in fig 5.24 (42.29694N, 13.48469E).*



*Figure 135. Detail of Fig. 5.23 showing the rock spur near the S.Angelo convent (42.30087N, 13.47829E).*

Debris Flows (Type c)

Landslides occurred on the southern flank of Mt. San Franco (to the north-east of L'Aquila) and crossed the SP86 highway between Assergi and Capannelle Pass. The area had been affected by debris flows involving the talus debris as the image in Figure 136, taken before the earthquake, illustrates. In the days following the earthquake the debris flows re-activated and a slide mass consisting of debris and snow/ice crossed the road (Figure 137).

The role of the earthquake is to be clarified; in fact the debris flows are not co-seismic with the mainshock. Their triggering can be due to the combined action of the aftershocks and the severe rainfall conditions that occurred in the days following the main seismic event. Furthermore it is worth noting that the snow depths were unusually high for the mid-April time frame of these observations. The role of the mainshock in triggering snow avalanches deposited on the debris cannot be excluded.




*Figure 136. Left view of the Mt. San Franco flank on 4-30-2009. Right: image from Google Earth taken before the earthquake showing the debris flows (42.4368N, 13.5796E).*



*Figure 137. Debris flow body invading the SP86. (Courtesy of Dr. Roberta Giuliani, DPC-SISM) (42.4368N, 13.5796E).*

**Embankments and Fills**

Few observations of side-hill fill embankment failures were made, with the exception of failures within a series of tight switchbacks along an unpaved rural access road located approximately 8.0 km north of L'Aquila. Headscarps of the failures, as depicted in Figures 138 and 139, appear to coincide with the approximate cut-fill contact. Corresponding maximum lateral and vertical displacements are estimated at about 2.0 m and 1.0 m, respectively.

Along the Aterno River and south and west of Onna are two bridges that suffered significant damage. In both cases, evidence of ground failure was observed in the abutment areas. The failures were represented as fissures oriented approximately parallel to the river alignment, developed in the alluvial floodplain at distances up to about 150 m from the river (Figure 140). Additionally, significant ground cracking was observed along the approach fills and foundation abutment/flood protection levee, with orientations tending parallel to the local strike of slope.

Along the approach road to the bridge directly south of Onna are a series of about ten cracks oriented parallel to the river alignment and at distances ranging from about 15 to 160 m from the Aterno River (Figure 141). The cracks are primarily tensional, extending through the asphalt but not into the sub-base or approach fill embankment (Figure 142). These cracks, together with those such as depicted in Figure 140, record permanent ground displacement that is consistent with the possibility of minor lateral spreading of the alluvial floodplain sediments toward the Aterno River.

Adjacent to the bridge abutment south of Onna, significant but localized cracking of the flood protection levee was observed, as shown in Figures 143 and 144. The observed cracks are oriented subparallel to the Aterno River and are consistent with permanent displacement toward the free faces of the levee.

Approximately 1.3 km upstream and east of the ground failures summarized in Figures 140 through 144 is the site of a bridge collapse, north of the town of Monticchio (Figure 145). The approach fill exhibits linear cracks along the road shoulder that indicate on the order of 10-15 cm of permanent lateral displacement toward the local free face condition (Figure 146). Although the flood protection levee has side slopes up to about 1.25:1 (horizontal to vertical) and appeared to be in a rather loose condition at the surface, the levee generally performed well in the area of the bridge failure (Figure 147). An exception is the western abutment on the northern side of the river. As depicted in Figure 148, directly beneath the abutment, a levee crack having a maximum width of about 6 cm and down-dropped 2-3 cm toward the river developed. From the observations made, it is not clear if the levee damage occurred first and possibly contributed to the collapse, or if the deck collapse enabled localized failure of the levee.



*Figure 138. Failure of side-hill fill embankment (42.420N 13.376E).*



*Figure 139. Failure of side-hill fill embankment (42.420N 13.376E).*

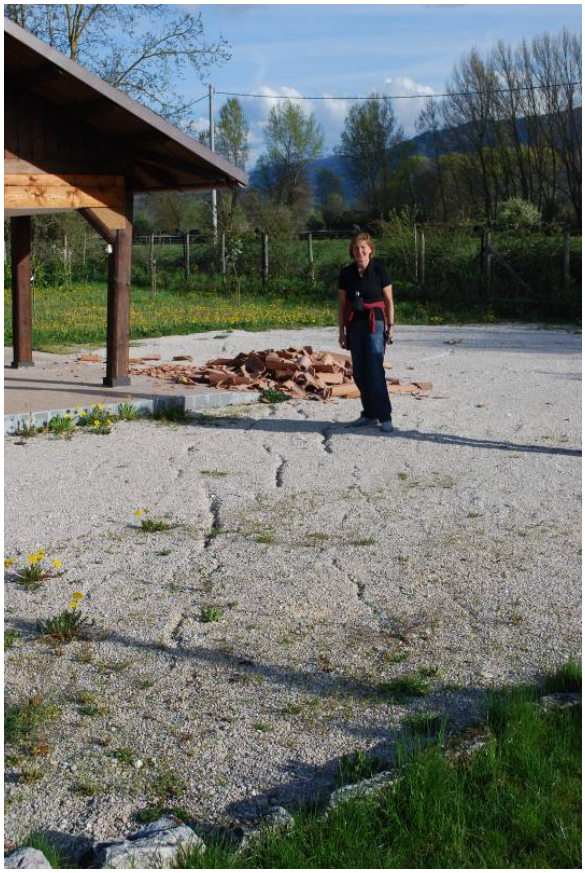


*Figure 140. Ground fissures developed in alluvial floodplain directly south of central Onna and approximately 150 m from the Aterno River. Orientation of fissures is approximately parallel to the river (42.325N, 13.480E).*



*Figure 141. Characteristic crack developed in bridge approach road directly south of Onna, at distances of 15 m to 160 m from the Aterno River (42.324N, 13.478E).*



*Figure 142. Typical tensile condition of road cracks, not extending into neighboring sub-base or approach fill embankment (42.324N, 13.478E).*



*Figure 143. Ground cracks up to 1.0 m deep, 20 m long, and with maximum of 15 cm vertical displacement (down-dropped toward river) developed directly adjacent to bridge abutment (42.324N, 13.478E).*



*Figure 144. Ground cracks developed along levee crest adjacent to bridge abutment (42.324N, 13.478E).*



*Figure 145. Bridge collapse along the Aterno River, approximately 450 m north of Monticchio (42.325N, 13.463E).*

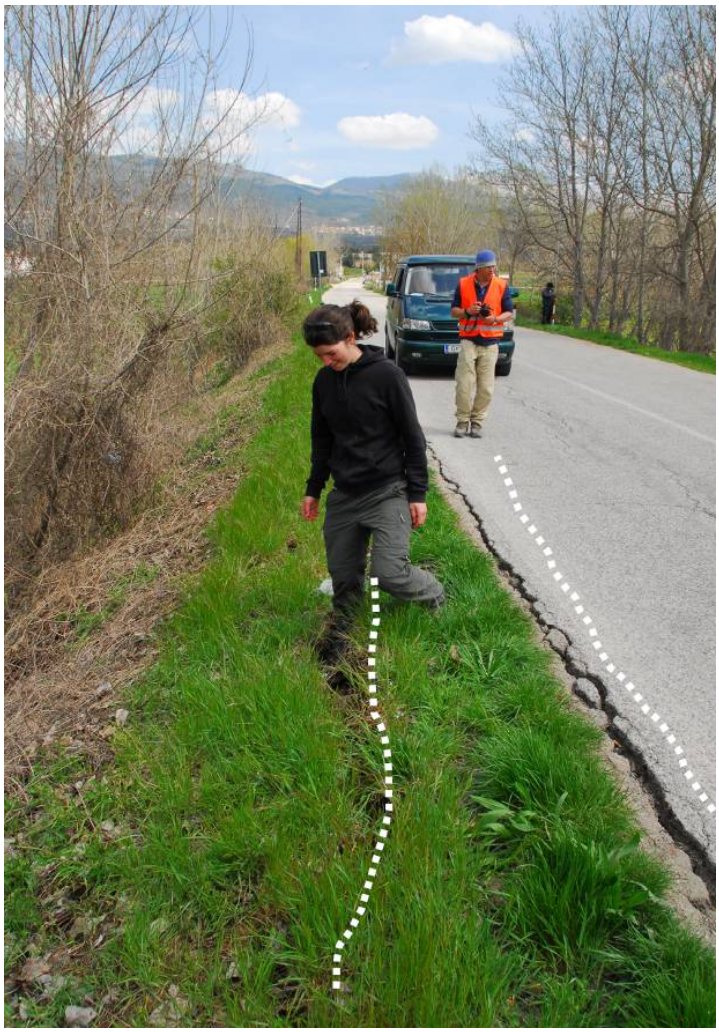


*Figure 146. Approximately 15-20 cm lateral displacement of approach fill (42.325N, 13.463E).*



*Figure 147. Flood protection levee in vicinity of bridge collapse (42.325N, 13.463E).*



*Figure 148. Ground cracking in levee directly beneath western abutment along northern side of Aterno River (42.325N, 13.463E).*

Within the cataclasite quarry northeast of Colle and depicted in Figure 128, two parallel shear failures in clayey sand fill materials were observed (Figure 149). The shear failures are oriented perpendicular to the free face of the fill slope, have approximately 15 m separation, with vertical displacement systematically increasing to a maximum of about 40 cm toward the free face. A block of soil between the parallel shears dropped, forming a graben structure (Figure 150), but no distinctive headscarp developed. These structural relations would not be expected for usual soil slope failure modes, and further inspection indicates the shear failures resulted from differential seismic compression of the fill.

Figure 151 reveals that the fill materials were placed in a tight bedrock notch, and considering the nature of mining operations it was likely loose dumped and poorly compacted. Such boundary conditions promote differential settlement from seismic compression. In this case, the resulting shear strain appears to have been sufficient to cause shear rupture through the soil.

Seismic compression was also observed in boulder fill placed along the sidewalls of a cut-and-cover tunnel structure located about 1.5 km northeast of L'Aquila. As shown in Figure 152, the boulder fill is of fairly uniform particle size, and Figure 153 shows 10-15 cm of settlement relative to the spanning parapet wall foundation. Some of this settlement may have existed prior to the earthquake. Fresh cracks in the overlying asphaltic surfaces and a narrow settlement trend along the sidewall of the cut-and-cover structure may indicate the boulder fill is continuous and not just at the portals (Figure 154). In addition, minor instances of utility trench backfill compression such as depicted in Figure 155 were observed sporadically.



*Figure 149. Shear failure developed in fill material, with vertical displacement increasing to approximately 40 cm at free slope face (42.435N, 13.330E).*

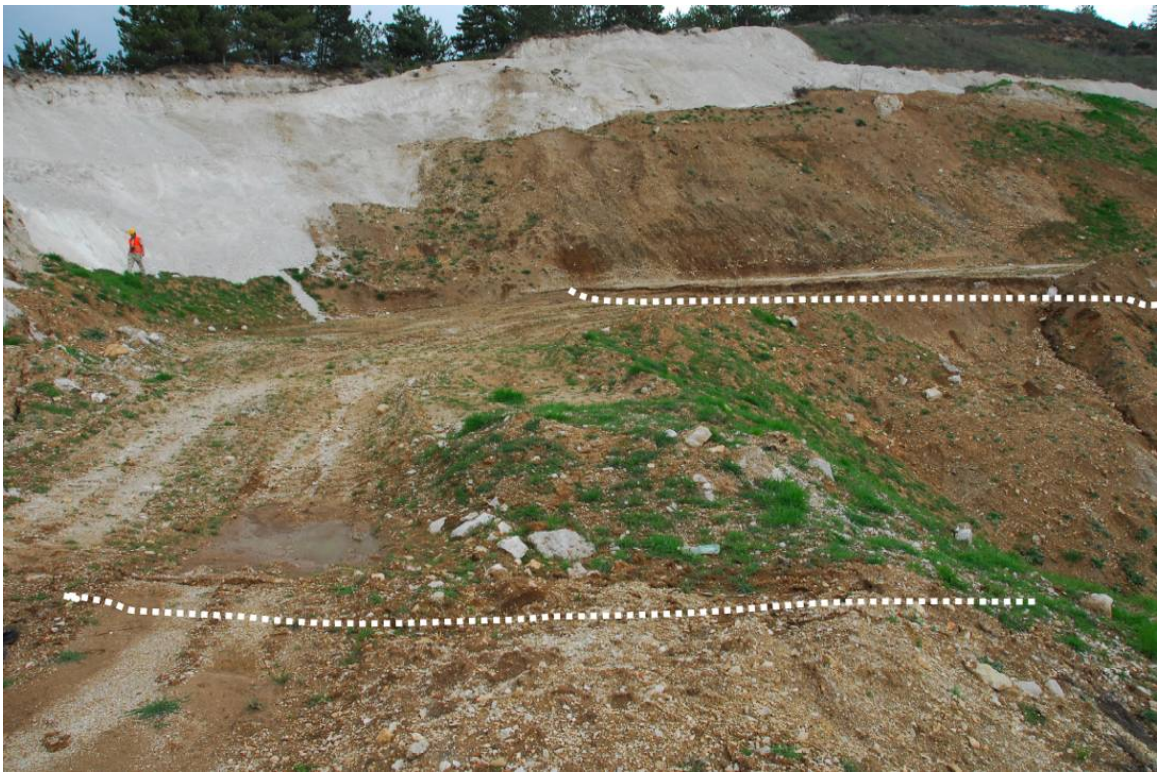


*Figure 150. Graben structure (between lines) created by parallel down-dropped shears (42.435N, 13.330E).*



*Figure 151. Graben structure (between vertical lines) and bedrock boundary conditions (42.435N, 13.330E).*



*Figure 152. Boulder fill placed along side wall of cut-and-cover structure (42.358N 13.415E).*

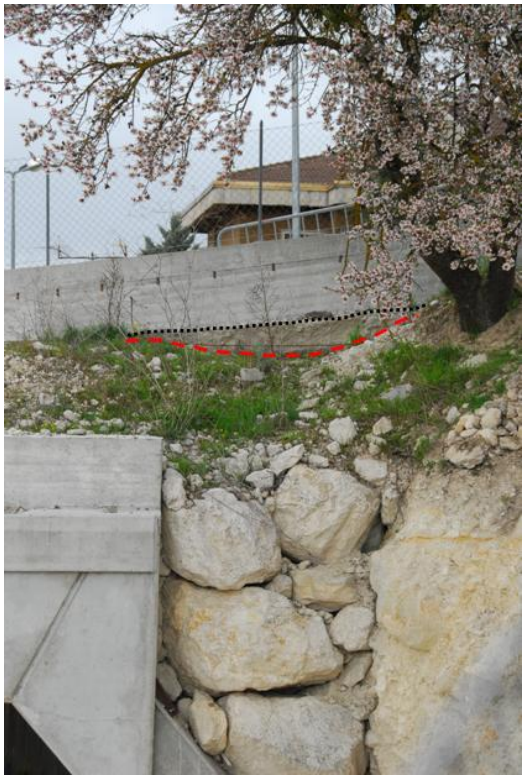


*Figure 153. Settlement trough reaching 10 to 15 cm maximum, relative to the spanning parapet wall foundation (42.358N 13.415E).*



*Figure 154. Cracks in the overlying asphaltic surfaces and a narrow settlement trend along the sidewall of the cut-and-cover structure (42.358N 13.415E).*



*Figure 155. Seismic compression of trench backfill in the town of Paganica (42.365N, 13.465E).*

**Lake Sinizzo**

General observations during field reconnaissance

Lake Sinizzo (42°17'27.23", 13°34'35.05") is situated in a natural karstic depression located east of San Demetrio ne' Vestini. The lake is roughly circular in plan view, with an average diameter of approximately 120 m. The lake appears to be partially impounded by a small embankment located as shown in Figure 156. A bathymetry survey by Tetè et al. (1984) is shown in Figure 157, indicating maximum side slope relief of about 10 m.

Significant ground cracking was observed along approximately 70-80 percent of the lake perimeter, such as depicted in Figures 158 and 159. Soils exposed in the sidewalls of the ground cracks were visually classified as clayey gravel (GC) to gravelly clay (CH), with notable high plasticity of the fines. These materials may have a mixed alluvial/lacustrian origin, and artificial near surface fill may exist locally.

Several meters of local slope displacement are evidenced by submerged trees and a prominent arcuate landslide scar near the western margin of Lake Sinizzo (Figure 160). Pre-and-post earthquake imagery, shown in Figures 156 and 161, respectively, indicate that submergence occurred as a result of slope displacement during the earthquake.




*Figure 156. Overview of Lake Sinizzo with location of impounding embankment indicated by vertical white line (42.291N 13.576E).*

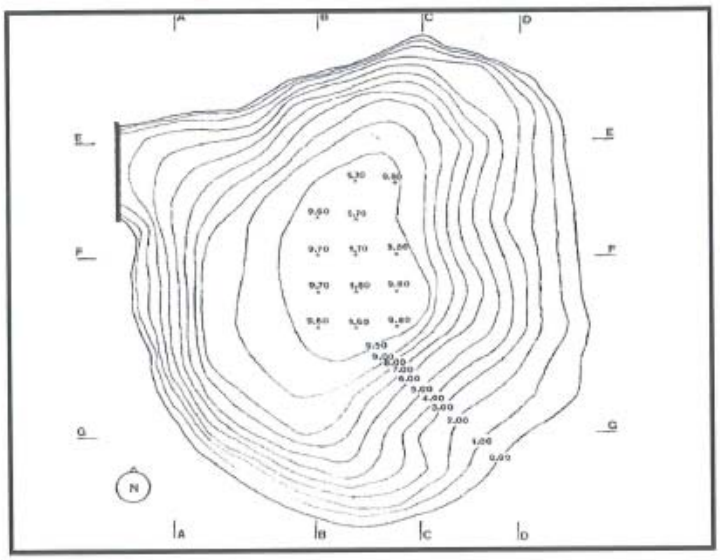



*Figure 157. Bathymetric survey of Lake Sinizzo; impounding embankment at upper left corner (Tetè et. al, 1984).*



*Figure 158. Ground cracks along the northwestern perimeter of Lake Sinizzo (42.291N, E13.576).*



*Figure 159. Ground cracks along the eastern perimeter of Lake Sinizzo (42.291N, E13.576).*



*Figure 160. Submerged trees located several meters from the western margin of Lake Sinizzo; picnic table within arcuate landslide scar at shoreline. (42.291N 13.576).*




*Figure 161. Post earthquake satellite imagery showing submerged trees within small circle and rock slope failures within large circle; compare to pre-earthquake imagery shown in Figure 146 (42.291N 13.576).*

Tape and Compass Displacement Measurements

Tape and compass measurements were performed to document permanent surface deformations along the banks of Lake Sinizzo. Linear traverses were measured utilizing a standard 60 m fiberglass tape and a Brunton Compass for each failure zone from the approximate shore line to the furthest observed ground cracks. The distance to each crack along the traverse and its opening were documented. Cracks with a minimum opening were assigned an opening of 1 mm.

The measurements were performed on 15 April 2009, 9 days after the mainshock. Our first observations were on April 11 2009 and no significant changes were observed by April 15. For example, Figure 162 shows the same ground deformations at the southwest corner of Lake Sinizzo (WP 18) photographed during each site visit. The camera position and lighting conditions were slightly different for the two photographs giving rise to slight differences between the two images.




*Figure 162. Ground cracks at the southwest corner of Lake Sinizzo (location WP 18) as observed on (A) 11 April 2009.*




*Figure 162. Ground cracks at the southwest corner of Lake Sinizzo (location WP 18) as observed on (B) 15 April 2009.*

Thirteen locations associated with ground failures were surveyed resulting in 19 data sets. The GPS waypoint (WP) for each location is indicated in Figure 163. Two waypoints are associated with multiple traverses for assessing the variability of the deformation within a single failure zone. This process was discontinued due to time constraints and the information related to the spatial variability was acquired by laser scanning. Sixteen of the measurement locations consisted of a linear traverse. The other three consisted of a system of fine cracks (WP 20), a single slump with no observable cracks in the block (WP 29), and a park bench (WP 31) associated with local ground surface deformation at base of a slope within a zone of permanent surface deformation. Waypoint 21 marks the top of the direct slope above the failures associated with Waypoints 22, 30, 31, and 32.

The results from the measurement campaign are available in both table and graphical format for each traverse in the appendix of GEER (2009). The corresponding waypoint, location, and the orientation of the measurement line are included in each table. The distance represents the location of each crack determined to be associated with slope deformations from the lake shore or the slope leading directly to the water surface. Desiccation cracks were identified based on the crack characteristics and patterns and are not included in the data sets. The opening associated with individual cracks crossing the traverse was measured at the intersection parallel to the traverse orientation. In some cases the opening may contain a component of shear displacement along the individual crack when the crack crosses the traverse obliquely.

The traverse length was based on the crack furthest from the lake shore. For waypoints with a single traverse, and the longest traverse within a multi-traverse location, the measured distance represents the maximum length of the displaced mass based on observable surface extension. The crest of the head scarp was identified and the tape was extended to the shore along the orientation normal to the crack orientation. The cumulative extension represents the total opening in the orientation of the traverse along its complete length. Each table is associated with a figure plotting the presented data. Table 8 summarizes the traverse lengths and the cumulative crack opening for all measured traverses. The cumulative opening for the traverses at WP 24, WP25, WP26, and WP 27 are minimum values; opening distance was not measured across displaced blocks that had moved into and under the water surface. Figure 164 shows an example of a block lying just below the waters surface near the end of the traverse WP 25. The location of Traverse WP 26 and WP 27 are also indicated on this figure.

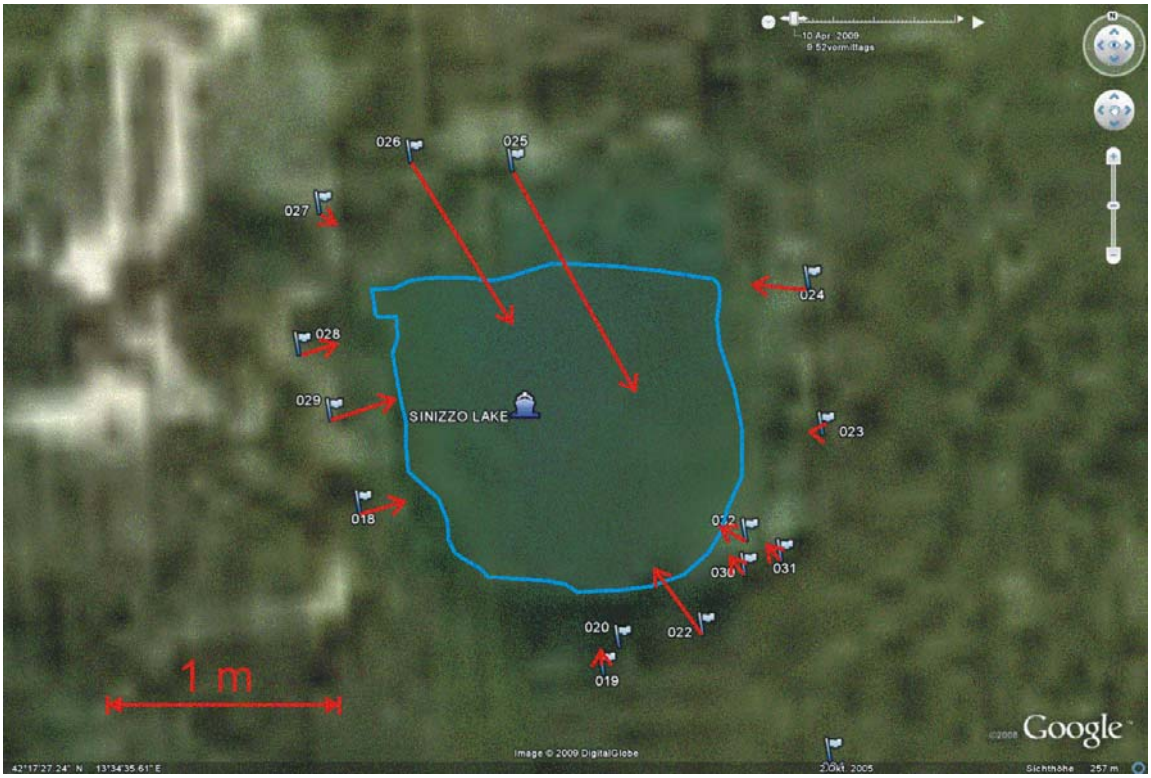



*Figure 163. GPS way points indicating measurement locations around Lake Sinizzo. The red arrows indicate the orientation and maximum cumulative crack opening measured at each location.*

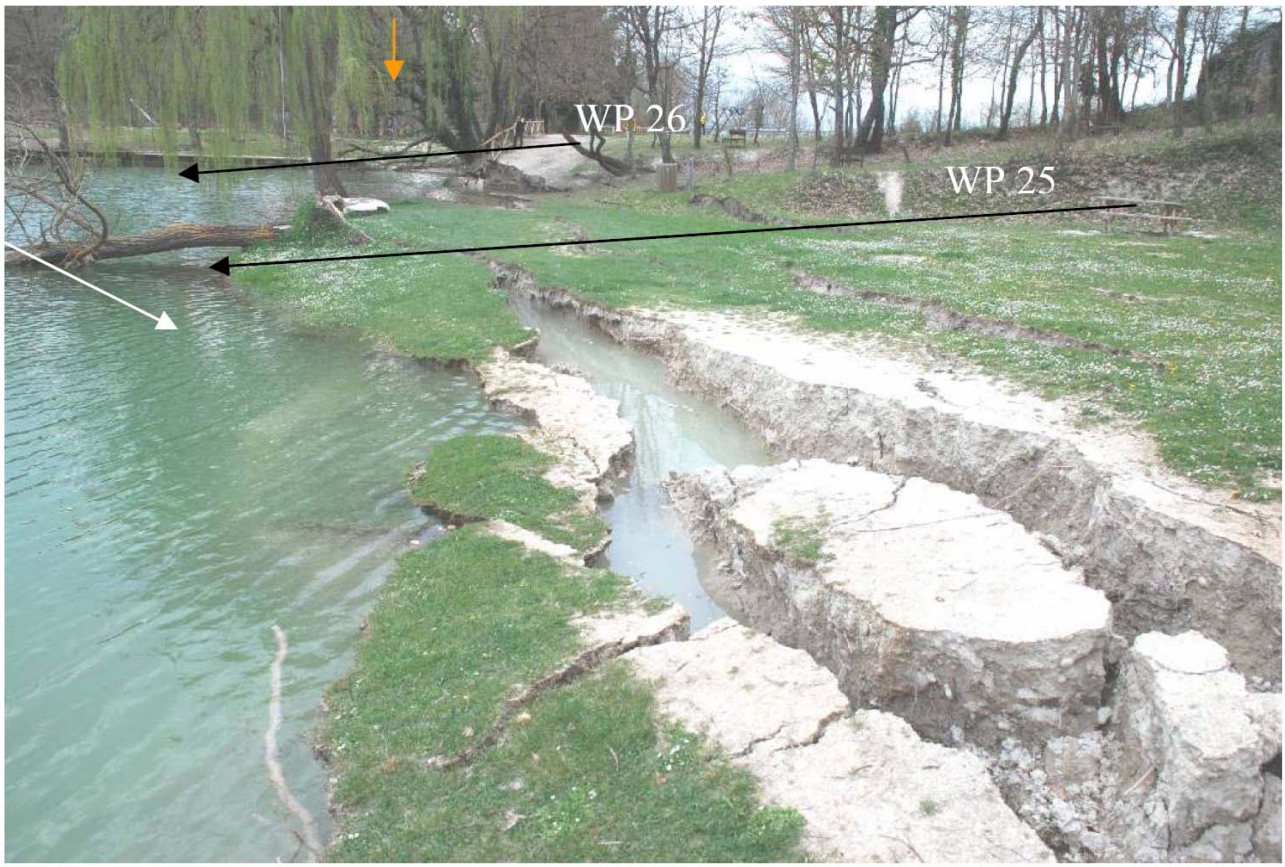



*Figure 164. Blocks lying under the water (white arrow) were not included in the traverses (WP 25 and WP26). The orange arrow shows where the fence (and the slump below it) truncated the traverse at WP 27. (Photo E. Button).*

*Table 8. Summary of the length, cumulative crack opening and the orientation of the 17 traverses and their corresponding way point.*

| | Length (cm) | Cumulative crack opening (mm) | Orientation |
|---|---|---|---|
| WP 18 A | 172 | 58.5 | 074° |
| WP 18 B | 236 | 90.5 | 074° |
| WP 18 C | 211 | 155 | 074° |
| WP 18 D | 251 | 224 | 074° |
| WP 19 | 175 | 77 | 356° |
| WP 22 A | 268 | 378 | 324° |
| WP 22 B | 258 | 274 | 324° |
| WP 22 C | 555 | 360 | 312° |
| WP 23 | 455 | 25 | 275° |
| WP 24 | 920 | 254 | 275° |
| WP 25 | 1320 | 1160 | 151° |
| WP 26 | 2180 | 877 | 148° |
| WP 27 | 1142 | 90 | 122° |
| WP 28 | 1248 | 176 | 072° |
| WP 29 | 614 | 320 | 072° |
| WP 30 | 1200 | 112 | 322° |
| WP 32 | 1940 | 145 | 300° |

Figure 163 plots the orientation and maximum cumulative crack opening distance for each measurement location superimposed on a Google Earth image of Lake Sinizzo. From this image it can be seen that the primary permanent displacements were towards the lake. However, the magnitude varies considerable with position around the lake.

Figure 165 summarizes the cumulative crack opening for all of the traverses at Lake Sinizzo. The largest permanent displacements occurred on the north and south shores respectively. The traverses at WP 25 and WP 26 document two locations associated with the largest permanent displacements at Lake Sinizzo with cumulative extension of more than 1 m. The traverses at WP 22 document three locations along the largest scarp observed on the south shore.

The measurements at WP 31 were associated with differential displacements occurring at a park bench bedded into the ground. Figure 166 shows a schematic diagram of the bench and the associated displacements. The features related to the bench displacement for C2 and C3 corners are shown in Figure 167.

In summary, the extensional displacements associated with permanent ground displacements at Lake Sinizzo ranged from several mm to over 1 m depending on the location around the lake. Extensional cracks could be documented at distances of more than 20 m from the shore in the relatively flat terrain on the north shore. On the south shore extensional cracks were observed up to a distance of approximately 20 m, the cracks furthest from the shore were located on a hill slope extending towards the south. While the bedrock is very shallow in this location (southeast corner of the lake), adjacent outcrops of limestone 2-3 m away showed no signs of continuous cracking along the strike of ground cracks. This could indicate that the deformations were constrained to be within the Quaternary cover materials. At approximately the same elevation on the southwest corner of the lake, weathered, friable marl bedrock stone was observed at a local slope failure. Thus the bedrock changes laterally along the southern shoreline and the potential for movements in the weathered bedrock cannot be excluded. The permanent displacements along the east shore of the lake were characterized by sub-parallel to anastomosing crack arrays with extensional displacements observable up to 9 m from the shoreline. The deformations along the east to southeast side of the lake were typically characterized by single slumps several of which slid into the lake (as shown in the post earthquake bathymetry) and only the scarps were visible. The furthest cracks were observed to be up to 12 m from the shore. The cracks with the largest opening distance were typically located less than 10 m from the shore.

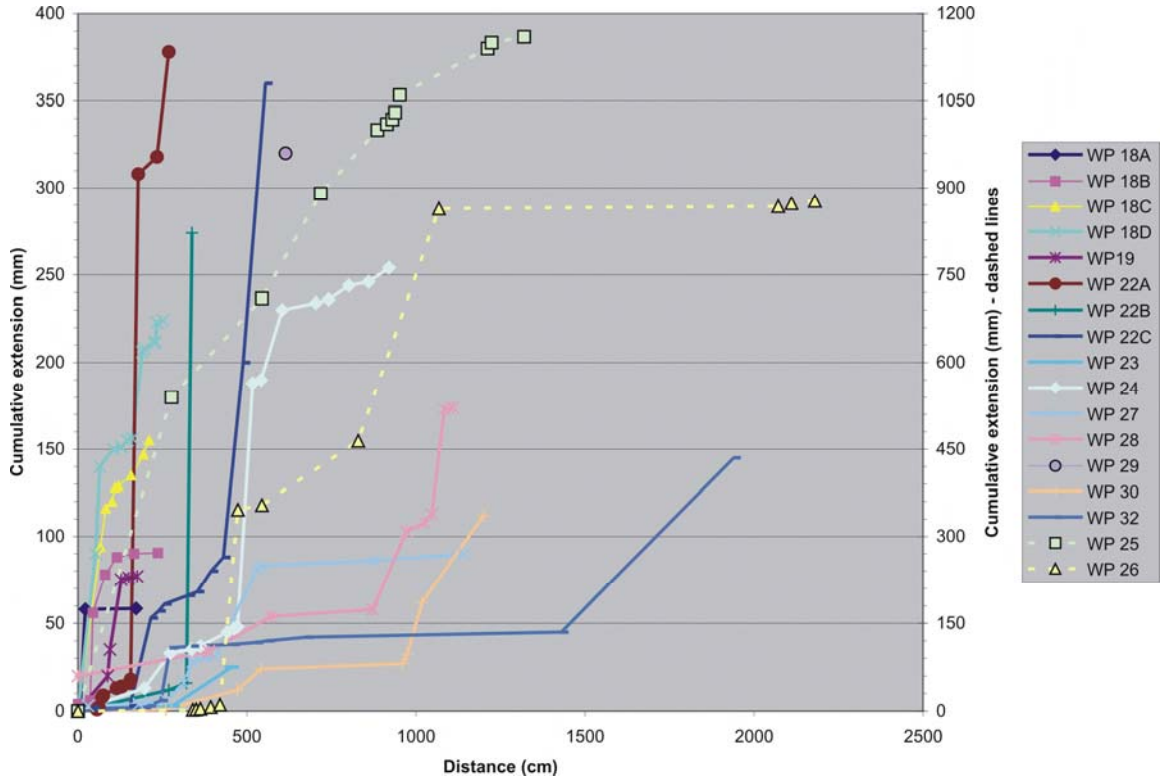
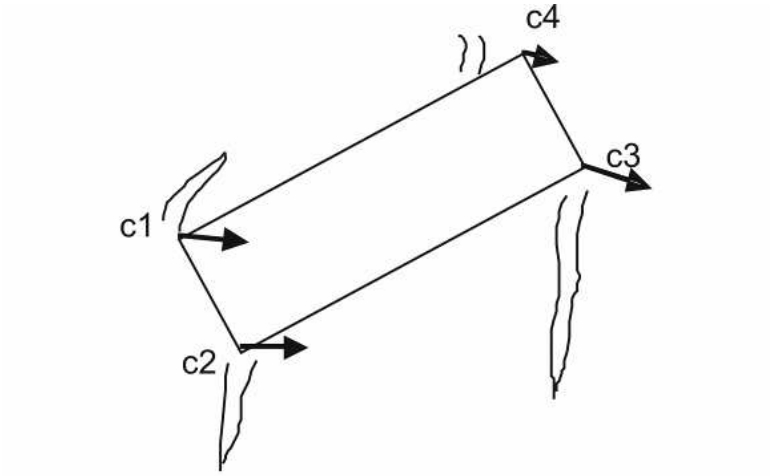



*Figure 165. Plot of the cumulative crack opening (extension) for all of the measurement locations. The data for WP 25 and WP 26 are plotted relative to the right axis (3X larger).*




| | Crack opening (mm) | Crack length (cm) |
|---|---|---|
| C1 | 60 | 40 |
| C2 | 60 | 60 |
| C3 | 42 | 90 |
| C4 | 38 | 11 cm overthrust |

*Figure 166. Schematic diagram and magnitudes of the cracks associated with the park bench at WP 31.*




*Figure 167. Characteristic deformations associated with the corners of the park bench at WP 31. (A) corner C2, (B) corner C3.*

A. Procedures and equipment

During the earthquake reconnaissance, we deployed lidar technology to image the ground-failures along the margins of Lake Sinizzo. At the Lake Sinizzo site, the terrestrial lidar laser beam systematically scanned over the shore margin to acquire the precise distances to objects. The laser repeatedly shot pulses of light at each rotation point of the scanner, sending light to reflect off an object and back to the scanner. Timing the two-way travel time of flight of each laser pulse allows for the determination of the range. A spherical coordinate system is initially used to map the targets, and then data are converted to a Cartesian scanner coordinate system centered on a scanner instrument datum. Terrestrial LIDAR technology was used at Lake Sinizzo because of its ability for characterizing ultra-fine scale changes in topography (Collins and Sitar, 2006; Collins et al. 2009; Kayen and Collins, 2005; Kayen et al., 2006, Kayen et al., 2007; Stewart et al. 2009). LIDAR technology is a natural extension of laser range finder systems or electronic distance meters (EDMs) commonly used in survey applications to measure distances.

The USGS LIDAR system used at Lake Sinizzo is manufactured by Riegl of Austria and is based on a near-infrared YAG 1064nm laser transceiver. The system, a Riegl z420i unit, is portable and designed for the rapid acquisition of high-resolution three-dimensional imagery. The maximum target range is about 1000 m for the Riegl under the best atmospheric conditions and is dependent on the reflectivity of the given target. For the Lake Sinizzo study, we operated at much shorter distances than the maximum range of the units. The minimum target distance is 2 m, the distance to the ground from a tripod-mounted system. The range accuracy is consistently about 4 mm for the Riegl at the range of interest in the study. The laser beam divergence angle is 3 milli-radians, meaning that at a range of 10 m, the beam footprint is approximately 30 mm across. Because of the footprint size, the shots are ideally spaced 3 milli-radians apart. The position of the center of the footprint is measured to a precision of 0.17 milli-radians by an encoder. The angular position of the laser-pulse leaving the scanner is controlled by precise servo-motors within the unit.

The USGS scanner (Figure 168) has a single scan sweep of 360° horizontally, and 80° vertically. The scanner takes several hundred thousand-to-several million individual x, y, z position measurements, at a rate of 12,000 points/second.

A tripod was used on the ground to deploy the instrument. The laser unit weighs 15 kg plus the weight of accessory cables, tripod, battery and laptop.



*Figure 168. Deployment of the tripod-mounted Lidar system on the lake margin. The laser unit is connected to a laptop, battery, and photogrammetric camera.*

3-D laser scanners cannot image behind objects, and the first object encountered casts a shadow over objects behind it. At low grazing-angles away from the scanner, the laser path angle decreases to only several degrees and proportionally larger shadows are cast on the ground behind the target. Also, at incident angles of less than approximately 4° on relatively flat surfaces, often, the laser cannot detect any backscattered signal. To minimize shadow zones and get full coverage of the target surface, the scanner was elevated as much as possible. The sensor was moved around the lake for 10 individual setups to capture data from various orientations around the lake margin to image the shadow-forming targets of the ground failures. Manipulation of that data is performed with specialized surface modeling software and a portable graphics workstation. We utilize two surface modeling software packages, I-SiTE Studio (I-Site Pty. Ltd) and RiSCAN Pro (Riegl Co.). These software packages collect the scan point-cloud data and can process multiple scans into geo-referenced surfaces.

B. Lake Sinizzo Data Collection

Ten scans were collected around the perimeter of the lake on April 15, 2009. The locations of the scans were irregular, with a higher density along portions of the lake margin that failed. Figure 169 shows a composite registered image of the 10 scans for the entire lake margin alongside the Google Earth image of the lake. Figure 170 shows high-resolution detail of the lake point cloud. The Google Earth image of Figure 169a was taken prior to the earthquake. The black central portion of the lidar image in Figures 169b and 170 is the surface of the lake water. The near infrared laser is unable to penetrate water, and therefore, all submerged portions of the lake are un-imaged. The images are colored from red to blue in a rainbow shade, with the red being the lowest typography and blue the highest topography. The point cloud data does not have vegetation removed through filtering and individual trees can be seen overhanging the lake water. On the left side of the image a clump of trees can be seen in the water, and are the vegetation of the displaced landslide block that entered the lake.

We did not use differential GPS to register the lidar imagery. The Google Earth image in Figure 169a is oriented with true north up, whereas true north in the lidar image is slightly N-NE. During the data collection, we tried to orient the scanner using a non-differential GPS unit. The individual scans were registered by finding the least squares best fit solution between point clouds of the surrounding scans. As such, the data are registered in a project coordinate system to an accuracy of approximately 5 cm. This allows us to make accurate estimation of the ground information that occurred around the perimeter of the lake, but does not allow for us to project the image as a map without the additional effort to link the imagery to a geodetic and geographic datum.

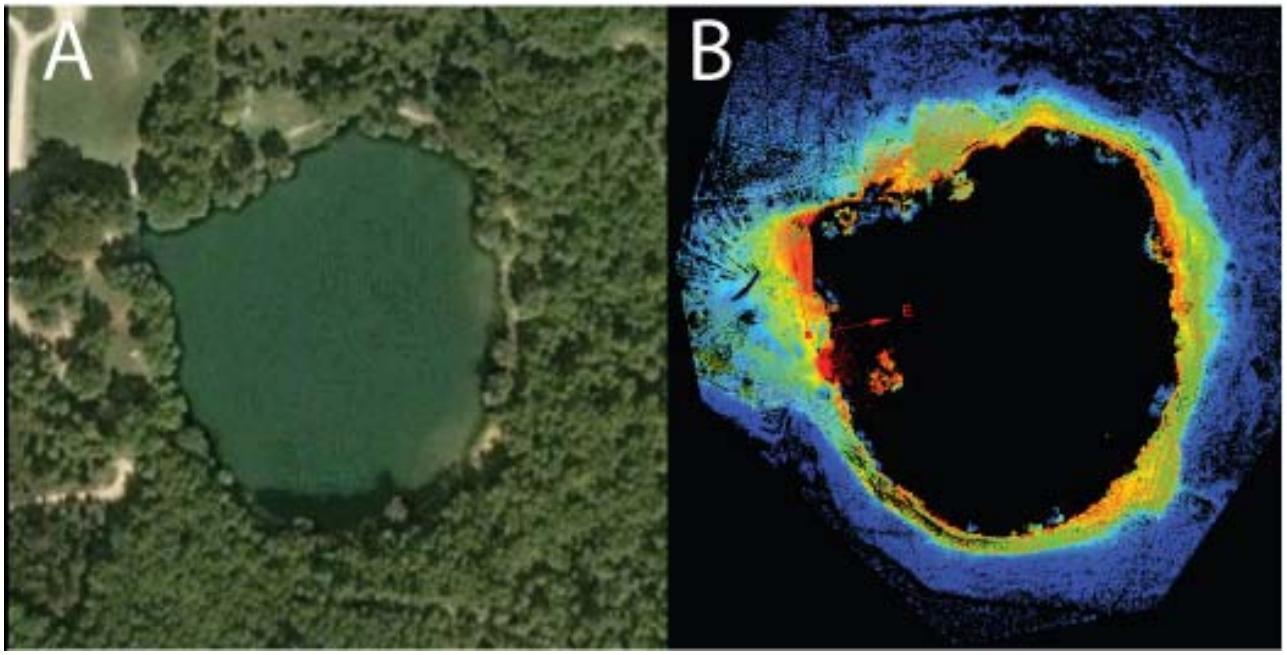



*Figure 169. (A) Google Earth image of the lake taken prior to the earthquake, (B) Lidar point cloud image of the lake taken on April 15, 2009. The coloring in the lidar imagery ranges from red (lowest typography) to blue (highest typography).*

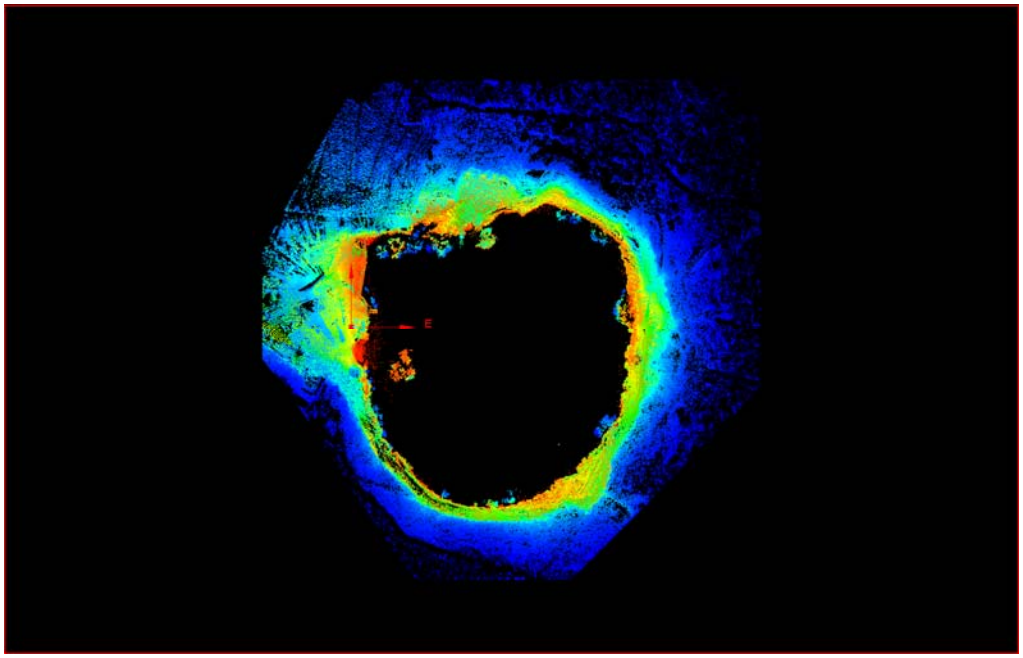


*Figure 170. High-resolution detail of the lidar point cloud image of the lake taken on April 15, 2009.*

Figure 171 shows oblique detail of ground failures along the lake margin, and overlapping imagery from three scans colored in red, purple, and green. Taking scans from different orientations allows for shadow zones to be filled. For example the central black circle in the image just above the "Z" axis is where the laser was set up during the capture of the purple data set. Subsequent scans, falsely colored, here as red and green, fill in the data hole beneath the scanner. In this image, areas can be seen where shadows cast by vegetation in one scan are filled by point cloud data from another scan. Fissures associated with lake margin soil sliding in toward the lake can be clearly seen in the green and purple scans. These features can be used to identify individual sliding blocks, and allow for reconstruction of pre-failure lake geometry needed to estimate ground deformation estimates, work that we are currently performing.

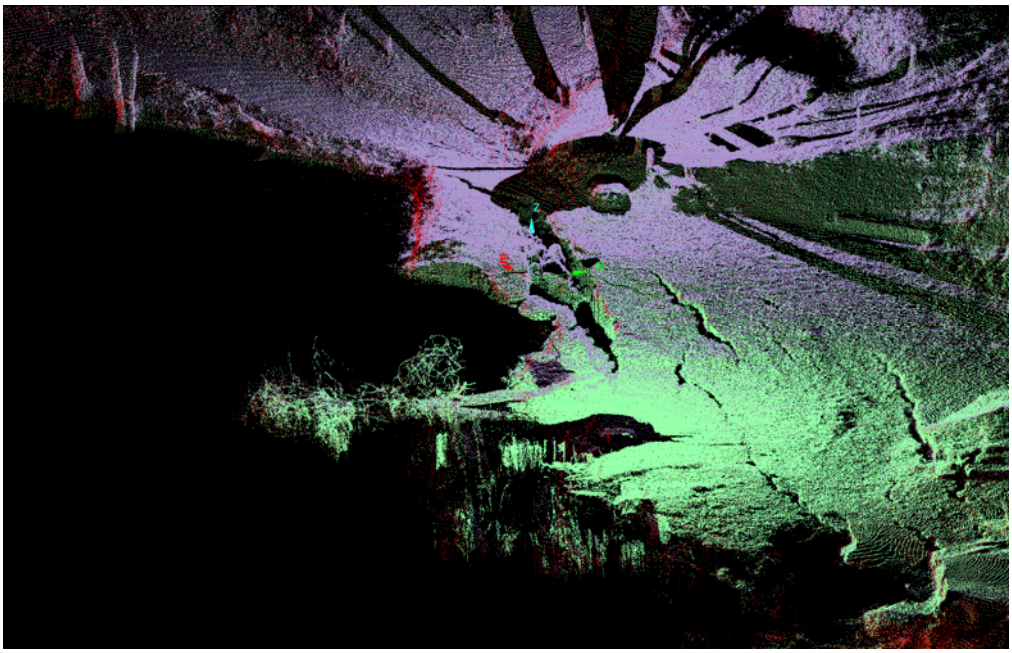


*Figure 171. Detail of ground failure along the perimeter of Lake Sinizzo, captured in three of the overlapping scans (red, purple, and green).*

High resolution multibeam bathymetry of Lake Sinizzio was performed by Violante (2009) on May 8 2009 (32 days following the mainshock) as part of the GEER investigation. Details on the equipment used and methodology are given by Violante (2009).

Multi-beam bathymetric data were collected from a rubber boat equipped with a dedicated pole and flange used to operate the sonar head (Figure 172). Vessel tracks were positioned so as to insonify 100% of the lake floor with a high percentage of overlap (Figure 173). The processed data were used to generate a digital elevation model (DEM) with cell size of 5x5 cm, with an accuracy meeting the requirements of the International Hydrographic Organization (IHO).



*Figure 172. Rubber boat equipped with the 8101 multibeam system.*

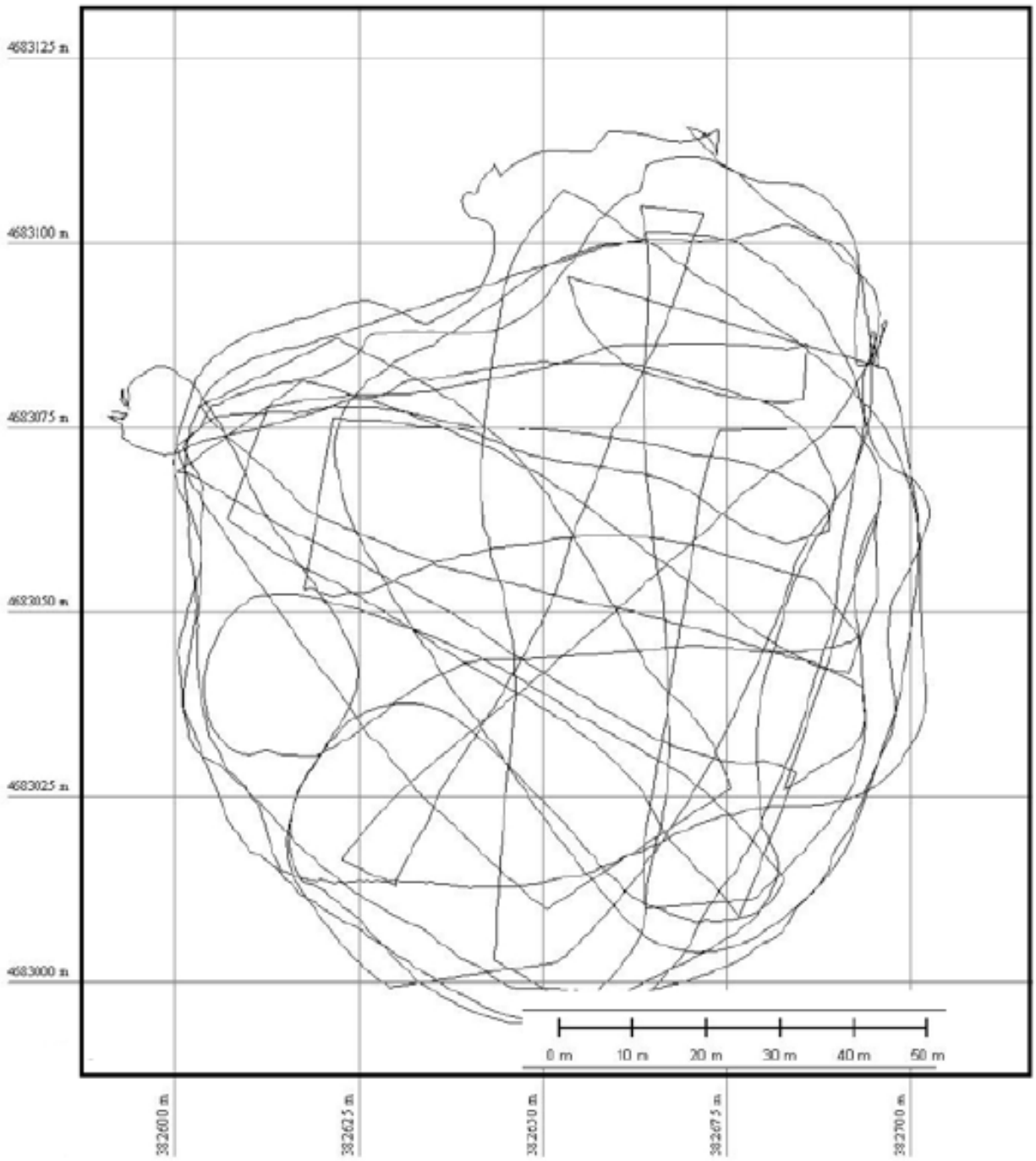



*Figure 173. Navigational plan for the Lake Sinizzo bathymetric survey.*

Figures 174 and 175 illustrate the main morphological features of the lake floor. Comparing the results to the 1984 single-beam bathymetry (Figure 175) indicates no significant differences in the general lake-floor configuration and relative depth distribution. The most relevant feature is an incipient instability denoted by an irregular morphological step (1 to 20/25 cm high) possibly locally evolving into a crack with an overall concave shape in plan-view, developing for about 120 m along the eastern side of the lake between -1.5 and -7.5 m. Some of these features may be underwater continuations of the cracks observed at lake banks. The western side of the lake seems to be affected by a shallow creep or decortication of the sediment cover. Also the multibeam data clearly show the area of detachment and accumulation of the "fallen trees" (Figure 160). The sliding block induced deformation of the lacustrine sediments during transportation towards the lake bottom.

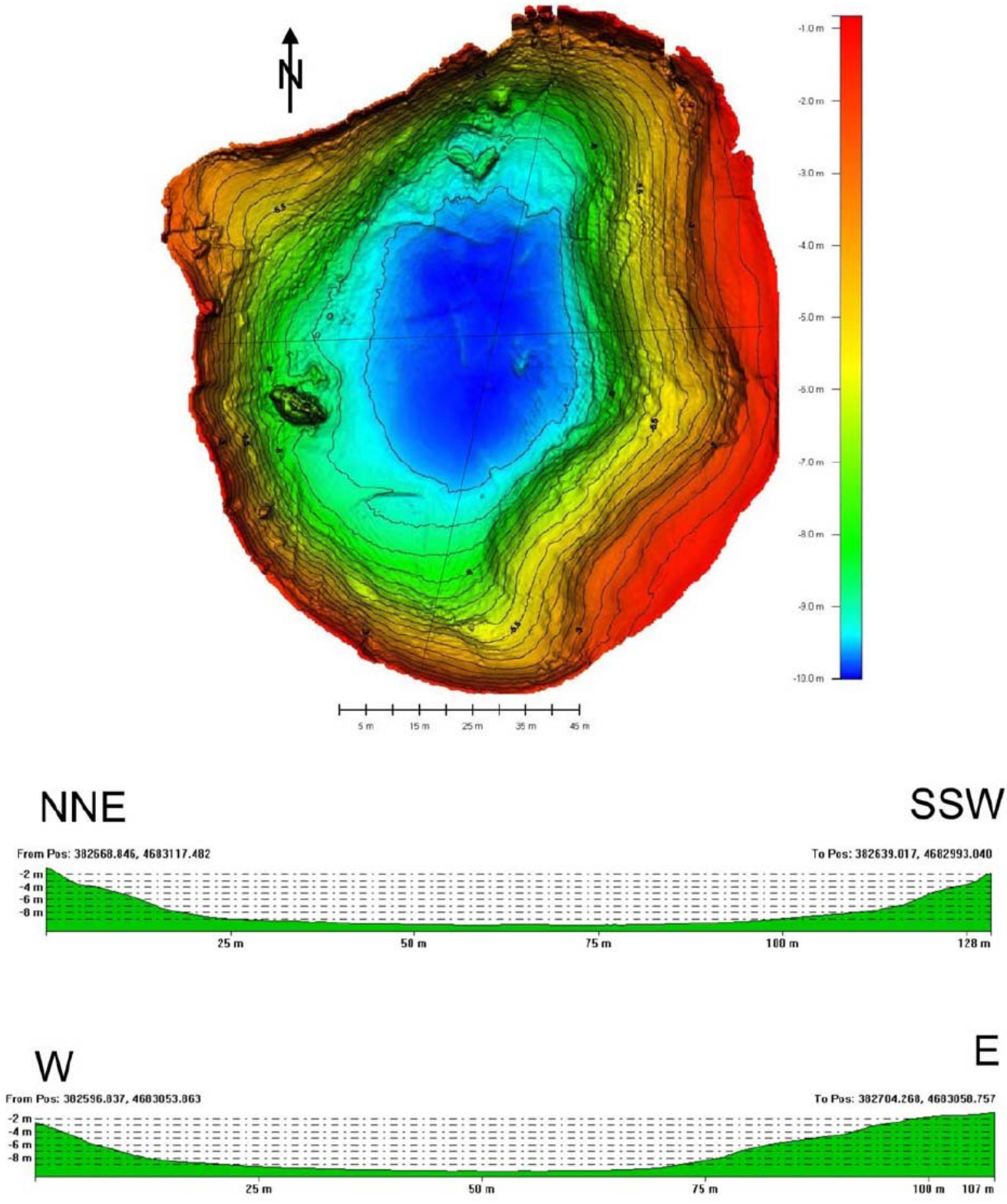



*Figure 174. Lake Sinizzo bathymetric survey results including cross sections.*

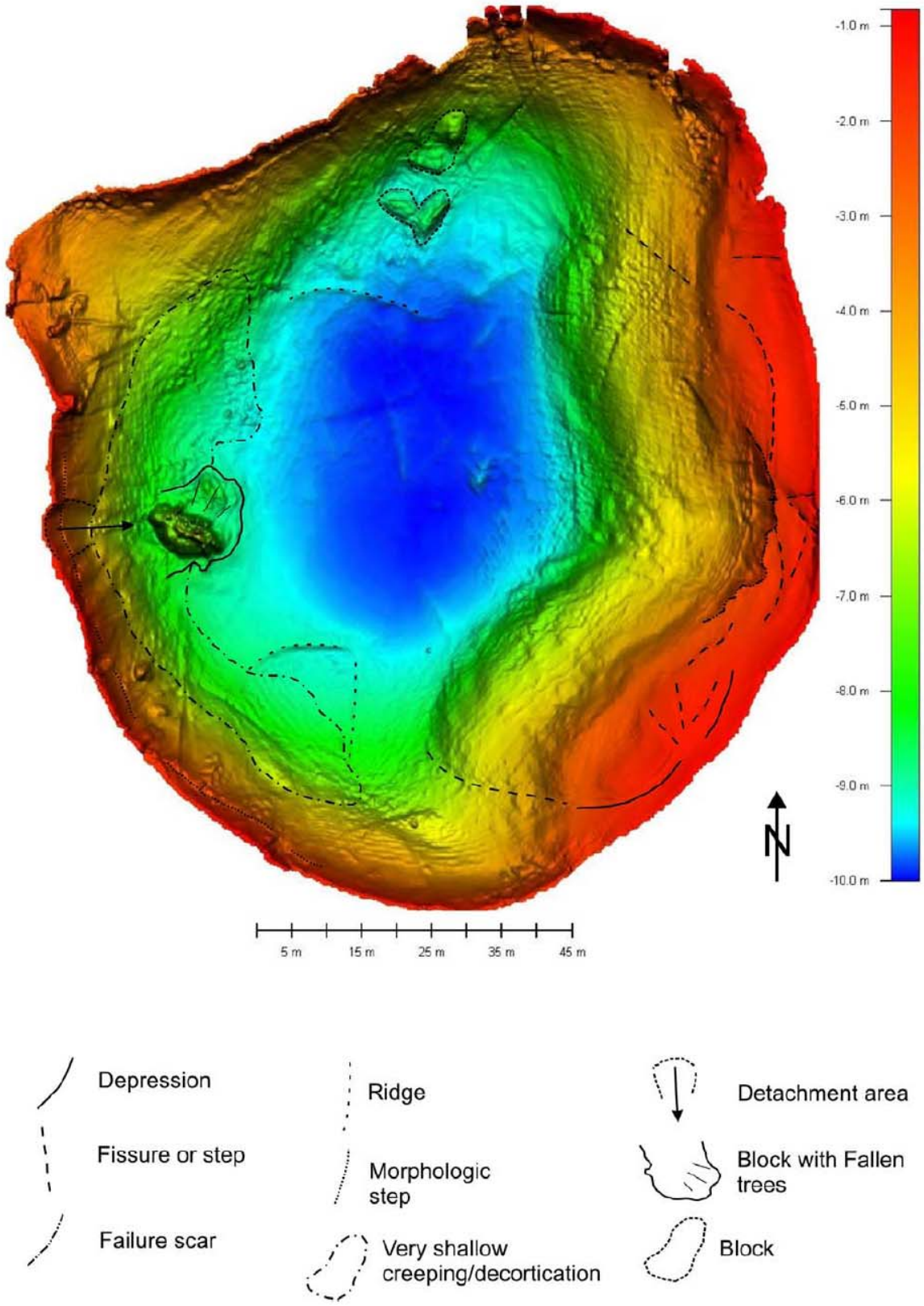



*Figure 175. Lake Sinizzo bathymetric survey results marked with interpretive symbols.*

**Campotosto Dams**

Campotosto lake is a man-made water reservoir with a capacity of 315.000.000 $m^3$, at an altitude of 1313 m above sea level. It is located approximately 20 km north of L'Aquila, between Gran Sasso and the Laga Mountains. As shown in Figure 176, the lake is impounded by three dams: Sella Pedicate (42.514954°N, 13.369194°E), Rio Fucino (42.535047°N, 13.410323°E) and Poggio Cancelli (42.558380°N, 13.338944°E). Reservoir filling was completed in the 1970's and its water is used for electrical power production. The dams were visited by the reconnaissance team on April 14 2009.




*Figure 176. Campotosto reservoir map with the location of the three dams.*

The Campotosto basin is placed at the site of an ancient lake which later became a peaty marsh due to mud silting. This is apparently the result of transport of bed load of the tributaries whose basins consist of highly erodible sandstone-marl rocks. A factor contributing to the drying up of the ancient lake was the constant deepening of the Fucino gorge by erosion. The basin consists of cemented sandstone layers and banks, chiefly clayish, alternating with marl banks and thin layers of clay schists of the middle Miocene (ENEL, 1980).

Over most of its length "Sella Pedicate" dam is a concrete dam while at one of its extremities it is a zoned earthfill embankment with an clayey central core and a concrete foundation diaphragm. It is 25 m tall and 750 m long. Its construction dates from the 1950's. Figure 177 shows a plan view of the dam from Google Earth. The upstream face is very steep (possibly 5 horizontal to 1 vertical) and is shown in Figure 178. The downstream face has a much milder inclination. Following the main shock of April 6 2009, the water level was lowered by ENEL by approximately 2 m to reduce water pressure on the structure. The reduction in water level is evident in Figure 178. At the time of the earthquake the water depth behind the dam was about 25 m. No earthquake damage was observed in the dam (crest, slopes, abutments). In addition, no soil liquefaction with sand ejecta was observed along the shoreline in the vicinity of the reservoir.

"Rio Fucino" is a concrete dam with a length of approximately 150 m and a reported maximum height of 49 m (Simonelli et al., 2009). Its construction dates from the same period as in the other dams. No damage was observed, as evident in Figures 179-181. According to ENEL employees of the local station, the dam is instrumented with seismic measuring devices, which recorded peak accelerations of the order of 0.1g. Acceleration histories from those instruments are not available as of this writing.

"Poggio Cancelli" is a zoned earth dam approximately 500 m length and 30 m in height. The inclination of the upstream face is about 3 horizontal to 1 vertical while that of the downstream face is approximately 1 horizontal to 1 vertical. No information as to instrumentation is currently available. At the time of the earthquake the freeboard was estimated to be about 20 m. Figure 182 and Figure 183 show the main embankment, which was found to have no visible damage from the earthquake. Moreover, no liquefaction was observed in the surrounding area.



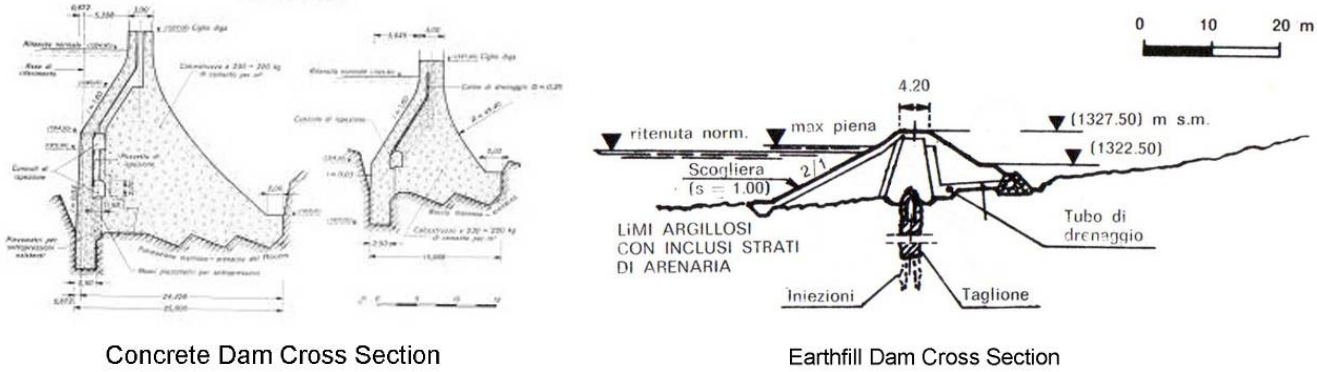




*Figure 177. Plan and cross sectional (concrete dam central portion, earthfill embankment end portion) views of Sella Pedicate (42.514954°N, 13.369194°E) dam and adjacent highway system.*




*Figure 178. Upstream face of Sella Pedicate dam. The lowering of water level decided by ENEL following the main shock is evident in the photo (42.514954°N, 13.369194°E).*



*Figure 179. Upstream face of Rio Fucino dam. Note the lowering of water level (42.535047°N, 13.410323°E).*



*Figure 180. View of the outlet tower of Rio Fucino dam (42.535047°N, 13.410323°E).*



*Figure 181. View of spillway of Rio Fucino dam (42.535047°N, 13.410323°E).*

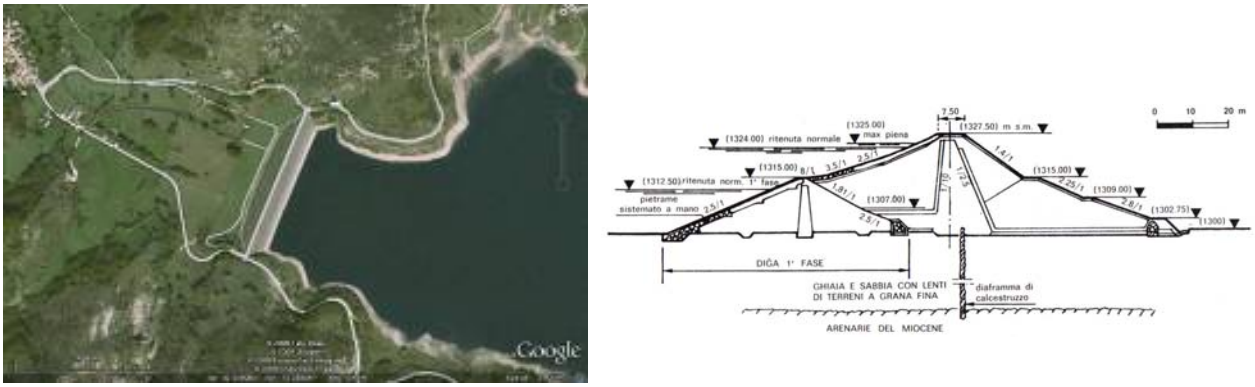



*Figure 182. Plan and cross sectional views of Poggio Cancelli dam (42.558380°N, 13.338944°E).*



*Figure 183. Downstream (left) and upstream (right) face views of Poggio Cancelli dam from the north abutment (42.558380°N, 13.338944°E).*

**Penne Dam**

Penne lake is a man-made water reservoir at an altitude of 250 m above sea level. It is located approximately 43 km east of L'Aquila and Gran Sasso Mountain. As shown in Figure 184, the lake is impounded by one earth dam (42.438809°N, 13.913265°E) 350 m in length. Although no members of the team have visited the dam to date, we have corresponded with ENEL staff who have surveyed the dam and found no evidence of structural or soil damage.




*Figure 184. Location map for Penne reservoir and dam (42.438809°N, 13.913265°E).*

**Earth Retaining Structures**

Earth retaining structures were generally observed to have performed well during the earthquake. No port structures (e.g., quay walls) were located in the meizoseismal area, hence the observed walls retain partially saturated (nonliquefiable) soils. In the region of interest, retaining structures are typically masonry walls, of the type shown in Figures 185-193. A number of reinforced concrete walls also exist in L'Aquila and did not suffer significant damage (Figure 192 and 194). In general, damage varied between minor detachments of stones, (Figure 188) to full collapse or toppling (Figure 191). No geographic concentration of retaining wall damage.

The wall failure shown in Figure 189 is nearly aligned with the pavement crack shown in Figures 190 and 191. Note that the offset of the nearby (250m away) cracked wall of Figure 192 is practically parallel to the pavement crack of Figures 190 and 191. There has been some speculation that these ground cracking patterns may be related to co-seismic rupture.



*Figure 185. Minor damage on masonry wall in severely shaken Pettino area (42.374011°N, 13.367498°E).*



*Figure 186. Stone masonry wall at L'Aquila city (42.348710°N, 13.403900°E). Note the (tolerable) outward movement at the center of the wall and the pavement cracks behind the wall.*



*Figure 187. Undamaged wall at the severely shaken Pettino area (42.373050°N, 13.366106°E).*



*Figure 188. Damaged wall at downtown L'Aquila (42.356056°N, 13.389524°E).*



*Figure 189. Partially collapsed wall at SS80 highway between L'Aquila and Campotosto (42.420510°N, 13.358394°E).*




*Figure 190. Pavement cracking in SS80 roadway (from L' Aquila to Campotosto) in the location of collapsed masonry retaining wall (42.420510°N, 13.358394°E).*




*Figure 191. Locations of observed pavement cracking and associated retaining wall failures.*



*Figure 192. Ruptured retaining wall due to slope instability at SS80 highway between L'Aquila and Campotosto (42.418117°N, 13.351591°E).*



*Figure 193. Toppling of masonry retaining wall at the outskirts of L'Aquila (42.366803°N, 13.376561°E).*



*Figure 194. Undamaged retaining wall at the city of L'Aquila (42.343672°N, 13.398821°E).*

**SUMMARY AND CONCLUSIONS**

The paper presents the findings from the geo-engineering reconnaissance carried out in the area affected by the April 6 2009 $M_w$=6.3 L'Aquila earthquake with the purpose of collecting perishable data and providing a preliminary summary of the principal seismological and geotechnical aspects of this important event.

The L'Aquila earthquake mainshock was a normal fault event ($M_w$=6.3) that occurred on April 6, 2009. This mainshock occurred after several weeks of elevated seismicity in the region. The mainshock was followed by two separate triggered events on April 7 ($M_w$=5.6) and April 9 ($M_w$=5.4). The latter events are considered to be "triggered" as opposed to aftershocks because they occurred on geographically distinct fault systems. All events involved normal slip, although the April 7 event was oblique with an element of right-lateral strike slip.

In the area affected by the seismic sequence there are many active faults, some of which are considered seismogenetic. The Paganica fault, which has been postulated as the source of the mainshock, was not viewed as a significant rupture hazard in the Abruzzo region prior to this event. Other active faults (e.g., the Pettino fault) were considered more hazardous. There are two working hypotheses on the causative fault for this earthquake: (1) the earthquake occurred on the Paganica fault, which demonstrated surface rupture over several kilometres of its length; and (2) the earthquake occurred on a deeper fault with shallower dip intersecting the Paganica fault, causing "passive remobilization" of the Paganica fault that was responsible for the observed surface rupture.

The surface fault rupture from this earthquake has been mapped by EMERGEO and other groups. Detailed LIDAR images of the fault displacements have been obtained. The slip is normal, involving approximately 4 km of rupture length and up to approximately 10 cm of displacement. Tectonic ground displacements have been inferred from GPS and InSAR data, which show a broad region of down-dropping and extension on the hanging wall of the fault. The displacements inferred from the two techniques are generally consistent, involving up to approximately 15 cm of downward vertical displacement along with lateral displacement. These data have been used to infer a preliminary fault plane solution for the mainshock, which is given in Table 3.

The mainshock strong-motion data have been recorded by 56 stations with digital instruments at distances up to about 250 km. This is the best-recorded earthquake to date in Italy. In addition, four instruments recorded near-fault ground motions near L'Aquila on various site conditions. We have compiled preliminary metadata, including site data and information on instrument housing, for all recording sites with the results presented in Table 4. The data have been processed by several groups, including Pacific Engineering and Analysis (which was performed according to NGA standards). Preliminary comparisons of those processed data with ground-motion prediction equations reinforces an earlier observation from Scasserra et al. (2009) that high frequency ground motions in Italy attenuate faster with distance than what is predicted from NGA GMPEs, which are based on a world-wide database. Additional more detailed analysis of the ground motion data is an important research need. This work will require careful characterization of geologic and geophysical conditions at the recording sites.

The main event caused locally heavy damage to nonductile reinforced concrete and unreinforced masonry buildings in portions of L'Aquila and in several villages in the Aterno valley. We performed systematic surveys in neighbouring villages having different site conditions and in adjacent regions of L'Aquila, also with varying site conditions, to evaluate possible site effects on building damage. Variations in damage intensity between villages were particularly striking, with several examples of catastrophic losses in a village adjacent to another with almost no damage, despite similar styles of construction. These differences suggested that local effects related to geologic/geotechnical conditions and different topographies significantly influenced the ground motions in the period range of interest for these structures. They also illustrate the well-known vulnerability of these styles of construction to earthquake losses.

Ground failure, defined as permanent ground displacement of non-tectonic origin caused by the earthquake, occurred in the form of several minor landslides and rockfalls, seismic compression of unsaturated fill materials including levees, and spread features around a lake. Slopes in pervasively-fractured and weak rocks experienced ravelling, but shallow slumps/slides were also recorded on subvertical cuts. The largest failures (some hundreds of $m^3$) involved poorly cemented rocks (conglomerate, cataclasite) and were influenced by morphologic effects (e.g. rock spurs with reduced lateral confinement). An incident of rockfall involving a large boulder (approximately the size of a car) was mapped in detail. Several incidents of longitudinal cracking along the crests of levees were documented, which may have resulted from softening of the underlying foundation soils.

The occurrence of ground failure that holds the greatest potential for advancing fundamental knowledge related to potential ground softening and strength degradation is a series of incidents of slumping and spreading around Lake Sinizzo. This lake lies along the fault zone, but is southeast of the rupture area. It is thought to be a sinkhole in the limestone bedrock. Ground cracking around the lake margin in Quaternary sediments indicates lateral displacements ranging from null to over 1.0 m. The displacements have been mapped with crack surveys and the morphology of the area (along with crack locations) has been imaged using LIDAR (above water) and bathymetry (below water). Soil conditions at the site are unknown. This is an important case history for detailed, follow-up investigation.

Major geotechnical structures in the shaken area include two concrete dams and one earth-fill dam, which remained functional with no observed damage. Earth-retaining structures also performed satisfactorily, with only minor damages at few locations.

This article provides a preliminary overview of the principal seismological and geotechnical aspects of this earthquake. We strongly recommend more detailed follow-up investigations be performed to fully leverage the valuable data to emerge from this event. Some of the most promising topics for further investigation include ground motion studies, damage pattern studies using aerial imagery, and ground failure investigations at Lake Sinizzo.

**ACKNOWLEDGMENTS**

Core support for the U.S. and Austrian participants in this work was provided by a grant from the U.S. National Science Foundation-sponsored GeoEngineering Earthquake Reconnaissance (GEER) Association through NSF Grant CMMI-00323914. Any opinions, findings, and conclusions or recommendations expressed in this material are those of the authors and do not necessarily reflect the views of the National Science Foundation.

Support for the Italian participants was partially provided by ReLuis Consortium (Italian University Network of Seismic Engineering Laboratories, with the assistance of Gaetano Manfredi, Università di Napoli) and partially by the Ministero dell'Università e della Ricerca (MIUR). These supports are gratefully acknowledged.

Aside from the authors, numerous individuals contributed data and observations that are reflected in this report including Margit Piber (U. Graz); Joe Smith (Montana Tech); Stefania Sica (University of Sannio); Augusto Penna (CIMA), Antonio Santo, Lorenza Evangelista, Emilio Bilotta, Domenico Calcaterra, Massimo Ramondini (University of Naples Federico II), Angelo Amorosi (Politecnico of Bari), Pietro Fargnoli (University of Rome La Sapienza, Rome, Italy), Luca Verrucci (CNR-IGAG, Rome, Italy), and Gerald Roberts (University of London). Stefano Aversa, chairman of AGI in Italy, is thanked for his participation in this effort. Alisa Facchini Stewart translated the earthquake setting and source characteristics section from Italian to English; her timely and accurate work is much appreciated.

**REFERENCES**

Ambraseys, N.N., Douglas, J., Smit, P., Sarma, S.K. (2005). "Equations for the estimation of strong ground motions from shallow crustal earthquakes using data from Europe and the Middle East: Horizontal peak ground acceleration and spectral acceleration". Bull. Earthquake Eng., 3(1), 1–53.

APAT (2006). Carta Geologica d'Italia alla scala 1:50.000 – Foglio n. 359 "L'Aquila". S.EL.CA. Firenze.

Athanasopoulos, G.A. (1995). Discussion of "1988 Armenia Earthquake II: Damage Statistics Versus Geologic and Soil Profiles", by M.K. Yegian, V.G. Ghahraman and G. Gazetas. Journal of Geotechnical Engineering, ASCE, 121 (4), 395-398.

Atzori, S., Chini, M., Hunstad, I., Stramondo, S., Bignami, C., Tolomei, C., Salvi, S., Moro, M. (INGV) & Saroli, M. (UniCass) (2009). Risultati dell'analisi interferometrica dei dati SAR e vincoli per la sorgente. Workshop on "The April 2009 L'Aquila earthquake (Italy): first results and future strategies". Chieti, June 4, 2009 (Italy): http://www.unich.it/geosis/PROGRAMMA.html) (in Italian).

Bagnaia, R., A. D'Epifanio e S. Sylos Labini (1992). "Aquila and subaequan basins: an example of Quaternary evolution in Central Apennines, Italy". Quaternaria Nova, II, 187-209

Bertini, T., Bosi, C., and Galadini, F. (1989). La conca di Fossa-S. Demetrio dei Vestini. In: CNR, Centro di Studio per la Geologia Tecnica, ENEA, P.A.S.: "Elementi di tettonica pliocenico-quaternaria ed indizi di sismicità olocenica nell'Appennino laziale-abruzzese". Società Geologica Italiana, L'Aquila, 26-58 (in Italian).

Boncio, P., Lavecchia, G., and Pace, B. (2004). "Defining a model of 3D seismogenic sources for Seismic Hazard Assessment applications: The case of central Apennines (Italy)". Journal of Seismology, 8, 407-425.

Boore, D.M. and Atkinson, G.M. (2008). "Ground motion prediction equations for the average horizontal component of PGA, PGV, and 5%-damped PSA at spectral periods between 0.01 and 10.0 s". Earthquake Spectra, 24 (S1). 99-138.

Boore, D.M., Watson–Lamprey, J., and Abrahamson, N.A. (2006). "Orientation-independent measures of ground motion". Bull. Seismol. Soc. Am., 96 (4a), 1502–1511.

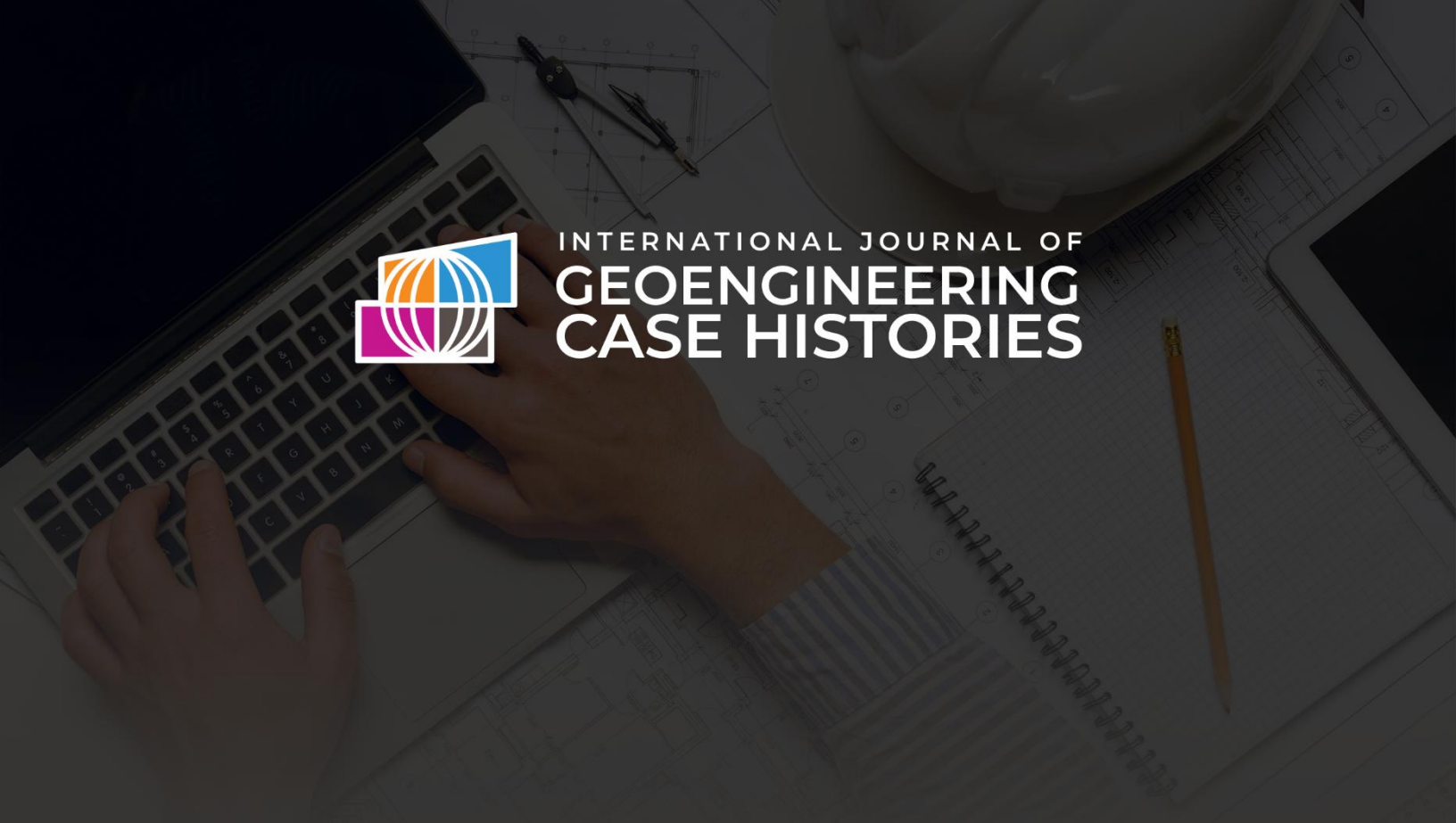
Bosi, C., and Bertini, T. (1970). "Geologia della Media Valle dell'Aterno". Memorie della Società Geologica Italiana, Volume IX, 719-777 (in Italian).

Bozorgnia, Y., and Campbell, K.W. (2004). "The vertical-to-horizontal response spectral ratio and tentative procedures for developing simplified V/H and vertical design spectra". Journal of Earthquake Engineering, 8(2), 175-207.

Bray, J.D., and Stewart, J.P.: coordinators (2000). "Chapter 8: Damage patterns and foundation performance in Adapazari". Kocaeli, Turkey Earthquake of August 17, 1999 Reconnaissance Report, T.L. Youd, J.P. Bardet, and J.D. Bray, eds., Earthquake Spectra, Supplement A to Vol. 16, 163-189.

Cavinato, G.P., and De Celles, P.G. (1999). "Extensional basins in the tectonically bimodal central Apennines fold-thrust belt, Italy: response to corner flow above a subducting slab in retrograde motion". Geology, 27, 955-958.
Chiarabba, C., & CNT Working Group (INGV) (2009). Terremoto de L'Aquila: il contributo della sismologia. Workshop on "The April 2009 L'Aquila earthquake (Italy): first results and future strategies". Chieti, June 4, 2009 (Italy): (http://www.unich.it/geosis/PROGRAMMA.html) (in Italian).
Cocco, M. (2009). INGV Internal Report: "The April 6th 2009 (Ml 5.8) earthquake preliminary results". EGU General Assembly, Vienna, Austria, 19-24 April (massimo.cocco@ingv.it; claudio.chiarabba@ingv.it; pasquale.degori@ingv.it).
Collins, B.D., and Sitar, N. (2006). "Monitoring of Coastal Bluff Stability Using High Resolution 3D Laser Scanning in Site Characterization and Modeling". Geotechnical Special Publication No. 138, ASCE GeoInstitute.
Collins, B.D., Minasian, D., and Kayen, R. (2009). "Topographic change detection at select archeological sites in Grand Canyon National Park, Arizona, 2006-2007". U.S. Geological Survey Scientific Investigations Report 2009-5116, 58 p. [http://pubs.usgs.gov/sir/2009/5116/].
D'Agostino, N. (2009). "Il terremoto dell'Aquila del 6 aprile 2009: risultati scientifici preliminary". INGV Internal Report (dagostin@ingv.it) (in Italian).
Devoti, R., Riguzzi, F., Cuffaro, M., and Doglioni, C. (2008). "New GPS costraints on the kinematics of the Appeninnes subduction". Earth Planet Sci. Lett., doi: 10.1016/j.epsl.2008.06.031.
DISS Working Group (2009). "Database of Individual Seismogenic Sources (DISS), Version 3.1.0: A compilation of potential sources for earthquakes larger than M 5.5 in Italy and surrounding areas". http://diss.rm.ingv.it/diss/, © INGV 2009 - Istituto Nazionale di Geofisica e Vulcanologia - All rights reserved
Doglioni, C. (1990). "The global tectonic pattern". Journal of Geodynamics, 12, 1, 21-38.
Doglioni, C. (1991). "A proposal of kinematic modelling for W-dipping subductions - Possible applications to the Tyrrhenian - Apennines system". Terra Nova, 3, 4, 423-434.
EMERGEO Working Group (2009). "Rilievi geologici di terreno effettuati nell'area epicentrale della sequenza sismica dell'Aquilano del 6 aprile 2009" (http://www.earth-prints.org/handle/2122/5036) (in Italian).
Galadini, F., and Galli, P. (2000). "Active Tectonics in the Central Apennines (Italy) – Input Data for Seismic Hazard Assessment". Natural Hazards, 22, 225-270.
Galadini, F., and Messina, P. (2001). "Plio-Quaternary changes of the normal fault architecture in the Central Apennines (Italy)". Geodinamica Acta, 14, 321-344.
Galli, P., and Camassi, R. (eds.), 2009. "Rapporto sugli effetti del terremoto aquilano del 6 aprile 2009". Rapporto congiunto DPC-INGV, 12 pp.
Sito Internet: http://portale.ingv.it/real-time-monitoring/quest/macrodef_sito.pdf (in Italian)
GEER Working Group (2009). "Preliminary Report on the Seismological and Geotechnical Aspects of the April 6 2009 L'Aquila Earthquake in Central Italy (Version 2.0 September 2009)". Report of the National Science Foundation-Sponsored GeoEngineering Extreme Events Reconnaissance (GEER) Team. http://research.eerc.berkeley.edu/projects/GEER/GEER_Post%20EQ%20Reports/Italy_2009/Cover_Italy2009.html.
Ghisetti, F., and Vezzani, L. (2000). "Modalità di riattivazione, circolazione dei fluidi e rottura sismica di alcune delle principali faglie normali nelle zone esterne dell'Appennino centrale". In: "Galadini F., Meletti C., Rebez A. (a cura di), Le ricerche del GNDT nel campo della pericolosità sismica (1996-1999). CNR-Gruppo Nazionale per la Difesa dai Terremoti – Roma, 2000, pp. 397 (in Italian).
Ghisetti, F., and Vezzani, L. (2002). "Normal faulting, transcrustal permeability and seismogenesis in the Apennines (Italy)". Tectonophysics, 348, 155-168.
Gruppo di lavoro CPTI (2004). "Catalogo Parametrico dei Terremoti Italiani, versione 2004 (CPTI04), INGV, Bologna" (http://emidius.mi.ingv.it/CPTI04/) (in Italian).
ISPRA (2009a). "Tabella sintetica sopralluoghi 7-8-9-10 Aprile 2009" (in Italian).
ISPRA (2009b). "Documentazione Fotografica sopralluoghi (periodo 6 - 10 Aprile 2009)" (in Italian).
Kayen, R., Pack, R.T., Bay, J., Sugimoto, S., and Tanaka, H. (2006). "Terrestrial -LIDAR visualization of surface and structural deformations of the 2004 Niigata Ken Chuetsu Earthquake". Earthquake Spectra. 22(S1), S147-S162.
Kayen, R., Collins, B.D., Abrahamson, N., Ashford, S., Brandenberg, S.J., Cluff, L., Dickenson, S., Johnson, L., Kabeyasawa, T., Kawamata, Y., Koumoto, H., Marubashi, N., Pujol, S., Steele, C., Sun, J., Tanaka, Y., Tokimatsu, K., Tsai, B., Yanev, P., Yashinsky , M., and Yousok, K. (2007). "Investigation of the M6.6 Niigata-Chuetsu Oki, Japan, Earthquake of July 16, 2007". U.S. Geological Survey, Open File Report 2007-1365, 230pg; [available on the World Wide Web at URL http://pubs.usgs.gov/of/2007/1365/].
Kayen, R., and Collins, B.D. (2005). "Terrestrial LIDAR Imagery and Analysis of Hurricane Katrina Levee Failures in the City of New Orleans". Eos Trans. AGU, 86(52), Fall Meet. Suppl, Abstract H42C-07.

Mantovani, E. (1991). "Evaluation of the seismic hazard in Italy". In: "Le Scienze – quaderni", 59, 51-59. Le Scienze S.p.A. Milano (in Italian).
Parotto, M. (1980). "Appennin Central". In: "Géologie d'Europe"; guide prepared for 26th International Congress of Geology, Paris.
Piatanesi, A., and Cirella, A. (2009). "Rupture process of the 2009 $M_w$=6.3 L'Aquila (Central Italy) earthquake from non linear inversion of strong motion and GPS data". INGV Report.
Praturlon, A. (1993). "Geological features". From "Structural Model of Italy 1:500.000" (1992), CNR. In: "Guide Geologiche Regionali - Lazio", 5, 18-25. Società Geologica d'Italia (in Italian).
QUEST (2009). "Rapporto sugli effetti del terremoto aquilano del 6 aprile 2009". Rapporto INGV (http://www.mi.ingv.it/eq/090406/quest.html) (in Italian).
Rovida, A., Castelli, V., Camassi, R., and Stucchi, M. (2009). "Terremoti storici nell'area colpita dagli eventi sismici dell'aprile 2009". INGV Report (http://www.mi.ingv.it/eq/090406/storia.html) (in Italian).
Sabetta, F., and Pugliese, A. (1996). "Estimation of response spectra and simulation of nonstationary earthquake ground motion". Bull. Seism. Soc. Am., 86 (2), 337-352.
Salvi, S., and Working Group (2009). "Risultati Preliminari SAR". INGV Report (http://portale.ingv.it/primo-piano/archivio-primo-piano/notizie-2009/terremoto-6-aprile/sar) (in Italian).
Scasserra, G., Stewart, J.P., Kayen, R.E., and Lanzo, G. (2009a). "Database for earthquake strong motion studies in Italy". Journal of Earthquake Engineering, 13 (6), 852-881.
Scasserra, G, Stewart, J.P., Bazzurro, P., Lanzo, G., and Mollaioli, F. (2009b). "A comparison of NGA ground-motion prediction equations to Italian data". Bull. Seism. Soc. Am., 99 (5), 2961-2978.
Simonelli et al. (2009). "Rapporto Preliminare Sugli Effetti Indotti Sull'ambiente Fisico Dalla Sequenza Sismica Dell'aquilano, Ver. 1.5, Parte II Ricognizioni Nell'area A Nord Di L'Aquila Fino All'invaso Di Campotosto". Gruppo di Lavoro UNISANNIO – CIMA – DIGA, available at www.reluis.it, (in Italian)
Stewart, J.P., Hu, J., Kayen, R.E., Lembo, A.J. Jr., Collins, B.D., Davis, C.A., and O'Rourke, T.D. (2009). "Use of airborne and terrestrial LIDAR to detect ground displacement hazards to water systems". J. Surveying Engineering, ASCE, 135 (3), 113-124.
Stucchi et al. (2007). "DBMI04, il database delle osservazioni macrosismiche dei terremoti Italiani utilizzate per la compilazione del catalogo parametrico CPTI04". Quaderni di Geofisica, Vol. 49, pp. 38, http://emidius.mi.ingv.it/DBMI04/ (in Italian).
Tetè, P., Pesce, G.L., and Leonardis, B. (1984). "Il Lago Sinizzo nei pressi di San Demetrio Nè Vestini (L'Aquila)". Natura (in Italian).
Tozzi, M. (1993). Deep structure of the central Appennine. In: "Guide Geologiche Regionali - Lazio", 5, 45-49. Società Geologica d'Italia (in Italian).
Valensise, G. (2009). "Alcune considerazioni sulla sismotettonica del terremoto del 6 aprile". INGV Internal Report, mailto:valensise@ingv.it (in Italian).
Violante, C. (2009). "High resolution morphobathymetric study of lake Sinizzo after the April-May 2009 Abruzzo seismic sequence". Report to GEER.
Working Group ITACA (2009). "Data Base of the Italian strong motion data": http://itaca.mi.ingv.it.
Yegian, M.K. et al., (1994). "1988 Armenia earthquake II: Damage Statistics Versus Geologic and Soil Profiles". Journal of Geotechnical Engineering, ASCE, 120 (1), 21-45.



INTERNATIONAL JOURNAL OF
GEOENGINEERING
CASE HISTORIES

***The Journal's Open Access Mission is generously supported by the following Organizations:***

dar
a Sidara company

Geosyntec consultants
engineers | scientists | innovators

ConeTec

MUD BAY DRILLING
LANKELMA
Geotech DRILLING

ENGEO
Expect Excellence

*Access the content of the ĪSSMGE Īnternational Journal of Geoengineering Case Histories at:*
*www.geocasehistoriesjournal.org*

Downloaded: Tuesday, November 10 2026, 14:18:30 UTC